Decellularized *Apium graveolens* Scaffold for Cell Culture and Guided Alignment of C2C12 Murine Myoblast

Santiago Campuzano

Thesis submitted to the University of Ottawa

in partial fulfillment of the requirements for the

Master of Science

Ottawa-Carleton Institute for Biology

Faculty of Science

University of Ottawa

ACKNOWLEDGMENT

First of all, I would like to acknowledge the unconditional support from New Harvest and the In Vivo Foundation. This work would not have happened without their support. Even if cultured meat does not happen in my lifetime, this was a life changing opportunity. Isha Datar, thank you for seeing something in me 3 years ago at the Georgia Hotel. Dr. Kate Krueger, thank you for always supporting my decisions. To be a New Harvest fellow was an absolute privilege.

As I sit here writing a grant proposal, I would like to thank Dr. Andrew Pelling for the constructive and insightful feedback provided throughout my studies. It made me a better scientist. As I stare at my grant, I ask myself "WWAS" (What would Andrew say).

A huge shout-out to the Pelling lab members, especially my good friends and incredible scientists, Maxime Leblanc, Ryan Hickey, Sebastian Hadjiantoniou, Matthew Walker and Daniel Modulevsky. Getting to see how you all tackled complex projects was an incredibly empowering opportunity.

As a proud Vancouverite, moving to Ottawa was not an easy decision for me or my family. Hannah, thank you for your patience and unconditional support. To my mom who has always believed in me and my crazy ideas, thank you. To my good amigos, Aaron, Timothy, Peter, Oliver, Terry and Bhaskhar, thank you for planning "family dinners" on the weeks that I visited. Much love gents.

Y para los que dudaron, apenas estoy empezando.

ABSTRACT

The development of *in vitro* meat from validated tissue engineering techniques has emerged as a more sustainable and ethical method of meat production. To date, the expansion of cellular agriculture is believed to be dependent on four pillars: animal free scaffolds, serum free media, bioreactors and cell lines or stem cells. In 2014, decellularized plant tissue emerged as an animal free scaffold for three-dimensional cell culture. Despite the fact that plant parenchyma provides a relatively porous and biocompatible substrate with stiffness values similar to those of muscle tissue, it lacks a number of physical, biochemical, and topographical cues necessary to recapitulate the microenvironment sensed by cells. A crucial characteristic of skeletal muscle tissue is the aligned arrangement of myofibers. Yet, a great deal of knowledge has come from *in vitro* studies where cells appear randomly scattered. This is turn has created a discrepancy between *in vivo* and *in vitro* studies due to widely supported observation that spatial orientation greatly influences gene expression. As part of this thesis, microchannels were developed by longitudinally cutting the vascular bundle of celery (*Apium graveolens*). Based on the guided alignment of cells on synthetic microchannels, I hypothesize that myoblast will not only align parallel to the vascular bundle but fuse into aligned myotubes. Results show that following 10 days in culture, the normalized orientation of F-actin filaments was determined to be 1.2 ± 2.0°. Subsequent to myoblast alignment, differentiation for 5 days led to the formation of myotubes with a normalized orientation of 8.6 ± 23.8°. Granted that alignment is a crucial characteristic of skeletal muscle tissue, it constitutes only one parameter. Fully recapitulating the microenvironment will need to extend beyond topographical cues, as plant vascularization is partially hydrophobic, approximately 30x stiffer than muscle tissue, and lacks the biochemical cues of mammalian extracellular matrix.

STATEMENT OF ORIGINALITY

I certify that, to the best of my knowledge, the research data and contents of this thesis are entirely original. Any copyrighted material, ideas, techniques or work included in this thesis are fully acknowledged in accordance with the standard referencing practices. Research and manuscript preparation were prepared under the supervision of Dr. Andrew Pelling in the STEM complex in the Department of Physics and Biology at the University of Ottawa.

MANUSCRIPTS IN THIS THESIS

Chapter 2 is a published article in *Frontiers in Sustainable Food Systems*:

Campuzano S. & Pelling A.E. (2019) Scaffolds for 3D Cell Culture and Cellular Agriculture Application Derived From Non-animal Sources. *Frontiers in Sustainable Food Systems*,3,38. Doi:10.3389/fsufs.2019.00038

Chapter 4 has been submitted to *Biomaterials Science* for peer review

CONFERENCE PROCEEDINGS:

Campuzano, S. & Pelling. A.E. "Decellularized celery scaffold for guided cell alignment" New Harvest conference 2019, Boston, Massachusetts, 2019 (Talk and poster)

Campuzano, S. & Pelling. A.E. "Decellularized celery scaffold for guided cell alignment" British Columbia regenerative medicine symposium 2019, Vancouver, British Columbia, 2019 (Poster)

TABLE OF CONTENTS

LIST OF ABBREVIATIOS

- Pax - Paired box genes
- MYHC - Myosin heavy chain
- Wnt - Wingless-related integration site
- BMH - Bone Morphogenic Protein
- MF-20 – Myosin heavy chain 1E antibody
- Shh - Sonic Hedgehog (Shh)
- Myf5 – Myogenic factor 5
- MyoD - Myoblast determination protein
- MRF4 – Myogenic regulatory factor 4
- HGF - hepatocyte growth factor
- ECM - Extracellular matrix
- FAK - Focal adhesion kinase
- PLA – Polylactic acid
- PCL - Polycaproctalone
- PH-4 - Prolyl 4-hydrolysase
- LH1-3 - Lysine hydroxylase
- Scl - streptococcal collagen-like protein
- PBS - Phosphate buffered saline
- DAPI - 4′,6-diamidino-2-phenylindole
- AFM – Atomic force microscopy
- SDS - Sodium dodecyl sulfate
- MAPK – Mitogen- activated protein kinase
- RGD – arginine-glycine-aspartate
- FBS -Fetal bovine serum
- H & E – Hematoxylin and eosin
- V.B. - Vascular bundle
- DMEM - Dulbecco’s Modified Eagle’s medium
- TBST - Tris-buffered saline, 0.1% Tween® 20
- SEM – Scanning electron microscopy
- BAR - Bin/amphiphysin/Rv
- PDMS - Polydimethylsiloxane

LIST OF FIGURES

THESIS PREFACE

The inception and expansion of tissue engineering as a multidisciplinary discipline capable of addressing medical issues with therapies ranging from localized *in vivo* treatment to the development of *in vitro* organs opened the door to a field beyond the biomedical realm: cellular agriculture (Kwon et al., 2018; Li et al, 2014). In response to the ethical (Verbeke & Viaene,2000) and environmental (Kraham, 2017) impact incurred by conventional meat production, cellular agriculture emerged as a more sustainable and ethical method of production (Tuomisto et al., 2011). This is yet to be determined, however (Lynch & Pierrehumbert, 2019). To date, the expansion of cellular agriculture is believed to depend on four major pillars: scalable bioreactors, cell lines or stem cells, serum free media, and animal free scaffolds (Datar & Betti, 2010; Specht et al., 2018).

The depiction of decellularized plant tissue as an abundant animal free scaffold for 3D cell culture by Modulevsky and colleagues (2014) opened the door to cellular agriculture applications. Furthermore, the wide array of structures with varying topographies and mechanical properties natively found in plants provides a plethora of substrates ripe for *in vitro* culture and tissue mimicry (Modulevsky et al.,2014; Gershlak et al.,2017; Fontana et al.,2017; Hickey et al.,2018; Modulevsky et al.,2016; Hickey & Pelling, 2019; Campuzano & Pelling, 2019; Adamski et al., 2018).

Taking into consideration that meat is often composed mostly of muscle tissue, which itself is composed in large part of aligned skeletal muscle cells (Listrat et al., 2016) has led to the development of fibrous and patterned substrates capable of recreating an aligned arrangement of muscle cells to more closely resemble native tissue (Cooper et al., 2010; Hume et al., 2012; Huang et al., 2010; Wang et al., 2010; Cha et al., 2017). As part of the structures natively found in plants, the vascularization of plants such as celery (*Apium graveolens*), which is composed of microchannels, presents a desirable topography for guided cell alignment through contact guidance. This in turn led me to hypothesize that the microchannels of the celery vascular bundle will provide topographical cues similar to the substrates mentioned previously; hence, guide muscle cell alignment through contact guidance (to be discussed in chapter 4, a manuscript in preparation). Prior to investigating this phenomenon, it's paramount that we first understand the physiological development of muscle cells *in vivo*. If we wish to develop biomaterials to better assimilate the *in vivo* environment, we must understand the physiological development of myoblast, transcription factors, and morphogens; and lastly the mechanical and physical factors known to influence muscle cells *in vivo*. Through chapter 1, I wish to provide an overview on the physiological development of muscle to lay a foundation for the forthcoming objectives, hypothesis, and results.

Through chapter two, a published review paper on animal free scaffolds, I will convey the importance of animal free scaffolds for the purpose of muscle tissue engineering and discuss in detail chitin/chitosan, decellularized plant tissue, and recombinant collagen. This chapter will also serve as a detailed overview on cellulose with emphasis on decellularized plant tissue. The

chapter will further discuss what has been shown regarding the varying mechanical properties and functionalization of decellularized plant tissue to date.

In chapter three, I will discuss the mechanical properties of the decellularized celery scaffold and its interaction with C2C12 murine myoblast. The phenotype, proliferation, and differentiation of cells on the scaffolds will be used to assess the biocompatibility of the decellularized celery scaffold. Chapter four will then shift the focus towards the vascular bundle of celery. I will show how the microchannels of the vascular bundle not only guide cell alignment but also lead to the formation of aligned myotube.

CHAPTER 1

Muscle overview

1.1. Muscle tissue

Throughout the body of mammals, amphibians, birds, and invertebrates, muscle tissue is responsible for a number of functions, including breathing, swallowing, movement, and blood flow. To accomplish these functions, each tissue possesses specialized muscle cells. These specialized cells are divided into cardiac muscle cells, smooth muscle cells, and skeletal muscle cells. These cells share one crucial characteristic: the ability to contract through a physical interaction between cytoskeletal proteins, actin and myosin (Fig.1). Each specialized cell portrays specific genes and overall phenotype.

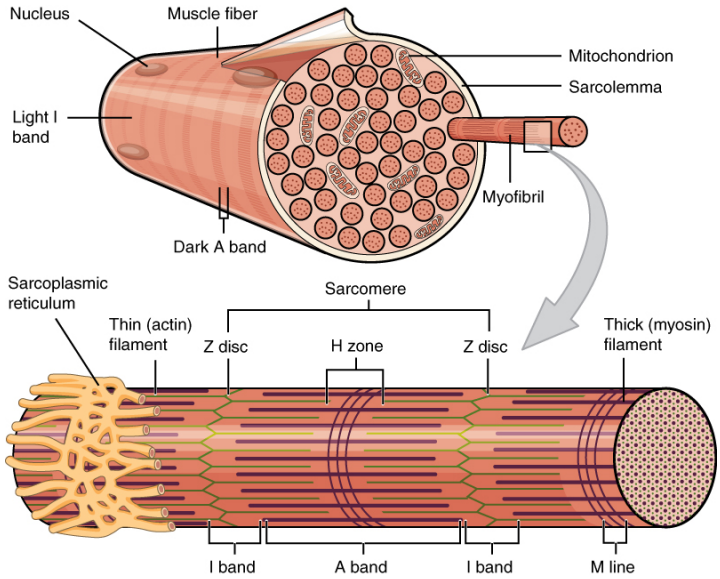

Figure 1. Skeletal muscle tissue at a glance. Skeletal muscle cells portray a clear striation from the rearrangement of myosin and actin filaments. The anisotropic arrangement of myofibers plays a crucial role in functionality of the tissue. Mature muscle fibres are also distinguished by the movement of the nuclei to the periphery and the even distribution of the sarcoplasmic reticulum to facilitate a synchronized depolarization. Image was retrieved from Anatomy and Physiology with written permission from OpenStax at https://openstax.org.

1.2 Skeletal muscle – *In vivo*

Skeletal muscle mass comprises approximately 38% of the total body mass of males and 21% in females (Janssen et al., 2000). Muscle as an organ consists of skeletal muscle tissue, connective tissue, nerve tissue, and vascular tissue. It portrays a number of crucial physical characteristics, such as aligned muscle fibers (Cornelison, 2008; Listrat et al., 2016; Frontera & Ochala, 2014). The alignment of muscle fibers allows for the synchronized generation of force along a predetermined axis when the skeletal muscle cell contracts in response to depolarization driven by acetylcholine release from nerve cells in the neuromuscular junction (Tintignac et al., 2015; Kuo & Ehrlich,2015).

1.3 Skeletal muscle development

The development of skeletal muscle begins in the somite originating from the paraxial mesoderm (Buckingham et al., 2003; Reshef et al.,1998). The specification of the somite towards the dermomyotome is dependent on Wingless-related integration site (Wnt) (primarily Wnt 1 and 3), bone morphogenic proteins, Noggin, and Sonic Hedgehog (Shh) signalling (Münsterberg et al., 1995; Bentzinger et al., 2012; Reshef et al., 1998; von Maltzahn et al., 2012). Bone morphogenic proteins in contrast to the other three delays differentiation while maintaining the $Pax3^{+}$ cells in a undifferentiated state. (Ben-Yair & Kalcheim, 2008; Bentzinger et al., 2012). The dermomyotome differentiates into central dermomyotome, dorsomedial lip, and ventrolateral lip. The skeletal muscle precursor cells within the dermomyotome are characterized by the expression of Pax3 and Pax7, and low expression of Myf5 (Chal and Pourquie, 2017; Bentzinger et al., 2012). Delamination of Pax 3^{+} myogenic precursors cells from the ventrolateral lip contribute to muscle formation of the limbs, whereas myocytes on the

myotome begin to form aligned primary muscle fibres along the anterior-posterior axis of the notochord giving rise to the trunk muscles (Fig.2A) (Eloy-Trinquet & Nicolas., 2002; Sacks et al., 2003; Chal and Pourquie, 2017) This alignment is predominantly influenced by Wnt 11 signaling. (Gros et al., 2009).

The first stage of myotube (multinucleated structure) formation arises from the fusion of a founder cells and fusion competent myoblast. (Kim et al., 2015). Founder cells attract the fusion competent cells, which influence the orientation, location, and number of muscle fibres (Dutta et al., 2004; Beckett and Baylies, 2007; Kim et al., 2015). The mechanism of fusion in mammals is still poorly understood as most of the experiments have been done on flies. However, it's understood that the fusion process is asymmetric, where actin-propelled protrusion from the fusion competent myoblast invade the founder cell forming the fusonegic synapse concomitantly with a number of push and pull forces to help destabilize the plasma membrane. (Hindi et al., 2013; Sampath et al., 2018; Kim et al., 2015; Duan et al., 2018; Abmayr & Pavlath, 2012). The formation of fusogenic synapse leads to the opening of fusion pores to allow cytoplasmic material to merge and form a multinucleated structure (Dhanyasi et al., 2015; Kim et al., 2015).

The formation of the myotome primary muscle fibers and limb primary muscle fibers provide the template for secondary muscle fibers throughout adulthood (Ontell & Kozeka, 1984; Buckingham et al., 2003). This process is highly regulated by transcription factors (e.g. Pax3) and muscle regulatory markers: Myf5, MyoD, MRF4 and Myogenin. Defining myogenic genes such as Myh7, Myh3, alpha actin (cardiac followed by skeletal) and Desmin appear as early as myotome stage (Chal and Pourquie, 2017). The primary fibers become slow twitch whereas the

secondary become fast twitch muscle fibers (Fiorotto, 2012). Muscle growth and elongation of primary muscle fibers at this stage is maintained by proliferating $Pax7^+$ (Allouh, et al., 2008).

Furthermore, a portion of somatic $Pax7^+$ will begin to relocate beneath the basal lamina (endomysium) to make up the quiescent satellite cell pool (Lepper and Fan, 2010). Satellite cells, quiescent myoblast precursors, are responsible for the repair and growth of myofibers throughout adulthood (Kassar-Duchossoy et al., 2005). Through asymmetric division, satellite cells maintain the pool of quiescent muscle and respond to damaged muscle following extrinsic signals, such as hepatocyte growth factor (HGF) release from the damaged ECM (Fu et al., 2015; Allen et al., 1995; Cosgrove et al., 2009). Following asymmetric division, the expression of Myf5, MyoD and Myogenin become markers of myoblast commitment (Sabourin & Rudnikci, 2000). Fusion and terminal differentiation is then driven by the expression of MyoD, MyoG and MRF4. All of which are expressed in mature muscle fibers (Fig.2B) (Murphy & Kardon, 2011; Bentzinger et al., 2012)

The mature skeletal myofibers are composed of aligned myofibrils attached to the myotendinous junction (Frontera and Ochala, 2014). The reorganization of myosin and actin leads to overlapping regions (Sarcomere) responsible for generating contractions (Fig.1) (Lemke & Schnorrer, 2017). The reorganization of the cytoskeletal proteins into the sarcomere is a clear depiction of optimal muscle fibre development (Engler et al., 2004*). In vivo* muscle fibres are also characterized by the formation of plasma membrane intrusions known as T-tubules, which assist in even depolarization distribution throughout the myofibrils (Franzini-Armstrong & Engel, 2012, p. 763-774). The calcium released from the cisternae following depolarization

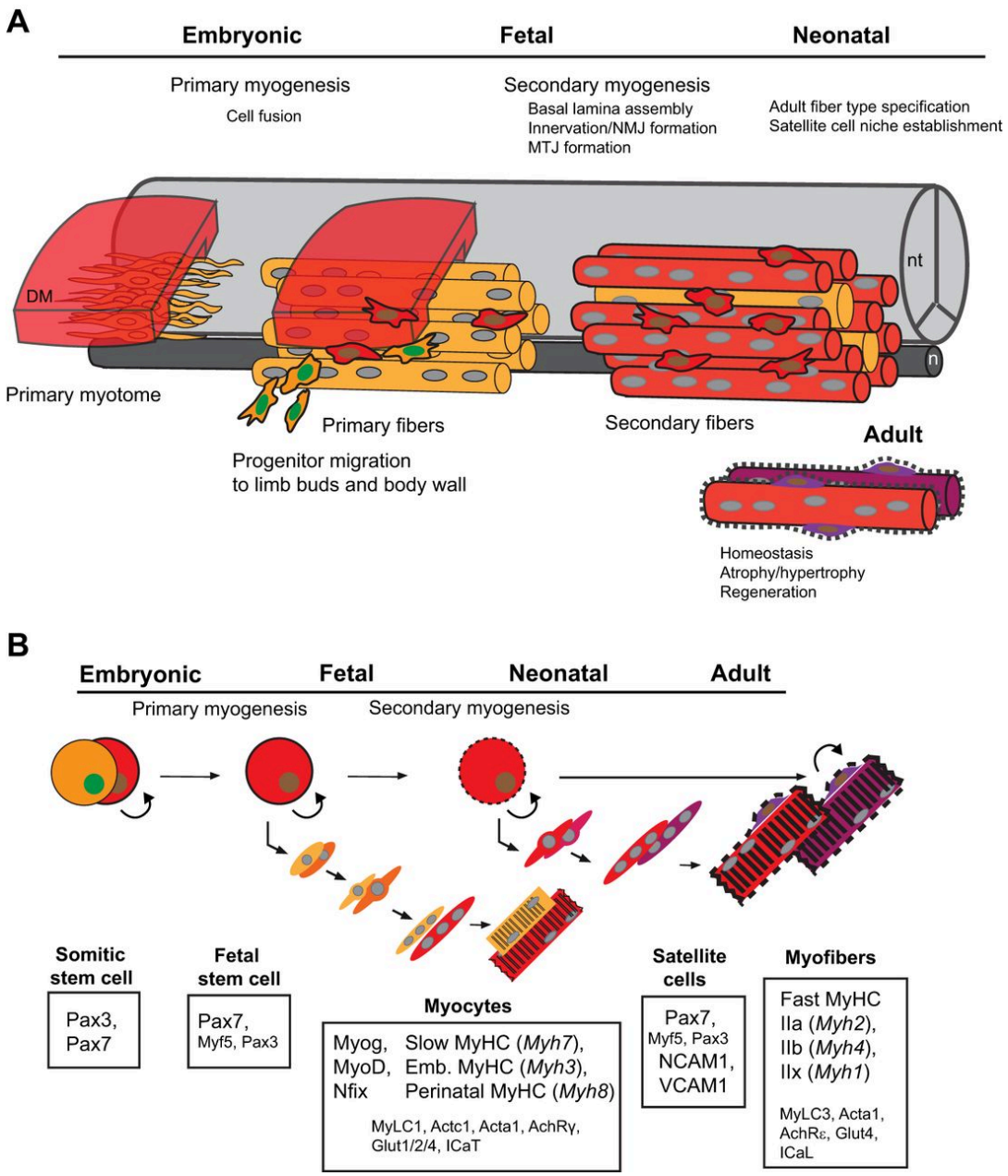

Figure 2. Stages of Skeletal myogenesis from embryo to adult.
(A) Developmental sequence of muscle formation from the dermomyotome. During primary myogenesis (middle), Pax3+ progenitors (yellow cytoplasm, green nuclei) delaminate from the dorsal side of the dermomyotome and contribute to the formation of large primary myofibers (yellow). nt, neural tube; n, notochord; DM, dermomyotome; MTJ, myotendinous junction; NMJ, neuromuscular junction. (B) Differentiation of somitic progenitors toward skeletal muscles and adult satellite cells. For each step, markers for the intermediates and differentiated skeletal myofibers are shown. Additional markers are also shown in smaller font. Differentiation stages along the myogenic lineages are color-coded according to A.

'Myocytes' encompasses also myotubes and myofibers. Emb., embryonic. Glut1, 2 and 4 are also known as Slc2a1, Slc2a2 and Slc2a4, respectively. Reproduced from Chal and Pourquie, 2017 with permission from *Development.*

binds to troponin, allowing for the interaction between myosin and actin (Szczesna et al., 1996). The defining genetic markers are dependent on the type of muscle fibre, where oxidative slow express MyHC type I and glycolytic fast express MyhC IIa,IIb,IIx (Schiaffino et al., 2015; Chal and Pourquie, 2017) .

1.4 Skeletal muscle - *In vitro*

In order to better understand muscle cells, these are routinely cultured in Petri dishes. However, the culture conditions oversimplify the actual *in vivo* environment: cells are no longer exposed to a number of physical and biochemical stimuli (Maleiner et al., 2018). Petri dishes have no resemblance to *in vivo* tissue; Petri dishes are stiff, smooth, flat, and lack a number of biochemical cues derived from the extracellular matrix (Gilles and Lieber, 2011), an everchanging blood serum, and paracrine signalling from a number of cell types (Cornelison, 2008). Connective tissue, nerve tissue, and vascular tissue embedded in skeletal muscle have been shown to play a role in the survival, repair, and functionality of skeletal muscle (Cornelison, 2008). However, myoblast or myogenic precursors cells are often cultured in isolation and in inconsistent media (Zheng et al., 2006), which doesn't represent the ever-changing conditions of blood serum.

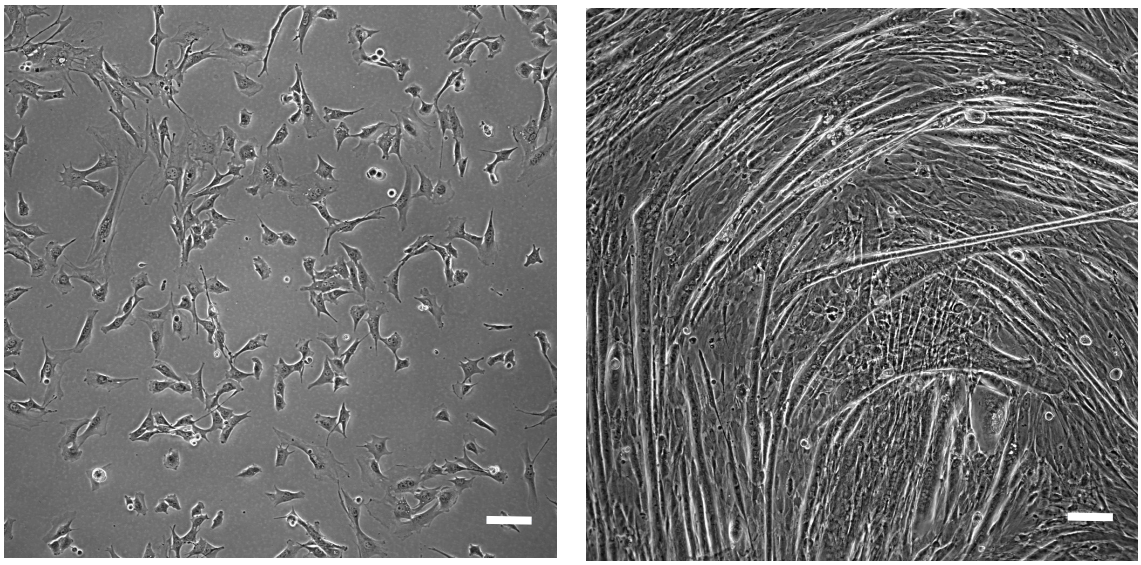

Figure 3. Phase contrast image of C2C12 murine myoblast and myotubes cultured on Petri dishes. (A) Myoblast portray an amorphous phenotype and appear randomly scattered. (B) Fusion of myoblast influenced by a low serum media leads to myotube formation. As expected, the myotubes cultured on Petri dishes don't portray a preferred orientation; yet, these often form parallel to eachother. Scale bar = 100μm

Physical cues, such as cyclic strain, topography, and matrix stiffness have been shown to play major role in myoblast development *in vitro* (Maleiner et al., 2018; Somers et al., 2017). Although a number of studies have elucidated the fact that cyclic strain has the ability to in part recreate the strain sensed by cells i*n vivo*, a caveat of factors clearly displays a number of limitations. Myoblast cultured in 2D under cyclic strain have been shown to differentiate faster when compared to those in static conditions (Pennisi et al., 2011). Yet, another group depicted how cyclic strain inhibited myogenesis and induced proliferation (Kumar et al., 2004). The conflicting evidence portrays the plethora of factors that play a role in stress/strain sensing of cells *in vivo*, and how *in vitro* mimicry of these factors fails to provide a reliable and consistent system.

Substrate stiffness has been shown to influence myogenesis *in vitro* (Romanazzo et al., 2012). Anchorage dependant cells sense matrix stiffness through integrin-rich regions referred to as focal adhesion (FA). Focal adhesion kinase (FAK) influences a number of signalling pathways, impacting cell behaviour (Graham et al., 2015; Wells, 2008). Gels with a muscle-like stiffness of approximately 12KPa have been shown to favour myogenesis through a clear depiction of sarcomere formation (Engler et al., 2004), and have also shown to favour prolonged self-renewal of skeletal muscle stem cells (Gilbert et al., 2010), which is rarely observed *in vitro* (Chal and Pourquie, 2017).

Topography has also been shown to alter morphology, proliferation, differentiation, and overall gene expression (Wang et al., 2012; Cooper et al., 2010; Mozetic et al., 2017; Kuppan et al., 2016; Foolen et al., 2018; Gao et al., 2016). As mentioned previously, spatial orientation or alignment of cells *in vitro* is a crucial characteristic of muscle. Yet, this valuable attribute is lost when cells are placed on Petri dishes. In order to assimilate 2D cell culture to the *in vivo* environment and further understand the role of matrix topography, substrates with a wide array of topographical structures, such as posts (Goedecke et al., 2015), microchannels (Humes et al.,2012), and nanofibers (Fee et al., 2016) have been developed (Goedecke et al., 2015). To further understand the role of directionality, microchannels/microgrooves, cyclic strain, and electrical stimulation have been shown to induce such phenomenon (Tanaka et al.,2014, Liu et al.,2008, Humes et al.,2012; Altomare et al., 2010; Charest et al., 2007; Pennisi et al., 2011). As mentioned previously, chapter 4 will continue to expand on the importance of alignment, and how the vascular bundle of celery can be used as an abundant animal free substrate for guided cell alignment

1.5 Conclusion

The expansion of cellular agriculture and *in vitro* meat relies on the ability to replicate the complex *in vivo* environment of skeletal muscle. The physiological development of muscle cells i*n vivo* depends on a wide array of morphogens, transcription factors, physical and biochemical cues. These factors are often lost when cells are cultured in 2D Petri dishes. Therefore, the ability to replicate these parameters *in vitro* has become of critical importance. Substrates with topographical cues capable of aligning, and overall influencing cell orientation have emerged in order to address the importance of spatial orientation. Active stimuli such as cyclic strain and electrical stimulation have been shown to enhance myogenesis. Most recently, bioreactors have emerged as way to control multiple parameters such as pH, temperature, active physical deformation and electrical stimulation (Heher et al., 2015; Donnelly et al., 2010; Giusti et al., 2017; Cerino et al., 2016; Allan et al., 2019). Control over this parameters allow for assimilation of the *in vivo* environment. I believe that complex bioreactors are currently nascent, but as research in the field continues, the biomimicry of bioreactors is expected to reach the complexity necessary to replicate *in vivo* conditions.

CHAPTER 2

Scaffolds for 3D cell culture and cellular agriculture applications derived from non-animal sources

This chapter was presented from:

Campuzano, S.[1], & Pelling, A. E.[2] (2019). Scaffolds for 3D cell culture and cellular agriculture applications derived from non-animal sources. *Frontiers in Sustainable Food Systems*, 3 doi:10.3389/fsufs.2019.00038

Motivation and Objectives

One of the main objectives of tissue engineering is to produce *de novo* tissue in vitro. Through reverse engineering, tissue engineers hope to recapitulate *in vivo* conditions to control the development of tissues from cells. Yet biomimetic scaffolds are often of animal origin, leading to environmental and ethical concerns. Furthermore, cellular agriculture hopes to utilize well established tissue engineering techniques to produce animal tissue for human consumption. To date, it's believed that the success of cellular agriculture relies on 4 major pillars: animal free scaffolds, bioreactors, continuous cell lines or stem cells, and animal free media (or serum free media). Through this peer reviewed mini review, I hope to convey the importance of animal free scaffolds, and discuss three scaffolding materials that have been widely studied in vitro and have potential applications in cellular agriculture.

2.1 Abstract

For decades, two-dimensional cell culture has been regarded as a major tool in cellular and molecular biology due to its simplicity, reproducibility and reliable nature. However, it is now recognized that 2D cell culture underrepresents the *in vivo* environment of living cells. The development and use of 3D scaffolds and biomaterials provide researchers an ability to more closely mimic the *in vivo* environment. However, many biomaterials are of animal origin, leading to variability, environmental and ethical concerns. Here we present three animal-free scaffolds: decellularized plant tissue, chitin/chitosan and recombinant collagen. Decellularized plant tissue provides a wide array of structures with varying biochemical, topographical and mechanical properties; chitin/chitosan-based scaffolds have shown synergistic bactericidal effects and improved cell-matrix interaction; and lastly, recombinant collagen has the potential to closely resemble native tissue, as opposed to the other two. These benefits, alongside potential scalability and tunability, open the door to applications beyond the biomedical realm, such as innovations in cellular agriculture and future food technologies.

2.2 Introduction

Since the early 20th century, two-dimensional cell culture has been regarded as a reliable, simple and reproducible study of cellular behavior (Jedrzejczak-Silicka,2017). However, a direct comparison between 2D and 3D cell culture is challenging due to dramatic differences in the cellular environment. *In viv*o, cells interact closely with other cells, a complex array of physical forces/stimuli, and biologically active extracellular matrix (ECM). In contrast, 2D cell culture is performed on a substrate with drastically different mechanical and biochemical properties (Fig.1). Comparisons between 2D and 3D cell culture have revealed significant differences in

proliferation, differentiation, drug toxicity resistance, gene expression and protein synthesis (Ravi et al.,2015; Antoni et al.,2015; Riedl et al.,2017; Huyck et al.,2012; Cavo et al.,2016; Fang and Eglen,2017). In order to overcome the gap between 2D cell culture and the 3D environment sensed by the cell *in vivo*, a plethora of natural and synthetic polymers, recombinant proteins, ceramics, and metal-composite scaffolds have been developed and reviewed previously (Carletti et al.,2011; Turnbull et al.,2018; O'Brien,2011). Yet, in order to produce scaffolds with similar characteristics to those of the ECM, animal-derived polymers such as collagen are often considered as the gold standard. However, the dependence on animals have made them undesirable due to variability (Shoseyov et al.,2013), environmental (Kraham,2017) and ethical concerns (Verbeke & Viaene,2000).

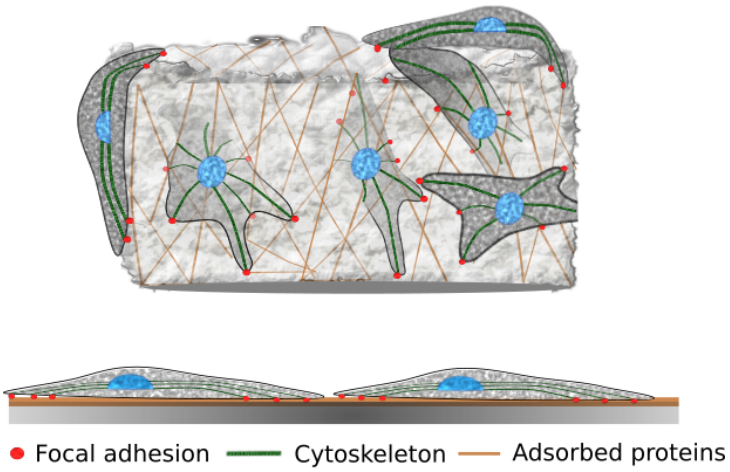

Figure 1. Cells on 3D porous substrate vs 2D substrate. Cells on 3D porous substrates can be found on the surface and interior, whereas cells on Petri dishes are bound to a 2D environment. Proteins naturally found in animal serum and those synthesized by cells adsorb to the surface of the material and facilitate cell adhesion. Through focal adhesion, adherent cells are able to interact with the substrate; therefore, the properties of the material (e.g. Stiffness) can influence the cells' behavior and morphology. Reproduced from Campuzano and Pelling, 2019 with permission from *Frontiers in Sustainable Food Systems.*

Moreover, the scalability and consumer acceptance of cultured meat products will rely on a disconnect from animal sources. Research into animal-free scaffolds has emerged as a potential source for consistent, chemically defined and low-cost materials.

Synthetic or natural animal-free polymers such as cellulose (Huber et al.,2012; Hickey et al., 2018), chitin/chitosan (Jayakumar et al.,2011), alginate (Lee et al.,2012), recombinant silk (Widhe et al.,2010), PLA (Serra et al.,2013), and PCL (Li et al.,2017) provide low cost, consistent and tunable scaffolds. In this concise review, we have chosen to focus on chitin/chitosan, cellulose (bacterial and plant), and recombinant collagen and their use in tissue engineering and potential applications in cellular agriculture. The biomaterials chosen here meet the criteria for cellular agriculture applications, such as animal-free, abundant, biocompatible, versatile, provide nutritional benefits, and are already part of commonly consumed products. However, we recognize that many other biomaterials and scaffolding approaches do exist and, as above, we refer the reader to other topical reviews for a deeper examination of those strategies (Carletti et al.,2011; O'Brien,2011; Derakhshanfar et al.,2018).

As tissue engineering and regenerative medicine continues to expand with promising results, the potential for novel food applications has arisen due to the similarity in techniques and approaches. Although meat/tissue has proven to be difficult to replicate *in vitro* due to its complex composition (muscle, nerve, water, minerals, growth factors, hormones and Extracellular matrix proteins) (Listrat et al.,2016.), the native structure of foods such as mushroom (Jo-Feeney et al.,2014) and jackfruit (John et al.,1992) have the potential to contribute the expected palatable properties of meat. In addition to rheological properties, these

foods contribute nutritional benefits, such as insoluble fiber (McDougall et al.,1995; Cheung et al.,2013),

2.3 Decellularized plant tissue and bacterial cellulose

As the most abundant polymer in nature (1.5 $x10^{12}$ tons of total biomass) and the main component of plants, cellulose, a 1-4β D-glucose polymer has shown great potential as scaffolding material due its low cost, versatility and overall biocompatibility (O'Sullivan,1997; Klemm et al.,2005). Cellulose hydrogels (Isobe et al.,2018), composites (Johns et al.,2018; Huber et al.,2012), functionalized plant cellulose (Fontana et al.,2017; Modulevsky et al.,2014) and decellularized plant tissue (Modulevsky et al.,2014; Gershlak et al.,2017.) have been developed. This in turn shows the versatility of cellulose. Moreover, cellulose and its derivatives (e.g. Methylcellulose and 6-carboxycellulose) have been functionalized and blended with other materials to improve its mechanical, biological and chemical properties (Novotna et al.,2013; Thirumala et al.,2013; Fontana et al.,2017). Cellulose as a biomaterial has been extensively reviewed previously (Hickey & Pelling,2019; Kalia et al.,2011). This section will emphasize on decellularized plant tissue and bacterial cellulose.

It was shown that decellularized apple hypanthium (Fig.2) can be used as a substrate for 3D cell culture. HeLa cells, 3T3 fibroblast, and C2C12 murine myoblast proliferated throughout the 3D matrix (Modulevsky et al.,2014). In order to decellularized the tissue, a surfactant, in this case SDS, was used to create pores in the plant cell membrane, leading to the release of cellular components. (Brown & Audet,2008; Modulevsky et al.,2014). The mechanical properties of these scaffolds which are known to influence cell behavior, have also been altered through functionalization and crosslinking (Modulevsky et al.,2014) and further shown to resemble

skeletal (Modulevsky et al.,2014; Hickey et al.,2018) and cardiac muscle tissue (Gershlak et al.,2017). However, cellulose based scaffolds do lack a wide array of mammalian biochemical cues; thus, biofunctionalization or coating with functional surface proteins may be required for specific cell lines, especially in a serum-free environment (Hayman et al.,1985; Courtenay et al., 2017; Johns et al.,2018). It was noted, however, that the viability of C2C12 cells was not affected by the bare cellulose scaffold when compared to collagen and gelatin coating (Hickey et al.,2018). Nonetheless, seeding efficiency has been shown to be greatly improved with surface coating and functionalization (Modulevsky et al.,2014; Hickey et al.,2018; Fontana et al.,2017).

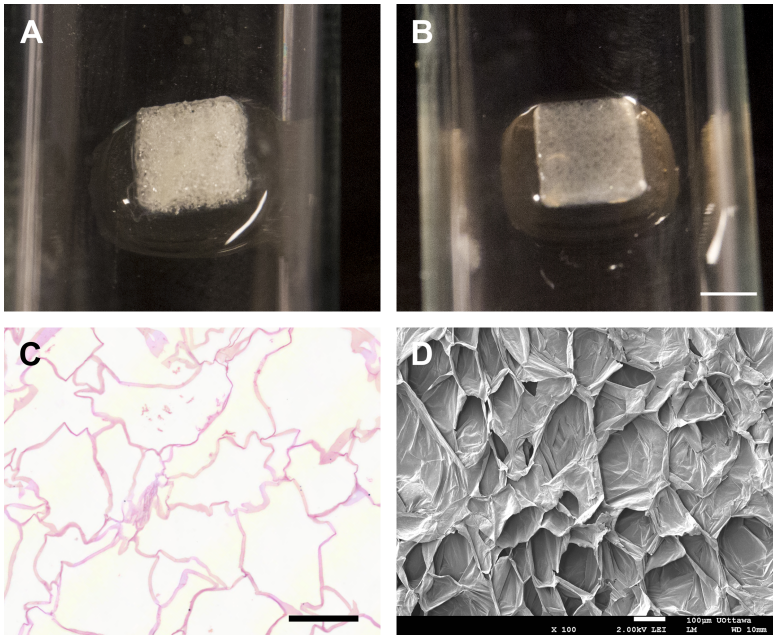

Figure 2. Preparation of cellulose scaffold. Macroscopic appearance of a freshly cut apple hypathium tissue (A) and the translucent scaffold biomaterial post decellularization and absent of all native apple cells or cell debris (B). H&E staining of cross sectioned decellularized cellulose scaffold(C). The cell walls thickness and the absence of native apple cells following decellularization are shown. The 3D acellular highly porous cellulose scaffold architecture clearly revealed by SEM (D). Scale bar: A-B = 2mm, C-D = 100µm. Reprinted from Modulevsky et al., 2016

An advantage of decellularized plant tissue is the wide array of natural topographies that can be used to study cellular behavior and potentially mimic *in vivo* conditions without long and costly processing (Modulevsky et al.,2014; Fontana et al.,2017; Modulesvky et al.,2016). By utilizing the topographical cues present in the vascularization of stems and leaves, guided cell alignment was noted (Fontana et al.,2017). In this case, cell alignment was likely due to the confinement of cells within the vascularization channels. Alignment in cell culture is a highly desirable characteristic, especially in musculoskeletal research. By inducing alignment, researchers try to mimic the physiological state of myoblast and myotubes (Zhao et al.,2009; Bettadapur et al.,2016). In comparison to synthetic microchannel development techniques, such as 3D printing (Tijore et al.,2018), softlitography (Glawe et al.,2005) and photolithography (Lee et al.,2006), the decellularized vascular bundle of plants depict a low cost, highly accessible and easy to use material.

The vascularization of a decellularized spinach leaf was postulated as a way to overcome the 100-200μm diffusion limitations of 3D scaffolds (Gershlak et al.,2017). Yet, it's still unclear if cells growing outside of the vascularization tracts can benefit from the circulation of nutrients. However, as of now, the need for vascularization in decellularized plant is not a requirement. Cells are able to grow throughout the porous decellularized apple hypanthium without developing a necrotic center (Hickey et al.,2018; Modulevsky et al.,2014). Yet, a necrotic center is likely to develop in very large scaffolds which may possibly be required in food applications. The porosity of the apple also supported angiogenesis when implanted *in vivo* (Modulesvky et al.,2016). This observation will not necessarily extrapolate to other decellularized plant scaffolds due to their underlying native tissue geometry which makes plant species/tissue choice important

(Gershlak et al.,2017). Although decellularization is depicted as a simple biomaterial development method, it lacks the customizability of "bottom-up" approaches, such as that of cellulose nanofibril scaffolds and cellulose composites with varying porosity, biological, and mechanical characteristics. (Courtenay et al.,2018; Khan et al.,2016; Courtenay et al.,2017).

Cellulose is not only found in the plant kingdom, but is also produced by certain strains of bacteria, such as *Acetobacter spp*. (Jonas and Farah et al.,1998; Schramm,& Hestrin,1954). Although plant and bacterial cellulose share an identical α-cellulose structure, bacterial cellulose possess greater crystallinity, degree of polymerization and water holding capacity. (Esa et al., 2014; Moniri et al.,2017). These attributes have been invaluable in a wide array of applications, including medical (Fürsatz et al.,2018; Petersen and Gatenholm,2011), cosmetics (Pacheco et al., 2017) and food (Shi et al.,2014). The food applications include cultural desserts such as *Nata de coco*; and functional properties such as gelling agent, stabilizer and thickener (Shi et al.,2014). Moreover, bacterial cellulose has been used to incur juiciness and chewiness in emulsified meats (Lin & Lin,2004).

An advantage of bacterial cellulose is the wide array of carbohydrate-rich by-products that have been used for its production (e.g. Wheat thin stillage, waste fiber sludge, pullulan fermentation waste water, beer culture broth) (Revin et al.,2018; Cavka et al.,2013; Zhao et al.,2018; Ha et al.,2008) and the wide array of chemical modifications that can be introduced to further improve biocompatibility and mechanical properties (Kurniawan et al.,2012; Lopes et al.,2014; Ostadhossein et al.,2015; Saska et al.,2012). The biocompatibility, low cost and nutritional attributes make this material a potential candidate for *in-vitro* meat production.

2.4 Chitin and chitosan

As the second most abundant polymer in nature, chitin is found in the exoskeleton of arthropods (e.g. crab and shrimp) and fungi (Percot et al.,2003; Deguchi et al.,2015). In this review, fungal chitin is of interest due to the animal-free nature. Although the chitin sources referenced throughout this section are either not disclosed or declared to be animal derived (likely due to abundance) there is currently no reason to believe that it can't be replaced with fungi chitin. (Bierhalz et al.,2016).

Through alkaline deacetylation, chitin is turned into chitosan. (Rodriguez-Vasquez et al.,2015). The degree of deacetylation of chitin leads to physical, chemical and biological changes, such as interaction with cells directly or with glycoproteins and proteoglycans through ionic complexes. In addition to the interaction with glycoproteins and proteoglycans, chitosan's resemblance to glycosaminoglycans has the potential of regulating and modulating bioactive factors (Madihally et al.,1999; Chicatun et al.,2013; Yang et al.,2011). Moreover, it was also shown that chitosan can be blended with other polymers to further improve the mechanical properties with the aim of resembling native mammalian tissue. (Zakhem et al.,2012; Hajiabbas et al.,2015)

Chitosan has shown to be a desirable material in tissue engineering due to its biocompatibility (Croisier & Jerome,2013; Tamura et al.,2011), antibacterial properties (Benhabiles et al.,2012), and accelerated healing rate on skin wounds (Tchemtchoua et al.,2011). It has been shown that chitosan and chitosan oligosacharaides provide a synergistic bactericidal effect on planktonic bacteria and biofilms when combined with antibiotics such cloxacilin

(Breser et al.,2018; Decker et al.,2005) and sulfamethoxazote (Tin et al.,2009). Chitin and chitosan alone portrayed a bacteriostatic effect on gram negative bacteria, *Escherichia coli*, *Vibrio cholerae*, *Shigella dysenteriae* and *Bacteriodes fragilis* (Benhabiles et al.,2012). The synergistic effect with antibiotics and overall bacteriostatic properties are a desirable attribute for applications in cellular agriculture; as antibiotic use decreases social acceptability (Karavolias et al.,2018), has the potential to cause long term health problems, and increase the development of antimicrobial resistance (Thanner et al.,2016). However, to our knowledge, the antimicrobial potential of these compounds in long term cell mammalian cell culture has yet to be tested or verified.

Often materials for medical applications are segregated into permanent or temporary. The degradation of chitosan by lysozymes found in the body can be controlled through the degree of deacetylation (Tomihata & Ikada,1997; Muzzarelli,1997; Rodriguez-vazquez et al.,2015). Degradability is not necessarily an undesirable characteristic, as degradation rates can be controlled; and the by-products have the potential to provide neuroprotective (Pangestuti & Kim,2010) and anti-inflammatory properties (Azuma et al.,2015; Kim,2018). Furthermore, biodegradable hydrogels with controlled degradation rates are expected to be a temporary matrix for adherent cells. The objective is to match matrix deposition by cells with the degradation rate of the scaffold (Bitar & Zakhem,2014; Ren et al.,2018; Berthod et al.,2006). This not only applies to medical applications, but also to potential applications for *in vitro* meat production. A temporary matrix can allow for cellular ECM deposition with the end of goal of obtaining a scaffold with characteristics similar to that of native tissue.

The structure of certain types of mushroom provide a mouthfeel and umami flavour which resembles that of meat, often perceived as a vegan alternative (Jo-Feeney et al.,2014). Moreover, the cell wall components of mushroom contain chitin, 1-3-alpha-D-gucans and mannans, which confer nutritional benefits, such as dietary fiber (Cheung et al.,2013; Fernandes et al.,2015). The antimicrobial and nutritional properties, alongside its animal-free nature and abundancy, make chitin/chitosan-based scaffolds a potential substrate for cellular agriculture applications.

2.5 Recombinant Collagen

The well-known and extensively studied extracellular matrix protein, collagen, is often derived from bovine (Chan et al.,2016), porcine (Smith et al.,2000), and murine (Isobe et al.,2012) sources. Collagen type I, a fibrillar heterotrimeric protein composed of two α1(I) chains and one α2(I) chain, has been produced in numerous forms, including porous hydrogels, composites and a number of substrates with topographical cues and varying mechanical properties (Rich & Crick,1955; Rich & Crick,1961; Stein et al.,2009; Wu et al., 2018; Antoine et al.,2014; Wang et al.,2016; Vernon et al., 2005). Yet, variability (e.g. age and physiological state of donor), potential pathogen transmission, and contaminants including cytokines and growth factors have been a concern for this animal derived product (Keefe et al.,1992; Banfield,1956; Kohn & Rollerson,1960; Shoseyov et al.,2013; Badylak & Gilbert,2008).

In order to overcome these issues, genetic engineering has led to the development of transgenic organisms capable of synthesizing the desired amino acid repeats. Through the insertion of COL1A1 and COL1A2 genes, the repeating amino acid sequence, Gly-X-Y, can be

translated and transcribed. In this case, the X and Y often correspond to proline and hydroxyproline, respectively (Shoseyov et al.,2014; An et al.,2014; Stein et al.,2009). The repeating amino acid sequence leads to the triple helical conformation and specific thermal stability of collagen (Bella,1995; Rich & Crick,1955; An et al.,2014).

The production of procollagen through recombinant methods has been observed in bacteria (An et al.,2014), mammalian cells (Geddis & Prockop,1993), insect cell culture (Myllyharju et al.,1997), yeast (Olsen et al.,2001), and plants (Stein et al.,2009; Xu et al.,2011). The introduction of COL1A1 and COL1A2 genes encode for the amino acid sequence. Yet, the post translational modifications are fundamental in the production of collagen with similar mechanical and biochemical properties to that of native collagen found *in vivo*. Procollagen for *in vivo* and *in vitro* use has been produced in a tobacco plant capable of expressing COL1A1 and COL1A2 proteins, alongside post translational modification proteins localized in the vacuole: Prolyl 4-hydrolysase (PH-4) alpha, PH-4beta and Lysine hydroxylase (LH1-3). P4H acts on the proline residues leading to directionality and thermal stability, whereas LH1-3 plays a role in collagen fibril formation and stabilization. (Pihlajaniemi et al.,1991; Shoseyov et al.,2013; Ruotsalainen et al.,2006).

Although the production of recombinant collagen has proven to be difficult in part due to the need for post translational modification machinery natively found in mammalian cells, (An et al.,2014; Werkmeister & Ramshaw,2012) a fibrillar protein with a similar melting point and overall chemical structure to collagen has been observed and isolated in microbes, such as *Streptococcus pyogenes*. The protein's properties have been attributed to the presence of

collagen like proteins*, scl 1* and *scl 2* (Yu et al.,2014; Lukomski et al.,2000; Lukomski et al.,2001). The production of this collagen like protein lacks the different biochemical cues found *in vivo* due to the lack of post translational modification; yet, the "blank slate" and gene customizability can be an attractive property for customization (Peng et al.,2010; Yu et al.,2014; An et al.,2014).

In order to fulfill the demand for recombinant collagen, yield optimization has been a major target. Standardized comparison has been difficult to accomplish due to the properties of the final product, influenced by the level and presence of post translational modification proteins. Collagen production in plants, more specifically, tobacco, has been considered to be the most promising. Production of up to 200mg of recombinant human type I procollagen per kg of fresh leaves (20g/L reported by Werkmeister & Ramshaw,2012) has been achieved through the vacuole targeted enzymes and genes (Stein et al.,2009). The biocompatibility of procollagen from transgenic tobacco plans was shown *in vitro* and *in vivo* (Willard et al.,2013; Shilo et al., 2013). *In vitro*, an increase in cell proliferation of human epidermal keratinocytes was noted when compared to bovine collagen (Willard et al.,2013). Bacteria collagen (Peng et al.,2010) and recombinant collagen produced in yeast (Liu et al.,2007) have also shown *in vivo* and *in vitro* biocompatibility.

Collagen type I is not the only ECM protein that has been produced recombinantly. Other types of collagen (e.g. Type II & III) (Ruottinen et al.,2008; Myllyharju et al.,2000; Pakkanen et al.,2003), tropoelastin (Martin et a.,1995), and fibronectin (Staunton et al.,2009) fragments have also been produced recombinantly.

Collagen production in transgenic tobacco plants, yeast and/or bacteria has the potential to alleviate issues encountered through the use of animal derived biomaterials. Subsequently, the animal-free nature and similarity to native collagen can be a major step forward in the development of *in-vitro* meat, especially if producers wish to replicate the characteristics of native tissue.

2.6 Conclusion

Here we present three biomaterials that have shown promising results in tissue engineering and that can be translated to cellular agriculture applications in large part due to their abundance, animal-free nature and current food applications. Moreover, the wide array of natural topographies and dietary fibre found in plants, alongside the antimicrobial and rheological properties of chitin/chitosan further extend their potential in cell culture and cellular agriculture. However, these materials do lack the biochemical cues found in native mammalian extracellular matrices, leading to a need for functionalization. This need further increases the complexity of the process, reducing the scalability potential. On the other hand, the emergence of recombinant collagen extracted from plants has important advantages as a scaffold in its own right or if used to functionalize the surfaces of the materials above. Furthermore, these materials have been modified, either as microspheres or bulk, to possess the porosity necessary for diffusion of nutrients through dynamic or static bioreactors (Varley et al.,2017; Huang et al.,2018; Wu et al., 2011; Garcia Cruz et al.,2012; Oh et al.,2009; Specht et al.,2018). In order to scale an animal-free product with similarities to that of native animal tissue, the need for foetal bovine serum, cost-effective engineering processes, antibiotic dependence, scaffold development, and cell line(s) (immortalized vs primary and cell co-culture) needs to be addressed (Lynch and

Pierrehumbert,2019; Stephens et al.,2018; Specht et al.,2018). It's currently believed that scaffolding will play a crucial role in the scalability of cultured meat. Therefore, the aim of this review was to summarize three animal-free materials with properties (e.g. rheological, nutritional and biological) that will likely be desirable in scaffolding for cultured meat applications. Yet, we wish to remind the reader that scaffolding is only one component of a much larger endeavor; and the scalability potential of the methods presented here is still unknown, and for some unlikely. Readers are encouraged to refer to Stephens et al. (2018) and Specht et al. (2018) for an overview on cellular agriculture and the major challenges.

2.7 Conflict of Interest

S.C. and A.P. are inventors on patent applications concerning the use of plant-derived cellulose for tissue engineering applications filed by the University of Ottawa.

2.8 Funding

This work was supported by the New Harvest grant number 0005. New Harvest is a 501c3 non-profit research institute based in the US. S.C was also supported by the Queen Elizabeth II graduate scholarships in science and technology (QEII - GSST). We also acknowledge generous support from the Natural Sciences and Engineering Research Council (NSERC) Discovery Grant and Canada foundation for Innovation grant.

CHAPTER 3

Decellularized Celery (*Apium graveolens)* Scaffold for Cell Culture

Motivation and objectives

As mentioned in the previous chapter, animal derived scaffolds portray a range of issues, including variability, environmental concerns, and ethical concerns. The motivation behind this chapter comes from the number of studies on decellularized plant tissue as an animal free substrate for cell culture and *in vivo* applications (Modulevsky et al.,2014; Hickey et al.,2018; Gershlak et al.,2017; Fontana et al.,2017; Modulesvky et al.,2016). The plant decellularization protocol first developed by Modulevsky et al., opened the door to a number of other plant tissues that natively posses a range of structures and physical properties ripe for *in vitro* applications.

In order to recreate the aligned morphology of skeletal muscle cells in native muscle tissue (Listrat et al., 2016; Frontera & Ochala, 2014), substrates composed of fibers, channels, and grooves in the micron and submicron range have been successful at recreating alignment (Cooper et al., 2010; Hume et al., 2012; Huang et al., 2010; Wang et al., 2010; Cha et al., 2017). Based on the perceived fibrous structure of celery (*Apium graveolens)*, I sought to determine if it can be repurposed as a simple, abundant, and animal free substrate for optimal skeletal muscle cell culture.

In this chapter, I sought to systemically determine the proliferation and differentiation of C2C12 as an indicator of positive cell-substrate interaction. Concomitantly with proliferation, SEM and confocal microscopy will be used to analyze the phenotype of the cells. A stretched or

elongated phenotype common to adherent cells is expected in a manner similar to that observed on decellularized apple hypanthium scaffolds (Modulevsky et al.,2014).

I next sought to determine the Young's modulus of the decellularized scaffolds, a mechanical property known to influence cell behavior (Wells, 2008; Engler et al., 2004; Gilbert et al., 2010). I also wished to determine if cells cultured on the scaffolds influence the mechanical properties of the biomaterial. The mechanical properties of this substrate are not only invaluable for *in vitro* applications but also for consumer perception. I, therefore, presume that the values presented here will be applicable for future work.

In this chapter, my goal is to provide evidence that celery scaffolds can be decellularized, support cell proliferation and differentiation, and to provide the reader with an overview on basic mechanical properties of the parenchyma and vascular bundle. In Chapter 4, I will examine the myogenic potential of C2C12 cells cultured on the vascular bundle of decellularized celery scaffolds in greater detail. I will also discuss the topographical influence of cells cultured on the vascular bundle.

3.1 Material and Methods

3.1.1 Scaffold Preparation

The decellularization protocol was performed as described previously (Hickey et al. 2018). Briefly, celery (*Apium graveolens)* stalk was cut parallel (XY) and perpendicular (CS) to the longitudinal axis using a mandolin slicer. A 6mm biopsy punch was then used to consistently obtain round scaffolds. The samples were then transferred to a 15mL Falcon tube containing 0.1% SDS at a ratio of one sample per mL of solution. Samples were then agitated in a shaker at

120RPM for 72 hours. Following treatment with SDS, the samples were washed three times with deionized water. After the final wash, 100mM solution of $CaCl_2$ (1mL per scaffold) was added and samples were incubated at room temperature for 24 hours. After 24 hours, the samples were washed with distilled water three times. On the final wash, the water was removed and 70% ethanol was added for 30min. At this point, the samples were brought into a class II biosafety cabinet and washed three times with sterile PBS. The samples were placed on PDMS coated 12-well plates with 2mL of growth media (refer to next section). The samples were incubated overnight at 37°C and 5% CO_2. Prior to cell seeding, the media was removed (Ch.4 - Fig.1A).

3.1.2 Cell culture

C2C12 murine myoblast were plated on tissue culture plates and maintained at 37°C with 5% CO_2. Cells were cultured in growth media consisting of high glucose DMEM with L-glutamine and sodium pyruvate (Hyclone) supplemented with 10% FBS (Wisent & Hyclone) and 1% penicilin (10000U/mL) & streptomycin (10000ug/mL) (Hyclone). Once the cells reached 70-80% confluency, they were trypsinized (Hyclone) (0.05%), resuspended in growth media, and spun down in the centrifuge at 1000RPM (97g) for 3 min. Following centrifugation, the pellet was resuspended in growth media to acquire 1.7 x 10^6 cells/mL. Cells were counted using a hemocytometer and Trypan Blue to determine viability. 30 μL of cells suspended in media was placed on the scaffolds and incubated for 4.5 hours. Following the incubation, 2mL of growth media was added and samples were incubated for 10 days with media change every 48 hours until day 7, followed by daily media change until day 10. For differentiation studies, cells were placed in differentiation media for 5 days. The differentiation media was composed of high glucose DMEM, 2% horse serum (Gibco) and 1% Penicillin and Streptomycin.

3.1.3 Fluorescent staining.

To first confirm decellularization of the *A. graveolens* scaffolds, native and decellularized samples without mammalian cells were washed three times with phospahte buffered saline (PBS) and placed in a 1:500 hoescht 33342(Invitrogen) solution made up in PBS for 30min at 37°C.

Following 10 days in growth media, decellularized scaffolds with cells were transferred to a microcentrifuge tube using a metal paddle, and washed three times with PBS. The samples were fixed with 3.5% paraformaldahyde in 2% aqueous sucrose solution for 10min and washed three times with PBS. Following the final PBS wash, room temperature triton-X100 was added to permeabilize the cells. The scaffolds were once again washed three times with PBS following tritron-X100 permeabilization. For F-actin imaging, scaffolds were stained using Alexa Fluor 488 phalloidin (Invitrogen) in PBS at a 1:200 concentration and incubated for 20min in the dark. Nuclei was stained with DAPI(Sigma) at a 1:500 concentration and incubated at 4°C for 10min. The samples were washed 3 times with PBS prior to imaging.

3.1.4 Confocal microscopy

Scaffolds were placed on coverslips with mounting medium (Vectashield H-1000) prior to imaging. The samples were imaged with a Nikon TiE A1-R high speed resonant scanner confocal microscope with a 10X and 40x lens. Image processing was done on Image-J FIJI. The images presented throughout this chapter are Maximun Intensity Projections(MIP) of approximately 249±39 μm (N=24) deep confocal volumes composed of images taken every 5μm. Brightness of fluorophore signal was enhanced to improve contrast of structures.

3.1.5 Scanning Electron Microscopy

Sample preparation was performed as described previously (Murtey and Ramasamy, 2016, p.173-175) Briefly, the sample was washed three times with PBS and placed in a solution containing 3.5% paraformaldahyde (in 2% sucrose solution) and 1.5% glutaraldehyde (Final concentration) overnight. Samples with cells were postfixed with 1% Osmium tetroxide in water (Sigma) for 2 hours. Following fixation, the sample was washed twice with distilled water and dehydrated through a sequential ethanol gradient (30,50,75,95 & 99%). The sample was dried using the Samdri-PVT-3D Critical point dryer in 99% ethanol. The dried sample was gold sputtered with a 5nm layer (LEICA EM ACE 200). The samples were image with a JEOL JSM-7500F FESEM at 2.0 KV.

3.1.6 Cell proliferation on decellularized *A. graveolens* scaffolds.

In order to determine the number of cells per scaffold, three images from the top and three from the bottom were used to acquire a representative number of nuclei per scaffold. The 249±39 μm (N=24) MIP images with an approximate area of 1.61mm^2 were thresholded using the Adaptive Threshold on ImageJ- FIJI to reduce noise. After thresholding, the total nuclei area was divided by the average nuclei size (84μm^2) (N=15). The average of the six images was then extrapolated to the surface area of a cylinder. All image processing and area quantification was done on FIJI Image-J.

3.1.7 Bulk compression for analysis of Young's modulus

The round, 6mm wide 2mm thick samples were stored in PBS until ready for use. Prior to compression, samples were placed in a humidifying chamber inside an incubator at 37°C for 1 hour. Mineral oil was used to coat the samples prior to bulk compression. Samples were

compressed using an in-house device at a strain rate of 50μm/s until 150g of force was reached. The slope of the first 10% strain from a stress-strain graph was used to calculate the Young's modulus.

3.1.8 Determination of vascular bundle stiffness through Atomic force microscopy (AFM)

JPK Nanowizard II AFM was used to determine the Young's modulus of the decellularized vascular bundle derived from celery stalks, (*Apium graveolens*). Three triangular PRP-TP tips (Nanoworld) with a spring constant of 41±16pN/nm (N=3) were used to produce 10 – 15 force indentation curves for 37 randomly chosen areas at a rate of 1Hz over 7 vascular bundles. The triangular tips were calibrated as previously described (Hutter & Bechhoefer, 1993). JPK software was used to fit the first 200nm (From contact point) using a Hertzian model for a conical indenter with a 35°opening angle and a Poisson ratio of 0.5. The equation (Eq.1) used to relate indentation to Young's modulus(E) is provided below, where F corresponds to the indenting force, ν to the Poisson's ratio, δ to sample indentation distance, and α to the semi-opening angle of the cone.

$$F = \frac{E}{1-\upsilon^2}\frac{2\tan(\alpha)}{\pi}\delta^2 \qquad \text{Eq. 1}$$

3.1.9 Statistical analysis

A one-way ANOVA followed by a Tukey post hoc analysis was performed to test for significance among the Young's modulus values within scaffold type. A student's t-test assuming equal variance was used to compare number of cells per scaffold between adjacent

incubation periods. All statistical tests were done on R. All values are presented as mean ± S.D unless otherwise specified. Statistical significance refers to $P<0.05$.

3.2 Results

3.2.1 Viability of *Apium graveolens* tissue post-decellularization and mammalian cell proliferation

Following the decellularization step, Hoescht 33342 was used to test for the presence of nuclei. The decellularization of the scaffold is clearly depicted by the loss in colour(Fig.1A & B), lack of nuclei in the ground tissue(Fig.1C & D), and lack of nuclei in the companion cells of the phloem (Fig.1E & F). In addition to the nuclei loss, decellularized tissue portrayed a collapsed morphology when compared to native tissue (Fig.1C & D). No structural changes can be observed in the vascular bundle post decellularization (Fig.1E & F).

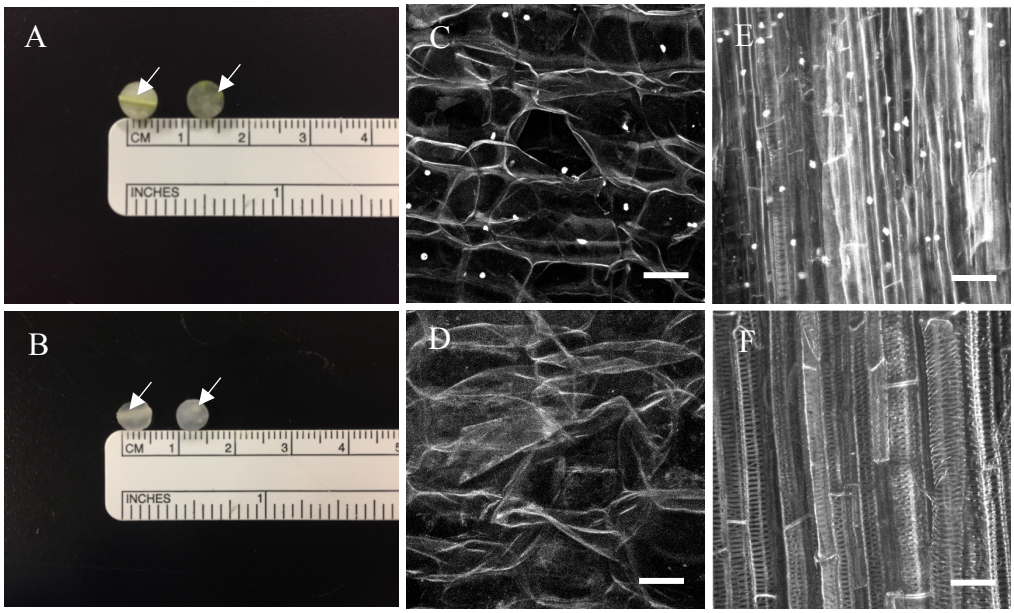

Figure 1. Macroscopic depiction of native and decellularized celery (*A. graveolens*) scaffold. (A) Native and (B) decellularized XY(Left) and CS(Right) celery scaffolds. Arrows =Vascular bundle. Live Hoescht 33342 staining of (C) native and (D) decellularized ground tissue. Hoescht staining of (E) native and (F) decellularized vascular bundle. Nuclei can be observed

inside the plant cells of the ground tissue and vascular bundle (C, D, E & F) scale bar = 50μm.

After confirming decellularization of the scaffold, we sought to determine the biocompatibility of the decellularized *Apium graveolens* scaffolds by measuring proliferation of C2C12 myoblast over a 10-day period. Cell proliferation was quantified at Day 1, 5, and 10 on based on the number of visible nuclei obtained from a 249±39 μm (N=24) MIP images. The number of cells at day 1 was determined to be 402 ± 222 cells/mm^2 , which accounts mostly for the number of cells that adhered to the scaffolds. By day 5, 786 ± 323 cells/mm^2 were present on the scaffold; yet not a statistically significant increase from day 1(P = 0.1, N =4). Lastly, by day 10, 2108 ± 541 cells/mm^2 were noted, leading to a statistically significant increase from day 5 (P = 0.006, N = 4).

Mammalian cells were noted crossing over the plant cell walls, growing on the cell wall junctions, and forming multicell spheroids inside the hollow plant cells (Fig.2B – D). The formation of multicell spheroids is presented here; yet, it was not pursued further as biocompatibility was assessed based on cell numbers, and cells predominantly portrayed a physiologically relevant phenotype. Therefore, pursuing such occurrence was considered to be unnecessary (Fig.2B).

The interior of the scaffolds portrayed minimal growth; hence, it was not included in the proliferation calculation. As shown on Figure 3, “streaks” of cells arising from the surface of the scaffold and travelling towards the interior were observed. The images presented here correspond to the internal area were cells were not confined to the surface. Aside from the

spheroid formation inside the plant cell skeleton, cells portrayed a stretched phenotype similar to that of adhered cells cultured on Petri dishes.

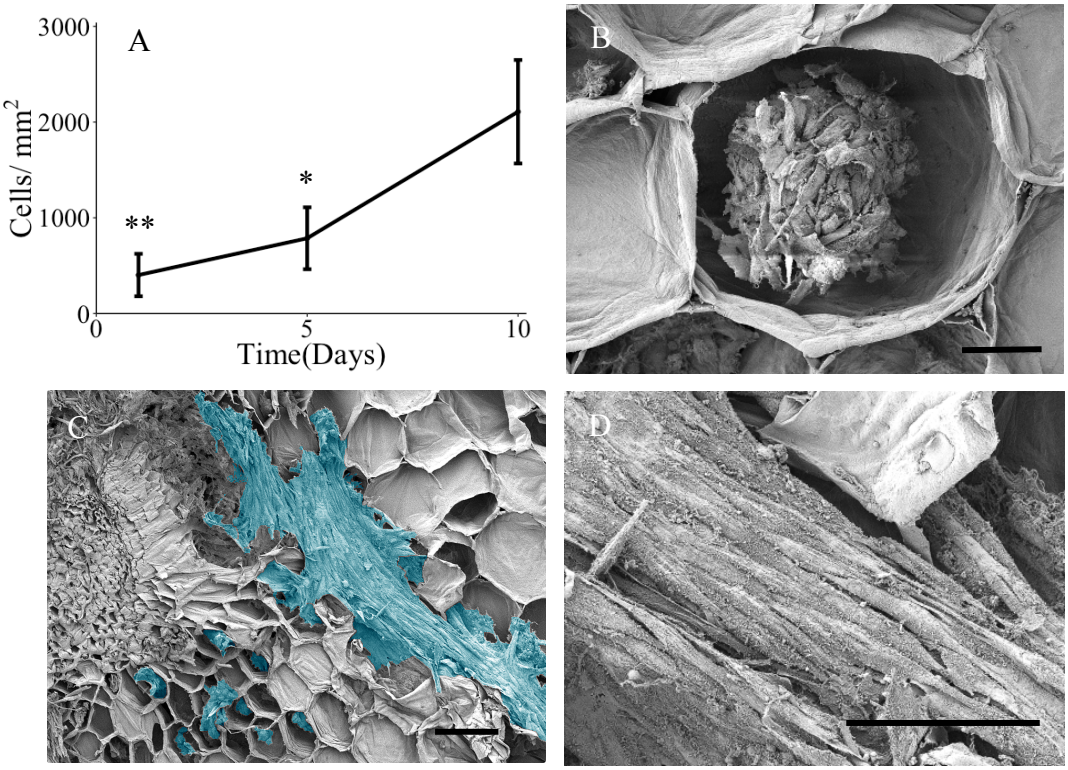

Figure 2. Proliferation and visualization of C2C12 murine myoblast on the surface of decellularized celery scaffold. (A) Proliferation over a 10-day incubation period. Data displayed as Mean ± SD (N=4). Four independent samples were used for each incubation period. * denotes $P<0.05$. ** denotes $P<0.01$. No statistical significance was observed between D5 and D1. SEM images of C2C12 myoblast on decellularized scaffold. Cells can be observed forming (B) multicell spheroids inside the decellularized plant cell wall, (C&D) and crossing over the hollow plant cells and cell walls. The formation of spheroids is shown here, but no follow-up experiments were performed to determine the occurrence. (C) Scale bar = 100µm. (B-D) Scale bar = 50µm.

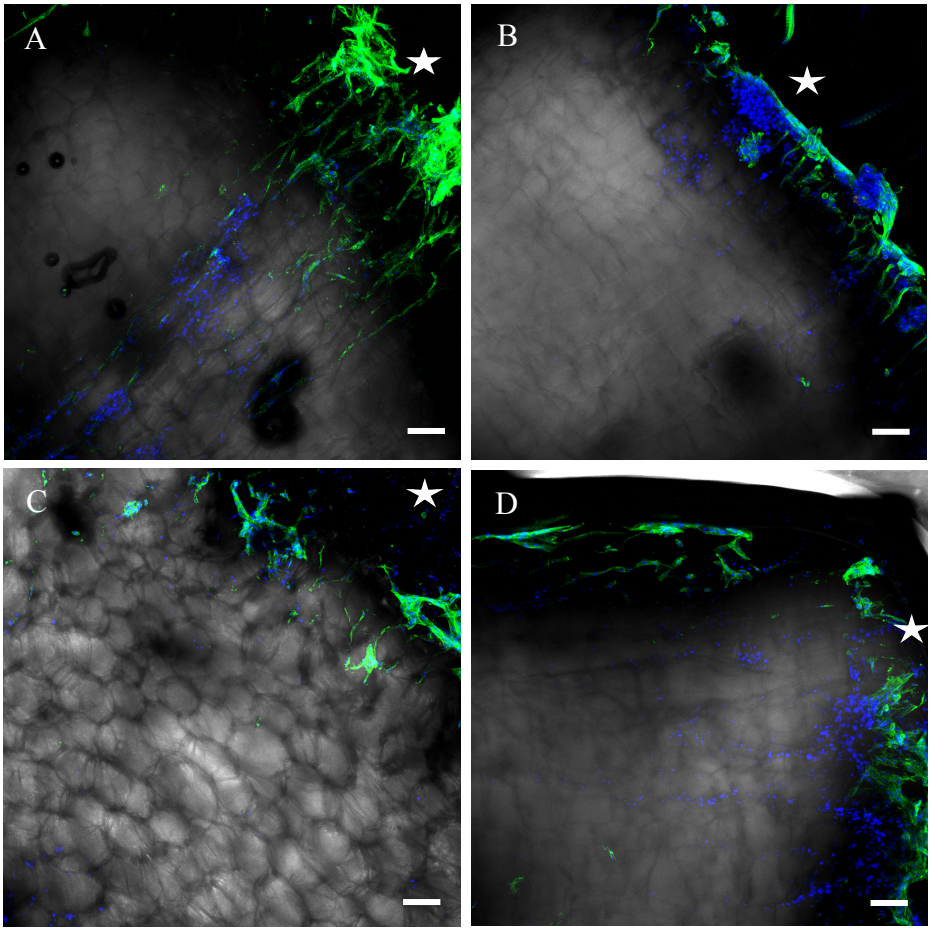

Figure 3. Migration of C2C12 muscle cells from the (Star) surface of the decellularized celery scaffold. (A-D)The images depicted here are only of the area(s) where cells were not bound to the surface. Actin filaments and nuclei were labelled with phalloidin 488(green) and DAPI (blue), respectively. Scale bar = 100 μm. N = 4.

3.2.2 Young's modulus of *Apium graveolens* parenchyma

Taking into consideration the effect of stiffness on cellular behavior, we sought to calculate the Young's modulus of the decellularized celery scaffold by compressing the round ,6mm wide scaffolds uniaxially to 150g of force. The slope of the first 10% strain was used to calculate the Young's modulus of the ground tissue/parenchyma. Subsequently, scaffolds with cells were also compressed to determine if the presence of myoblast (Undifferentiated) or

myotubes (Differentiated) influence the Young's modulus of the substrate. A significant decrease in Young's modulus following decellularization was only observed in the XY scaffolds ($P = 0.0005$, $N=5$. Fig. 4A). Lastly, based on our results, the presence of myoblast or myotubes didn't significantly influence the Young's modulus of the decellularized scaffold ($P>0.1$, $N = 5$. Fig.4B).

The bulk compression was performed on the two-scaffold types: XY and CS ground tissue samples. Depiction of myotube formation, which is based on MYHC positive structures with two or more nuclei after 5 days in differentiation media is presented in Chapter 4 - Fig. 4.

3.2.3 Young's modulus of *Apium graveolens* vascular bundle

In order to determine the Young's modulus of the vascular bundle, AFM was used to indent with 1nN of force using a cone-shaped cantilever. Due to the opacity of the vascular bundle and the experimental setup (Fig. 5A), the exact location of the AFM probe once it passed the periphery couldn't be accurately determined. Therefore, the data is presented in the form of a histogram, which depicts a range of values acquired from 37 randomly chosen areas (Fig. 5B).

However, despite this uncertainty, I suggest to assign values in the range of 5-20KPa, which constitute 66% of the tallest peak, to the phloem as these were acquired predominantly on the periphery. These are "representative" of the phloem's mechanical properties when compared to the ylem (Lee, 1981; Hepworth and Vincent, 1998).

To examine if damage was incurred by the AFM probe, the Young's modulus values for the last three curves of 4 randomly selected areas (0.46 ± 0.36MPa) were compared with the

initial three values of the same areas (0.51 ± 0.51MPa), leading to us to conclude that there was not significant difference (N=4. P = 0.71);hence, no damage to vascular bundle was incurred. The percent difference, which is the variation in young's modulus values with respect to the mean value of a specific area, was calculated to be 11 ± 1.4% for a total of 10 areas (mean ± SE. N=100).

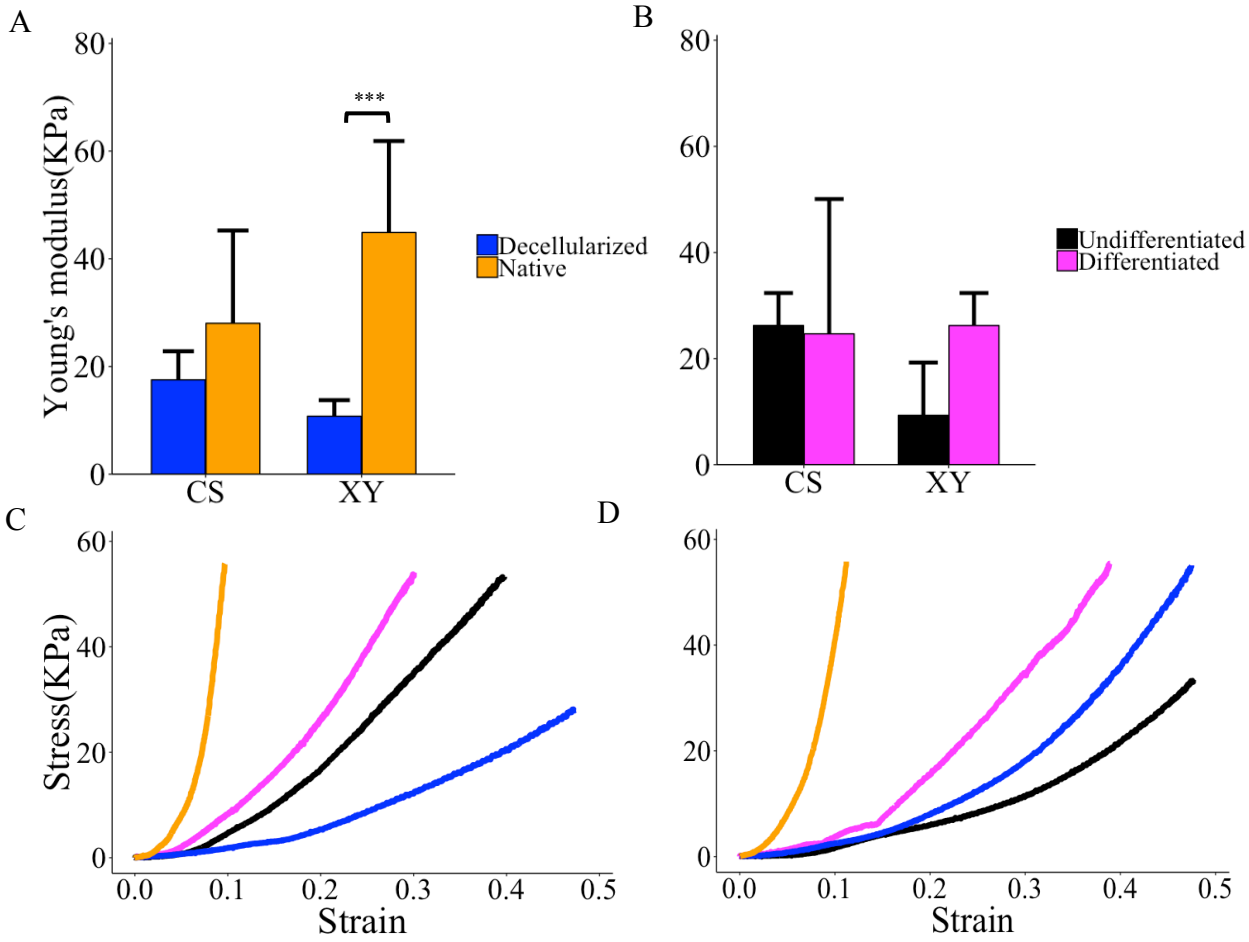

Figure 4. Young's modulus of decellularized, native, undifferentiated and differentiated *A. graveolens* scaffolds (A) Young's modulus of decellularized and native *A. graveolens* ground tissue (*** indicates P<0.001). (B) Youngs modulus of scaffolds with myoblasts (Undifferentiated) and myotubes (Differentiated). Data displayed as Mean ± SD. N=5 for all treatments. Representative Stress vs Strain sample graphs for (C) CS and (D) XY decellularized, native, undifferentiated, and differentiated celery scaffolds.

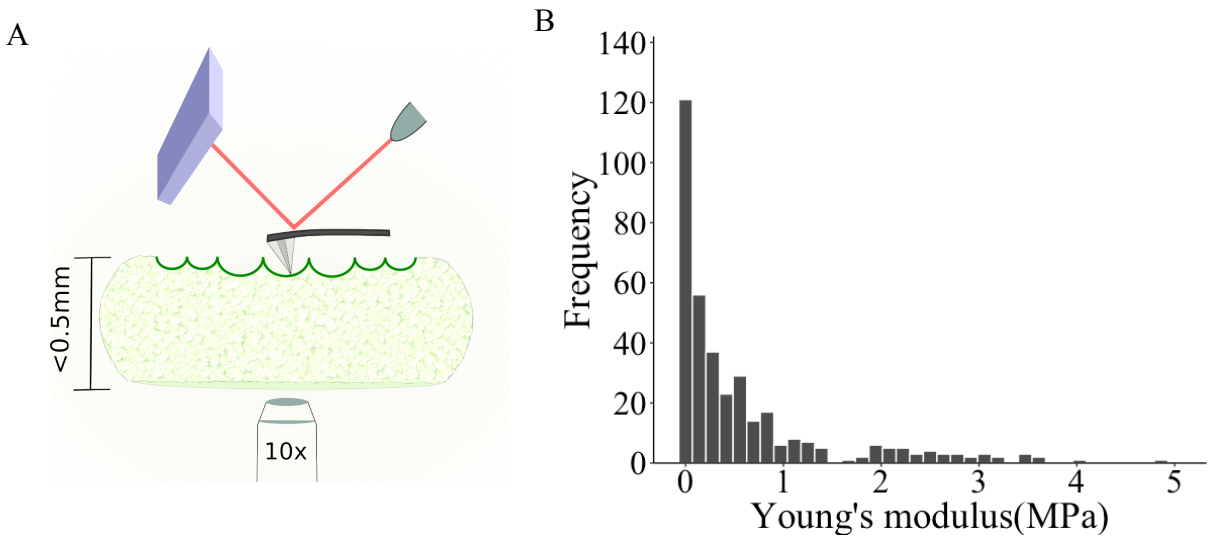

Figure 5. (A) Young's modulus of 37 randomly chosen areas within the vascular bundle determined with AFM. (B) Graphical representation of experimental setup. Laser reflection is dependent on the bending of tip, which is reflective of the substrate stiffness.

3.3 Discussion

To date, the expansion of cellular agriculture is believed to be dependent on 4 pillars: Animal free scaffolds, serum free media, bioreactors, and continuous cell lines or stem cells. The depiction of decellularized plant tissue as an abundant, highly accessible, and biocompatible animal free scaffold for 3D cell culture by our group opened the door to applications beyond the biomedical realm, such as cellular agriculture. Furthermore, the range of structures natively found throughout the plant kingdom displays a range of possible topographies and biomaterials with varying mechanical properties (Gershlak et al.,2017; Hickey et al.,2018; Modulevsky et al.,2014; Fontana et al.,2017). Short term, these structures have the ability to provide researchers with a range of abundant and highly accessible animal free scaffolds to study a range of cellular phenomena. Subsequently, the range of scaffolds can assist in the development of animal-plant hybrid as an alternative food. We hypothesize that the perceived fibrous structure of celery will be beneficial in assimilating native skeletal muscle.

The decellularization of the celery scaffold was performed as previously shown (Hickey et al., 2018). Sodium dodecyl sulfate, a surfactant, was used to disrupt the phospholipid bilayer leading to cell lysis. Following SDS incubation, calcium chloride is then used to reach the cloud point and facilitate washing (Hickey et al., 2018; Sammalkorpi et al., 2009). To confirm decellularization, native and decellularized scaffolds were stained with Hoescht 33342 (Chazotte, 2011). Nuclei were observed in the ground tissue (Fig.1C) and vascular bundle, more specifically, the companion cells within the phloem (Fig.1E). In contrast, nuclei were no longer visible on the decellularized tissue (Fig.1B & F).

The potentials of decellularized plant tissue as a scaffold for cell culture has been shown in a number of studies (Gershlak et al.,2017; Hickey et al.,2018; Modulevsky et al.,2014; Fontana et al.,2017). The mechanical properties previously depicted by these authors, potential for tunability, and animal free nature makes this scaffolding material a promising biomaterial for cellular agriculture applications. Taking into consideration the perceived fibrous structure of celery, the dimensions of the vascular bundle, the biocompatibility, porosity, and abundance of decellularized plant tissue, we sought to determine if this native structure would be beneficial for *in vitro* myoblast culture. The number of cells on the ground tissue increased approximately 2-fold from day 1 to day 5, and a significant 5-fold increase on day 10 (Fig.2A) ($P = 0.006$, $N = 4$). The proliferation rate observed on the celery scaffolds is greater than that previously depicted on decellularized apple scaffolds by our group (Modulevsky et al., 2014). The explanation behind this observation likely relies in the introduction of $CaCl_2$ to facilitate the removal of SDS (Hickey et al., 2018). In comparison to these previous studies, a Live/Dead analysis was not performed as

cells will readily detach following apoptosis and numerous PBS washes. In contrast to apple hypanthium, decellularized celery didn't allow for extensive migration of cells throughout the scaffold (Modulevsky et al., 2014; Hickey et al., 2018). Cells were noted crossing over the plant cell walls and growing on the cell wall junctions (Fig.2C-D). The formation of multicell spheroids presented in Figure 2B was an occurrence worth noting, but not pursued any further as biocompatibility was assessed based on cell numbers, and cells predominantly portrayed a physiologically relevant phenotype. It's likely that shallow plant cells allowed for the crossing over observation, whereas deeper cell walls caused cells to form groupings. The multicell spheroid appears to be an unlikely occurrence, which can be attributed to poor cell-matrix interactions leading to removal during the washing steps. The elongated phenotype, in contrast to a spheroid phenotype, depicts a strong attachment and interaction between the cell and scaffold resembling the native structure of muscle tissue (Trovato et al., 2016; Kassianidou et al., 2019; Modulevsky et al., 2014).

In addition to superficial growth, streaks of cells (Fig.3A-D) were observed migrating from the surface of the scaffold towards the interior. This was observed in 4 scaffolds following a 10-day incubation period. Muscle cells likely migrated through the intercellular space that forms at the junction of the plant cells (Duckett & Pressel, 2018; Earles et al., 2018).

In comparison to another group, human dermal fibroblast underwent a 14.5-fold expansion on RGDOPA- coated parsley stems over a 50-day incubation period (Fontana, et al., 2017). It was also shown how stem cells and primary cells behave on this plant derived scaffolds. For example, human pluripotent stem cell derived cardio myocytes were shown to contract

spontaneously on decellularized spinach leaf. Yet, in comparison to tissue culture plastic, the contractile strain was lower on the spinach leaf. (Gershlak et al., 2017). In comparison to 2D, the doubling time of C2C12 has been recorded to be approximately 13.5 - 15 hours (Forterre et al., 2014; Sato et al., 2011). Conversely, we conclude that proliferation was in fact lower on the decellularized celery scaffold than on Petri dishes. Matrix stiffness could be considered a major variable as proliferation and differentiation increase with stiffness (Engler et al., 2004; Trensz et al., 2015; Wells, 2008). There are a number of other factors, such as variability between cell lines (Ben-David et al., 2018) and biochemical properties of the substrate (Hickey & Pelling, 2019; Zeiger et al., 2013) which could have also contributed to this observation.

In order to further assess the biocompatibility of the scaffolds and influence on myogenesis, cells were placed in differentiation media for 5 days to minimize the risk of detachment induced by active contractions (Denes et al., 2019; Hosseini et al., 2012; Griffin et al., 2004). As shown on chapter 4, fusion of C2C12 into myotubes was prevalent after 5 days in differentiation media based on the pronounced presence of MHC positive structures with 2 or more nuclei (Chapter 4 - Fig.4). Yet, sarcomere formation was not observed after 5 days in differentiation media. The cells were also cultured for 7 and 14 days, and sarcomere formation was also not observed (data not shown). The development of striated myotubes is rarely observed *in vitro*, especially in immortalized cell lines (Chal & Pourquié, 2017; Denes et al., 2019; Hosseini et al., 2012). Based on the data presented here, we can conclude that the scaffold didn't promote or inhibit myogenesis beyond that observed in a Petri dish.

Taking into consideration the effect of substrate stiffness on cell behavior, such as proliferation, viability, and differentiation (Engler et al., 2004; Trensz et al., 2015; Gilbert et al., 2010), measuring the Young's modulus becomes a crucial mechanical characteristic. Furthermore, the mechanical properties of this animal free scaffold are not only invaluable for *in vitro* cell culture, but also consumer perception as part of an *in vitro* food product.

The bulk Young's modulus of the scaffolds was calculated by measuring the first 10% strain. This range was chosen based on the knowledge that *in vivo,* tissue viability decreases following 20% strain (Bader et al., 2008). This in turn supports the conclusion that cells rarely experience deformation beyond this point. Therefore, for biocompatibility studies and influence of substrate stiffness on cells, strain beyond this point falls outside the scope of this chapter. A significant decrease in the stiffness was observed in the XY scaffolds ($P<0.001$, $N=5$) following decellularization. It has been shown that the vacuole plays a critical role in the rigidity of the plant, a term known as turgor pressure (Beauzamy et al., 2014; Wiebe, 1978; Lang et al., 2014). Therefore, it is likely that following cell lysis the vacuole becomes compromised, leading to the significant decrease in stiffness (Fig.4A). The observed decrease in stiffness following decellularization resembles that of apple hypanthium (Hickey et al., 2018), and more importantly, it resembles that of skeletal muscle tissue (Feng et al., 2018; Engler et al., 2004; Gilbert et al., 2010).

As shown previously by our group, the cell laden scaffolds didn't portray a significant change in Young's modulus (Hickey et al., 2018). Due to the insignificant cells-to-substrate

ratio, it comes as no surprise that cells didn't significantly influence the bulk Young's modulus of the decellularized celery scaffold (Fig.4B) ($P>0.1$, $N = 5$).

As mentioned already, the wide range of structures natively present in plants have the potential to be repurposed into substrates with varying topographical structures. In the case of celery, the vascularization is composed of channels with dimensions that have previously been shown to influence the spatial orientation of cells (Hume et al.,2012; Sun et al.,2013; Altomare et al., 2010; Charest et al., 2007). The vascular bundle of celery is composed of two major structures: xylem and phloem. The alignment of cells on the vascular bundle will be discussed thoroughly in chapter 4. In this chapter, I sought to determine the Young's modulus of the vascularization channels through atomic force microscopy, which allowed for localized measurements. As a way to represent the range of stiffness values throughout the vascular bundle, we present a histogram of 37 randomly chosen areas throughout the vascular bundle (Fig.5A). It has been shown that the xylem is 1000x stiffer than the phloem (Lee, 1981; Hepworth and Vincent, 1998). Therefore, taking into consideration the range of values presented in the histogram and the values acquired at the periphery, we speculate that values greater than 1MPa likely correspond to the xylem. An independent study on the stiffness of *Populus deltoides* stem following the removal of lignin depicted Young's modulus values $1x10^4$ greater than those shown here (Farahi et al., 2017). Before making a direct comparison, however, we must consider the processing method and natural variability among plant species. The study also depicted a 4-fold increase in Young's modulus following removal of lignin, which explains the observed stiffness of the ylem (Farahi et al., 2017). Conversely, the conspicuous presence of lignin

explains the known fact that xylem tissue is dramatically stiffer than phloem tissue (Lee, 1981; Hepworth and Vincent, 1998).

The decellularization protocol pioneered by our group opens a door to a range of plant tissues with a broad range of structures and desirable properties for *in vitro* research. Although decellularized celery portrayed a bulk Young's modulus similar to skeletal muscle and allowed for extensive proliferation and differentiation, it only allowed for superficial confinement. In addition to the lack of migration throughout the scaffold, decellularized plants present a number of disadvantages; such as inconsistency in their composition, heterogeneous structure, and poor tunability. Yet, a number of structures with desirable dimensions are ripe for further exploration, Therefore, in the next chapter we will look beyond the celery parenchyma and investigate the potential applications of the vascular bundle for *in vitro* studies.

3.4 Conclusion

The perceived fibrosity of celery presents an opportunity to repurpose an abundant and highly accessible animal free scaffold for *in vitro* meat research. Here, decellularization was confirmed by the loss of colour and absence of nuclei following Hoescht 33342 staining. A significant decrease in Young's modulus supports this observation based on the knowledge that intact plant cells are under turgor pressure. In addition to the celery parenchyma, the Young's modulus of the vascular bundle was determined independently of the ground tissue through atomic force microscopy. Indentation of 37 randomly chosen areas yielded a Young Modulus of 0.60 ± 0.86MPa (N=37) for all of the areas within the vascular bundle. Values ranging from 5-20KPa were assigned to the phloem based on literature values and experimental setup. The

biocompatibility of the decellularized scaffold was assessed through proliferation growth curve, which depicted an approximately 5-fold increase over a 10-day incubation period. Although we present celery as a biocompatible and structurally relevant scaffold for *in vitro* meat research, we must take into consideration a number of limitations such as the inconsistent heterogeneous composition and low porosity preventing cell migration.

CHAPTER 4

Decellularized Celery Scaffold for Guided Cell Alignment of C2C12 Murine Myoblast

Manuscript submitted to *Biomaterial Science*

Motivation and objectives

As shown on the previous chapter, plant parenchyma provides a relatively porous substrate with stiffness values similar to those of skeletal muscle tissue. Yet, it fails to recapitulate an invaluable characteristic of skeletal muscle tissue: the aligned arrangement of myofibers. Taking into consideration the dimensions of the vascular bundle channels and large body of literature on synthetic microchannels for guided cell alignment, I sought to determine if microchannels derived from longitudinally cut celery stalks can be repurposed as a simpler and more accessible substrate for cell alignment.

4.1 Abstract

Alignment and orientation of cells *in vivo* plays a crucial role in the functionality of tissue. In the laboratory, however, 2D Petri dishes fail to recreate alignment. This in turn has shown a difference in gene expression, leading to inaccurate results. To overcome this discrepancy, a wide array of methods including topographical cues, cyclic strain, and electrical stimulation have been used to recreate alignment. However, these methods are often laborious and rely on the use of specialized equipment. Consideration of recent publications on decellularized plant tissue as 3D substrates for cell culture has led us to speculate that a wide array of structures natively found in plants have yet to be explored. Here we depict the alignment of C2C12 murine myoblast on the decellularized vascular bundle of celery (*Apium graveolens)*.

The xylem channels (17± 5μm) and phloem channels (16 ± 6 μm) lie within the 10-100μm diameter necessary for optimal myoblast alignment. Following 10 days in proliferation media, the normalized mean direction of F-actin filaments was determined to be 1.2 ± 2.0°. Subsequently, after 5 days in differentiation media, 308 ± 169μm long myotubes formed parallel to the vascular bundle grooves. We can therefore conclude that the microtopography of the vascular bundle guides muscle cell alignment. The results presented here highlight the potential of this plant-derived scaffold for *in vitro* studies of muscle myogenesis, where structural anisotropy is required to more closely resemble *in vivo* conditions.

4.2 Introduction

The orientation and arrangement of cells *in vivo* plays a crucial role in the functionality of tissue (Feng et al., 2013; Komuro et al., 1982; Frontera & Ochala, 2015). The multinucleated structures in muscle tissue, known as myofibers, are bundled and arranged along a predetermined axis to synchronously contract and generate force (Chal & Pourquié, 2017; Narayanan et al., 2002). Airways, arteries, and veins rely on the circumferential alignment of smooth muscle cells to facilitate the transport of fluids and gases (Clark & Pyne-Geithman, 2005; Komuro et al., 1982). In the laboratory, however, *in vitro* studies are performed on flat 2D Petri dishes which lack biologically active adhesion sites, dimensionality, microtopography, and proper mechanical stimuli. This in turn causes cells to appear randomly scattered; and portray dissimilarities in proliferation, differentiation and overall gene expression (Wang et al., 2012; Cooper et al., 2010; Mozetic et al., 2017; Basso et al., 2018; Kuppan et al., 2016; Foolen et al., 2018; Gao et al., 2016). In order to assimilate 2D cell culture to the *in vivo* environment and further understand the role of matrix topography, substrates with a wide array of topographical structures, such as

posts (Goedecke et al., 2015), microchannels (Hume et al.,2012), and nanofibers (Fee et al., 2016) have been developed (Goedecke et al., 2015). In addition to topographical features such as microchannels/microgrooves, cylclic strain and electrical stimulation have also been shown to influence spatial orientation of cells (Liu et al.,2008; Tanaka et al., 2014).

It has been shown that smooth muscle cells (Kuppan et al., 2016), skeletal muscle cells (Cooper et al., 2010), neurons (Basso et al., 2018) and tendon derived cells (Foolen et al., 2018) portrayed a difference in gene expression when compared to those cultured on the smooth surfaces of tissue culture dishes. Skeletal muscle cells upregulate troponin T, myosin heavy chain, and myogenin when cultured on uniaxial microchannels (Cooper et al.,2010).

Substrate topography has also been shown to influence differentiation lineage of mesenchymal stem cells. Mesenchymal stem cells cultured on grooves and ridges committed to myogenic and adipogenic line, whereas smooth surface induced osteogenic differentiation (Wang et al., 2012).

Microchannel development has proven to be a popular method for guided cell alignment due to tunability and reproducibility. Photolithography (Camelliti et al.,2006; Leclerc et al., 2013), femtosecond pulsed laser (Yeong et al.,2010), 3D printing (Tan et al., 2017; Tijore et al.,2018) and electron-beam lithography (Wang et al., 2010; Idota et al., 2009 have all been shown to produce substrate topographies capable of inducing alignment. It has been shown that microchannel width ranging from 5-200μm can induce alignment of myoblasts, where channels 20 to 100μm wide induced optimal myotube maturation (Hume et al.,2012; Sun et al.,2013;

Altomare et al., 2010; Charest et al., 2007). The depth of the channels has also been shown to play a role in cell alignment. Cells cultured on 2μm deep microgrooves exhibited limited alignment after 24 h when compared to 7um deep channels, which provided a permanent alignment (Zhao et al.,2009). This observation appeared to be cell line specific: C2C12 responded to grooves below 0.5μm differently than primary myoblasts (Altomare et al., 2010). On the discussed substrates, cell alignment is attributed to confinement and contact guidance. Cells were considered aligned if the mean angle of cells with reference to the direction of the substrate pattern fell below 10° (Altomare et al., 2010 & Charest et al., 2007)

Anchorage dependent cells interact with the extracellular matrix through integrin binding, often through the RGD (arginine-glycine-aspartate) motif present in fibronectin, vibronectin and laminin (Janson & Putnam, 2015). Non-animal derived scaffolds lack binding motifs; yet, the presence of adhesion proteins naturally found in serum (e.g. Fetal bovine serum) and those extruded by cells facilitate interaction between a foreign matrix and the cell (Hayman et al., 1985; Turoverova et al., 2009). Clusters of integrins, GTPases and other enzymes form focal adhesion (FA) complex, which undergo active restructuring in response to substrate stiffness and topography (Wozniak, 2004; Wu, 2007). Stretch sensitive channels such as Bin/amphiphysin/Rv (BAR) domain-containing proteins work in part as topographical sensors, and are believed to play a role in the sensing of curved structures. (Mim & Unger, 2012; Kulangara & Leong, 2009; Sheetz & Vogel, 2006). The reorganization of cytoskeletal proteins in response to topography is mandated in part by the regulation of Rho, Rac, and Cdc 42 (Kulangara & Leong, 2009). This phenomenon is referred to as contact guidance (Linke et al., 2018; Teixeira et al., 2003; Kim et al., 2012; Kulangara & Leong, 2009). Information received through focal adhesion complexes

influences focal adhesion kinase (FAK) signaling, which in turn triggers downstream signaling of the mitogen activated proteins kinase (MAPK) cascade (Kim et al., 2012; Janson & Putnam, 2015). Although the interaction between cells and matrix has been an area of interest for over 20 years, locomotion, local restructuring, and molecular mechanisms governing intracellular changes is still not fully understood.

A series of recent studies have depicted the biocompatibility of decellularized plant tissue *in vitro* and *in vivo.* Through the use of surfactants, such as SDS, the cell membrane becomes compromised leading to cell lysis. (Fontana et al.,2017; Modulevsky et al.,2014; Brown and Audet, 2008; Modulevsky et al., 2016; Hickey et al., 2018). Immortalized cell lines were shown to proliferate throughout the relatively porous decellularized apple tissue without the need for biofunctionalization (Modulevsky et al.,2014; Hickey et al., 2018). *In vivo* studies showed that implanted decellularized apple tissue showed minimal immune response and guided angiogenesis (Modulevsky et al., 2016). In addition to biocompatibility, the mechanical properties have been shown to resemble that of skeletal (Hickey et al.,2018) and cardiac muscle (Gershlak et al.,2017) tissue. However, decellularized plant tissue lacks the biochemical cues natively found in mammalian extracellular matrix (Thorsteinsdóttir et al.,2011). Yet, the lack of biochemical cues in plant cellulose, bacterial cellulose, and cellulose derivatives has not impeded applications in tissue engineering (Novotna et al., 2013; Hickey & Pelling, 2019). Furthermore, the tunability potential of cellulose, including biofunctionalization, can further extend its applications (Hickey et al., 2018; Modulevsky et al., 2014; Courtenay et al., 2018; Courtenay et al., 2017; Fontana et al., 2017).

As part of the wide arrays of structures found in plants, the vascularization of plants is composed of vessels with diameters in the micrometer scale (Scarpella & Meijer, 2004; Karam, 2005; Myburg et al.,2013). In the case of celery (*Apium graveolens*), a dicot plant, the vascularization is composed of two major structures composed of channels with varying diameters: xylem and phloem (Scarpella & Meijer, 2004). Therefore, based on the diameter of these structures, we hypothesized that C2C12 myoblast cells will align along the longitudinal direction of the vascular bundle. After 10 days in growth media, we found that the actin filaments and apex of nuclei align parallel to the vascular bundle. After differentiating the cells into fused myotubes, we found that myotubes maintain their align morphology.

We hereby depict how the natural topography of the vascular bundle can be exploited to induce the uniaxial orientation of muscle precursor cells and myotubes. The method presented exploits the use of a simple, highly accessible, biocompatible and tunable substrate for guided cell alignment. This in turn is expected to facilitate research and broaden our knowledge of *in vitro* cell alignment. Although we only discuss skeletal muscle cells, we wish to remind the reader that spatial orientation is a property of all tissues. Therefore, based on recent publications depicting biofunctionalization and tunable mechanical properties (Hickey et al., 2018; Modulevsky et al., 2014; Fontana et al., 2017), we expect that the vascular bundle of celery will become a foundational substrate for further development to more closely resemble the microenvironment of other cell types.

4.3 Materials and Methods

4.3.1 Scaffold Preparation

The decellularization protocol was performed as described previously (Hickey et al. 2018). Briefly, celery (*Apium graveolens)* stalk was cut parallel and perpendicular to the longitudinal axis using a mandolin slicer. A 6mm biopsy punch was then used to obtain round scaffolds with the exposed vascular bundle in a longitudinal and cross section orientation. (Fig.1A-B) The samples were then transferred to a 15mL Falcon tube containing 0.1% SDS at a ratio of one sample per mL of 0.1% SDS solution. Samples were then agitated in a shaker at 120RPM for 72 hours. Following treatment with SDS, the samples were washed three times with deionized water. After the final wash, 100mM solution of $CaCl_2$ (1mL/scaffold) was added and samples were incubated at room temperature for 24 hours. After 24 hours, the samples were washed with distilled water three times. On the final wash, the water was removed and 70% ethanol was added for 30min. At this point, the samples were brought into a class II biosafety cabinet and washed three times with sterile PBS. The samples were placed on PDMS coated 12-well plates with 2mL of growth media (refer to next section). The samples were incubated overnight at 37°C and 5% CO_2. Prior to cell seeding, the media was removed (Fig.1A).

4.3.2 Cell culture

C2C12 murine myoblasts were plated on tissue culture plates and maintained at 37°C with 5% CO_2. Cells were cultured in growth media consisting of high glucose DMEM with L-glutamine and sodium pyruvate (Hyclone) supplemented with 10% FBS (Wisent) and 1% penicilin (10000U/mL) & streptomycin (10000ug/mL) (Hyclone). Once the cells reached 70-80% confluency, they were trypsinized (0.05%)(Hyclone), resuspended in growth media, and

spun down in the centrifuge at 1000RPM (97g) for 3 min. Following centrifugation, the pellet was resuspended in growth media to acquire 1.7 x 10^6 cells/mL. Cells were counted using a hemocytometer and trypan blue to determine viability. 30 μL of media containing cells were placed on the scaffolds and incubated for 4.5 hours. Following incubation, 2mL of growth media was added and samples were incubated for the 10 days with media change every 48 hours until day 7, followed by daily media change until day 10. For differentiation studies, cells were placed in differentiation media for 5 days. The differentiation media was composed of high glucose DMEM, 2% horse serum (Gibco) and 1% penicillin and streptomycin (Hyclone).

4.3.3 Fluorescent staining.

To first confirm decellularization of the *A. graveolens* scaffolds, native and decellularized samples without cells were placed in 1:500 hoescht 33342(Invitrogen) made up in Phospahte buffered saline (PBS) for 30min at 37°C.

Following 10 days in growth media, decellularized scaffolds with cells were transferred to a microcentrifuge tube using a metal paddle (to minimize contact with exposed vascular bundle) and washed three times with PBS. The samples were fixed with 3.5% paraformaldahyde in 2% aqueous sucrose solution for 10min and washed three times with PBS. Following the final PBS wash, room temperature triton-X100 was added to permeabilize the cells. The scaffolds were once again washed three times with PBS. For F-actin imaging, scaffolds were stained using Alexa Fluor 488 phalloidin (Invitrogen) in PBS at a 1:200 concentration and incubated for 20min in the dark. Nuclei was stained by first placing the scaffolds in 10% RNAse in PBS (DNase and protease-free) (Thermo Fisher) for 30 min at 37°C, followed by PBS wash (3X). After the third

wash, propidium iodide(1mg/mL) (Thermo Fisher) was added at a 1:1000 concentration for 30min. In order to observe the cells morphology with respect to the substrate, cellulose was stained with 10% calcofluor in PBS for 20min at room temperature.

To test for the presence of myotubes, scaffolds from the 5-day differentiation treatment were fixed and permeabilized as described above. These samples were then washed three times with cold wash buffer (5% FBS in PBS) and placed at 4°C for 20min. The cold wash buffer was removed and MF-20 (DSHB Hybridoma Product) was added at a 1:200 concentration made up in cold wash buffer and incubated for 24 hours at 4°C. The MF-20 solution was removed and the scaffolds were washed three times with cold wash buffer. Samples were stored in cold wash buffer for 20 min at 4°C before adding the secondary antibody. Anti-Mouse IgG (whole molecule)–FITC (Sigma) was added at a 1:100 concentration and placed in the refrigerator for 1 hour. The samples were then washed 3 times with PBS prior to imaging.

4.3.4 Confocal microscopy

Scaffolds were placed on coverslips with mounting medium (Vectashield H-1000) prior to imaging. The samples were imaged with a Nikon TiE A1-R high speed resonant scanner confocal microscope with a 10X and 40x lens. Image processing was done on FIJI- ImageJ. The images presented throughout this manuscript are Maximun Intensity Projections (MIP) of 210 ± 51μm (N=9) and 49 ± 24μm (N = 7) confocal volumes for 10X and 40X magnification, respectively. Brightness of fluorophore signal was enhanced to improve contrast of structures.

4.3.5 Scanning Electron Microscopy

Sample preparation was performed as described previously (Murtey and Ramasamy, 2016, p.173-175) Briefly, the sample was washed three times with PBS and placed in aqueous solution containing 3.5% paraformaldehyde (in 2% sucrose solution) and 1.5% glutaraldehyde (Final concentration) overnight. Post fixation, the sample was washed again with PBS and dehydrated through a sequential ethanol gradient (30,50,75,95 & 99%). The sample was dried using the Samdri-PVT-3D Critical point dryer in 99% ethanol. The dried sample was gold sputtered with a 5nm layer (LEICA EM ACE 200). The samples were image with a JEOL JSM-7500F FESEM at 2.0 KV.

4.3.6 Orientation measurement

1.61mm^2 images with a 24 ± 6% (N=20) actin coverage and 20 ± 10% (N=20) MYHC coverage were analyzed to determine the orientation of the labeled structures. The images were captured 1mm away from the edge of the vascular bundle to minimize the influence of damaged channels brought upon by the biopsy punch and mandolin. The labeled MYHC and F-actin were first thresholded with the *Adaptive Threshold* plug-in on ImageJ-FIJI to isolate labeled cytoskeletal proteins and vascular bundle. The directionality of the structures was determined using the *Directionality* plug-in on FIJI ImageJ. We quantified the degree of alignment by examining the broadness of the Gaussian distribution. In a manner similar to signal processing techniques, we defined the alignment in a manner reminiscent of a Quality Factor(Q-factor). In this case, the Degree of Alignment = Average Angle / Width of the distribution at half maximum. Tightly aligned myotubes will therefore have a small distribution and large Degree of

Alignment. Conversely, a population of myotubes which are randomly oriented will have a broad distribution and a small Degree of Alignment.

4.3.7 Histology

The scaffolds were rinsed with PBS three times and fixed overnight with 10% formalin (Sigma). Following formalin fixation, the scaffolds were rinsed with PBS and stored in 70% ethanol until paraffin embedding. The vascular bundle was serial cut into 4μm sections (longitudinally) and stained with H&E. The slides were scanned using the Aperio AT2 pathology slide scanner. Image viewing and processing was done with Aperio ImageScope.

4.3.8 Immunohistochemical analysis

Formalin-fixed, paraffin-embedded sections were deparaffinized in xylene and rehydrated through a sequential 100-70% ethanol gradient. Heat induced epitope retrieval was done at 110°C for 12 min with citrate buffer pH 6.0. Sections were then blocked with Rodent Block M blocking reagent (BioCare) and incubated overnight at 4°C at a 1:12 dilution using MF-20 antibody (DSHB). Following overnight incubation, sections were washed with 1xTBST and then incubated with goat anti-mouse-568(Abcam) secondary antibody at a 1:500 dilution for 2 hours in the dark at room temperature. Sections were washed with a 1X TBST, incubated for 5 min with a quencher (Vector TrueView Autofluorescence Quenching, Vector Labs). Sections were washed and incubated with 5ug/mL DAPI (ThermoScientific), washed and cover slipped.

4.3.9 Migration Measurement and channel diameter

In order to determine the migration of cells throughout the vascular bundle, nuclei on longitudinal cuts 12 μm apart were counted to minimize the probability of counting the same nuclei twice or underestimating the actual number. This was done based on an average nuclei size of 10 μm (Roman & Gomes, 2018). An Open Computer Vision (OpenCV) Python script was developed to batch process images. The location of each nuclei was then determined by exporting the coordinates of a mouse-click. Once a nucleus was counted, an overlay green dot would mark it to prevent overestimation (Appendix II).

An OpenCV Python script was also used to measure the diameter of the vascular bundle channels. The script first isolates the edges and then draws built-in Contours. The contour area was fitted to a circle based on the correlation between diameter and surface area (Appendix I).

4.3.10 Statistical analysis

Student's t-test assuming equal variance was used to analyze the results presented in this manuscript. All of the statistical tests were done on R studio. Statistical significance refers to $P<0.05$. Values throughout this manuscript are displayed as mean ± standard deviation.

4.4 Results

4.4.1 Substrate preparation

We first sought to create two distinct scaffolds with different topographies. The scaffolds were created by cutting the *A. graveolens* stalk longitudinally and cross-sectionally (Fig. 1A & B). Cross sections had an amorphous topography, whereas the longitudinal scaffolds portrayed

highly aligned vascular bundle grooves. Following 3 days in 0.1% SDS, the scaffolds lost their green color due to the loss of cellular components (Fig.1B). In order to facilitate removal of SDS, 100mM concentration of $CaCl_2$ was added to the scaffolds for 24 hours. The decellularization of the vascular bundle was determined using a membrane permeable stain, Hoescht 33342 (Fig.1 – Supplementary material). A comparison between native and decellularized phloem was expected to depict the nuclei of companion cells in the phloem, as opposed to the outline of companion cells lacking a nuclei in the decellularized scaffolds. The xylem and sieve tube elements don't possess a nucleus (Schuetz et al., 2013)**.** The loss of the natural green colour and nuclei of companion cells depict successful decellularization of the *A. graveolens* scaffolds.

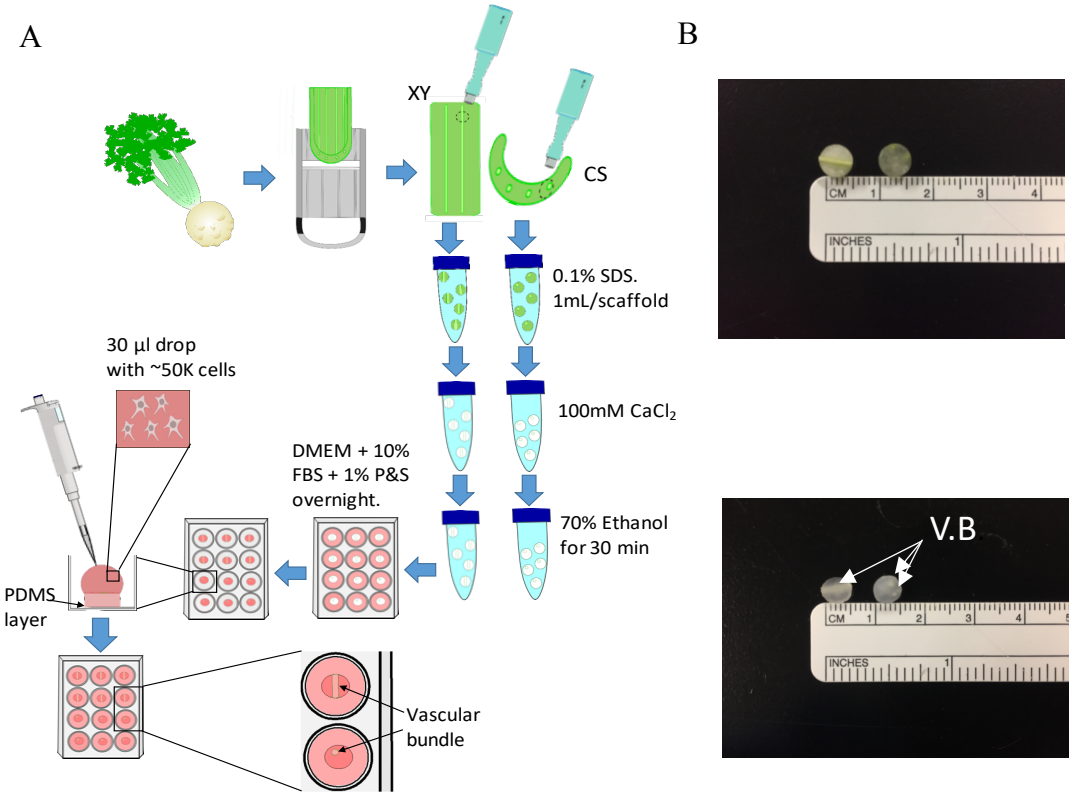

Figure 1.(A) Visual representation of celery(*A. graveolens)* scaffold preparation. (B) Samples were 6mm wide and 2.15±0.15mm thick. "XY" corresponds to scaffolds cut (left) longitudinally with respect to the celery stalk, whereas" CS" corresponds to (right) cross sections. Approximately 50,000 Cells were seeded on (C) decellularized scaffolds and left on scaffold for 4.5 hours. V.B.= Vascular bundle

The lignified tissue in the xylem interacts with propidium iodide leading to the observed red fluorescence. In contrast, the parenchyma and phloem labelled with calcofluor led to blue fluorescence (Depicted in Fig. 2A & Fig.2B as yellow and purple, respectively). The diameter of the phloem vessels was determined to be 16 ± 6µm (N=3.), whereas the xylem vessels were 17 ± 5µm (N=3) wide (Fig.2E). Based on these results, we conclude that were able to acquire grooves with diameters within the 5-100µm region necessary for optimal alignment.

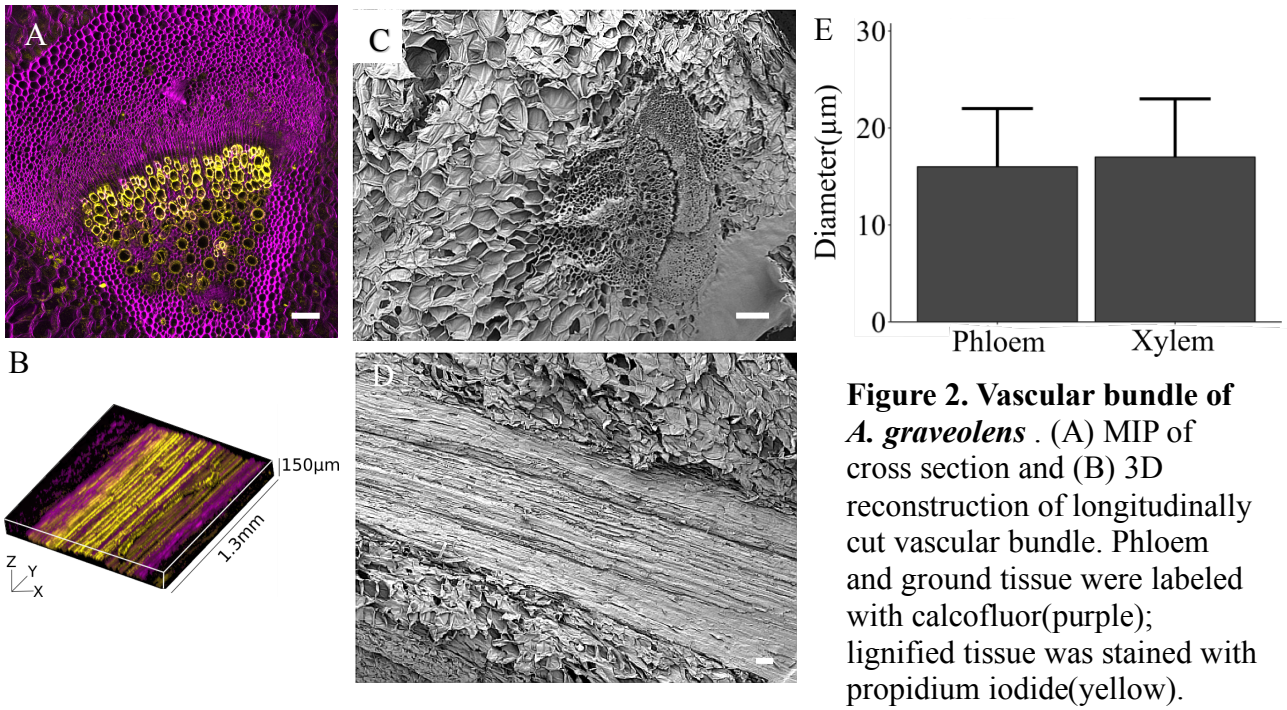

Figure 2. Vascular bundle of *A. graveolens* . (A) MIP of cross section and (B) 3D reconstruction of longitudinally cut vascular bundle. Phloem and ground tissue were labeled with calcofluor(purple); lignified tissue was stained with propidium iodide(yellow). SEM images of vascular bundle (C) cross section and (D) longitudinal cut.(E) Phloem and xylem channel diameter(N=3.

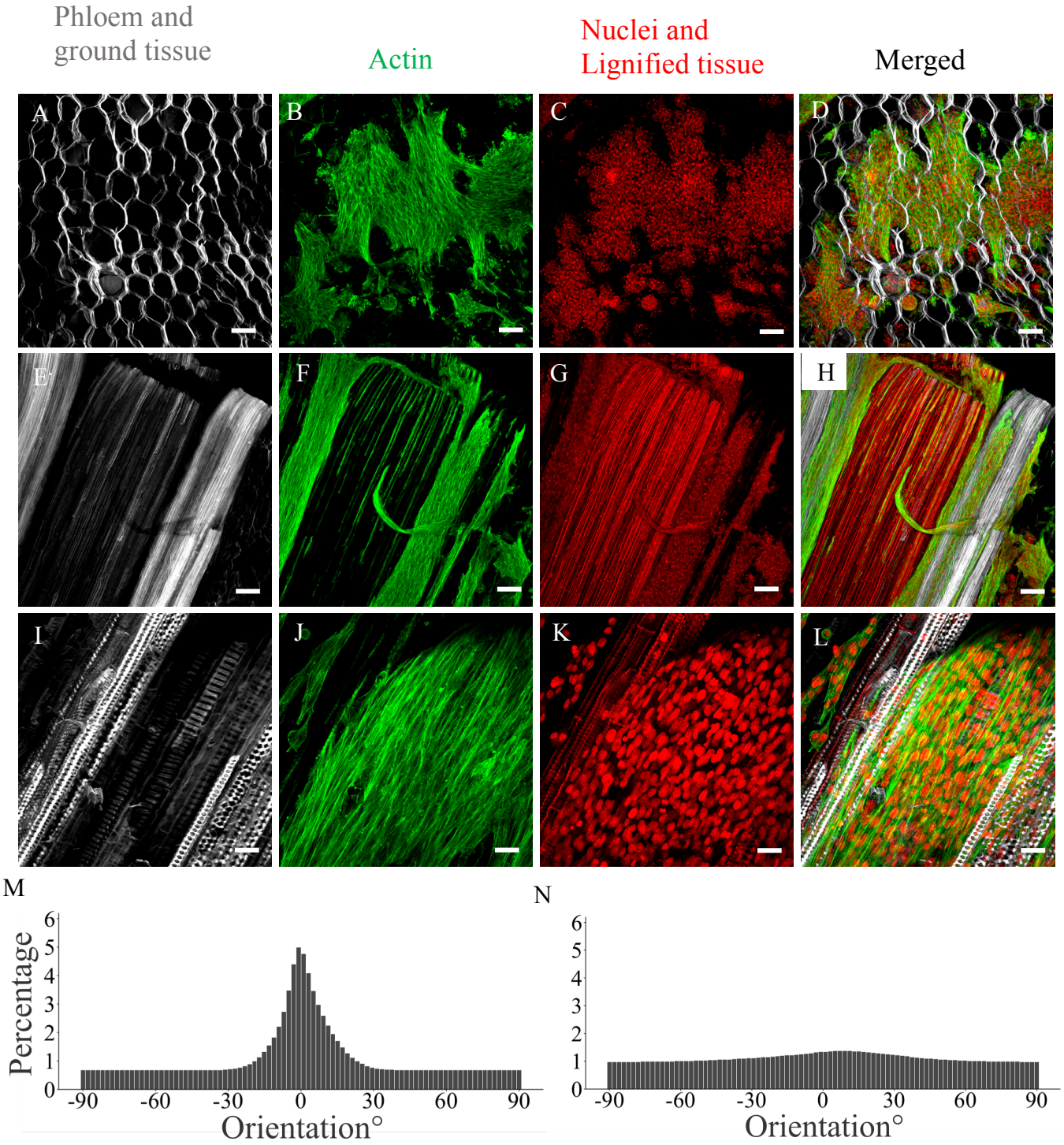

Figure 3. **Myoblast alignment on the decellularized vascular bundle of celery (*A. graveolens)* following 10 days in growth media**. (A,E & I) Phloem and ground tissue were labeled with Calcoflour (gray); (B, F, & J) F-actin was labeled with Phalloidin Alexa fluor 488(green) ; (C ,G & L) nuclei and lignified tissue were labeled with propidium iodide (Red) (A - H) Scale bar = 100µm. (I-L) Scale bar = 25µm. Histograms representing average F-actin filament orientation on (M) vascular bundle and (N) parenchyma (N=10 MIP images).

4.4.2 F-actin alignment on vascular bundle derived from *A. graveolens* stalks

We next sought to test our hypothesis that microscale grooves in a plant scaffold would lead to cellular alignment. Cells were seeded on the decellularized scaffolds at a concentration of ~5 x 10^5 cells/mL. A 30µl drop of cells was left on the scaffold for 4.5 hours. The scaffolds were incubated in growth media for 10 days. By the end of the incubation period, F-actin filaments were observed to be oriented parallel to the longitudinal axis of the vascular bundle (Fig.3F & 3J) as opposed to those on the parenchyma (Fig.3B). This in turn leads to a visible unimodal distribution in Figure 3M (0.5 ± 41.2°), whereas isotropic F- actin filaments on the parenchyma are represented by a uniform histogram (Fig.3N) (0.7 ± 50.2°). Furthermore, a significant difference was observed between the Degree of Alingment of myoblast seeded on the vascular bundle and those on the parenchyma. (Aligned myoblast Degree of Alignment: 4.7 ± 2.7. Isotropic myoblast Degree of Alignment: 0.7 ± 0.4. P = 2 x 10^{-4}, N = 10). Consequently, the normalized mean value with respect to the vascular bundle was calculated to be 1.2° ± 2.0 (N =10). This led us to conclude that the vascular bundle topography had a clear influence in the phenotype and reorganization of F-actin filaments.

4.4.3 Fusion of aligned myoblast on vascular bundle derived from *A. graveolens*

The clear reorganization of F- actin filaments and the orientation of the nuclei-apex led us to hypothesize that 5 days in differentiation will lead to the formation of aligned myotubes. Cells were first incubated for 10 days in proliferation media, then switched to differentiation media for 5 days to induce fusion; yet, minimize the risk of detachment induced by active contractions (Szustakowski et al.,2006; Denes et al., 2019; Hosseini et al., 2012; Griffin et al., 2004).

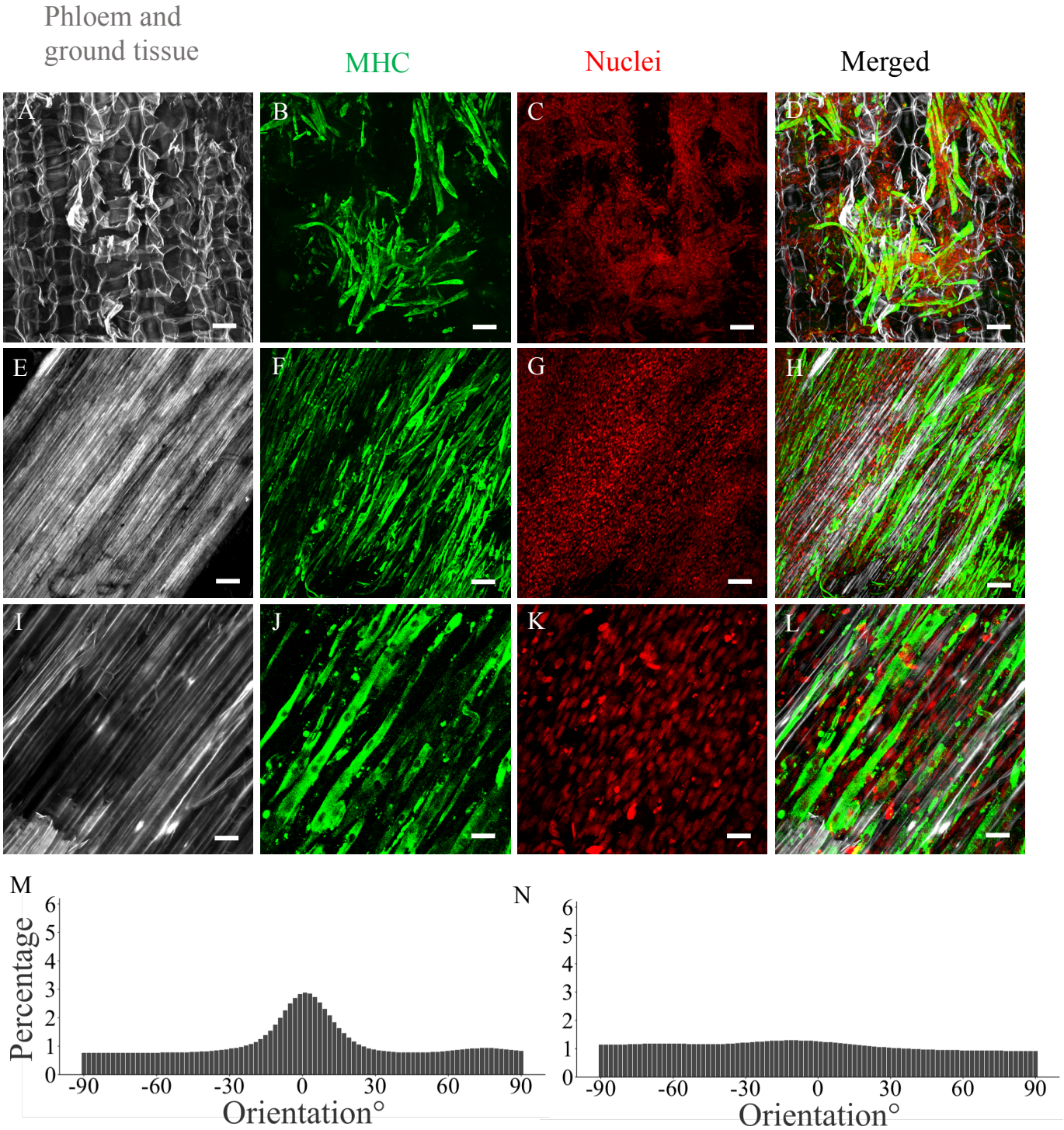

Figure 4.(A-D) Myotube alignment on the decellularized vascular bundle of celery(*A. graveolens)*. Myotubes were labeled with MF-20 followed by FITC-conjugated secondary antibody (green); nuclei were labeled with propidium iodide (Red); ground tissue and vascular bundle were labeled with calcofluor (gray). Scale bar = 100µm. Histograms representing average myotube orientation on (M) vascular bundle and (N) parenchyma(N = 10 MIP images).

Myosin heavy chain (MYHC), an early differentiation marker, was labeled with the MF-20 antibody (Fig.4B, 4F& 4J). The average myotube length was determined to be 308 ± 169μm (N=103). Myotubes were predominantly observed to have an elongated morphology (Fig.4F & 4J). Concomitantly with the F-actin orientation, a statistically significant difference was also observed between the orientation of the myotubes cultured on the vascular bundle and those on the parenchyma (aligned myotubes Degree of Alingment: 3.3 ± 1.1. Isotropic myotubes Degree of Alignment: 0.6 ± 0.6. $P = 2 \times 10^{-6}$, N =10). Concomitantly with F-actin filament orientation, a unimodal histogram with a broader distribution of 1.7 ± 45.5° represents the orientation of myotubes on the vascular bundle (Fig.4M). Conversely, and in support of isotropic F-actin filament formation on celery parenchyma, a uniform histogram (-4.4 ± 51.1°) depicts the orientation of myotube orientation on celery parenchyma (Fig.4N). In addition, the normalized mean value for the orientation of myotubes with respect to the vascular bundle was calculated to be 8.6° ± 23.8 (N = 10). As shown on Figure 3 & 4, the histograms corresponding to myoblast and myotubes on the vascular bundle portray a uniform distribution, whereas the histogram of cells cultured on the parenchyma yielded a uniform histogram. Taking into consideration the natural variation of biological samples and the preparation method, we can't disregard the formation of smooth or damaged areas with outlying topographical cues or void thereof (Figure 2 – Supplementary material).

4.4.4 Migration of C2C12 through vascular bundle and immunohistochemical analysis of MYHC expression

In addition to studying the effects of alignment, we lastly sought to determine if cells seeded on cross section scaffolds would be able to migrate the full extent of the vascular bundle.

Therefore, cells were seeded on the decellularized scaffolds as mentioned previously and incubated for 10 days. The scaffolds were serial cut (4 µm) cross sectionally (Fig.5B & 5E) and longitudinally (Fig.5A & 5F). The average migration distance was determined to be 0.91 ± 0.80mm (N=5)(Fig.5C). Cells were predominantly observed on the surface of the vascular bundle as depicted by the bars at the 0 and 2mm mark. Throughout the bundle, however, cells appear to be uniformly distributed (Fig.5C). As shown in Figure 5A & 5D, cells present an elongated phenotype, which corresponds to optimal cell-matrix interaction.

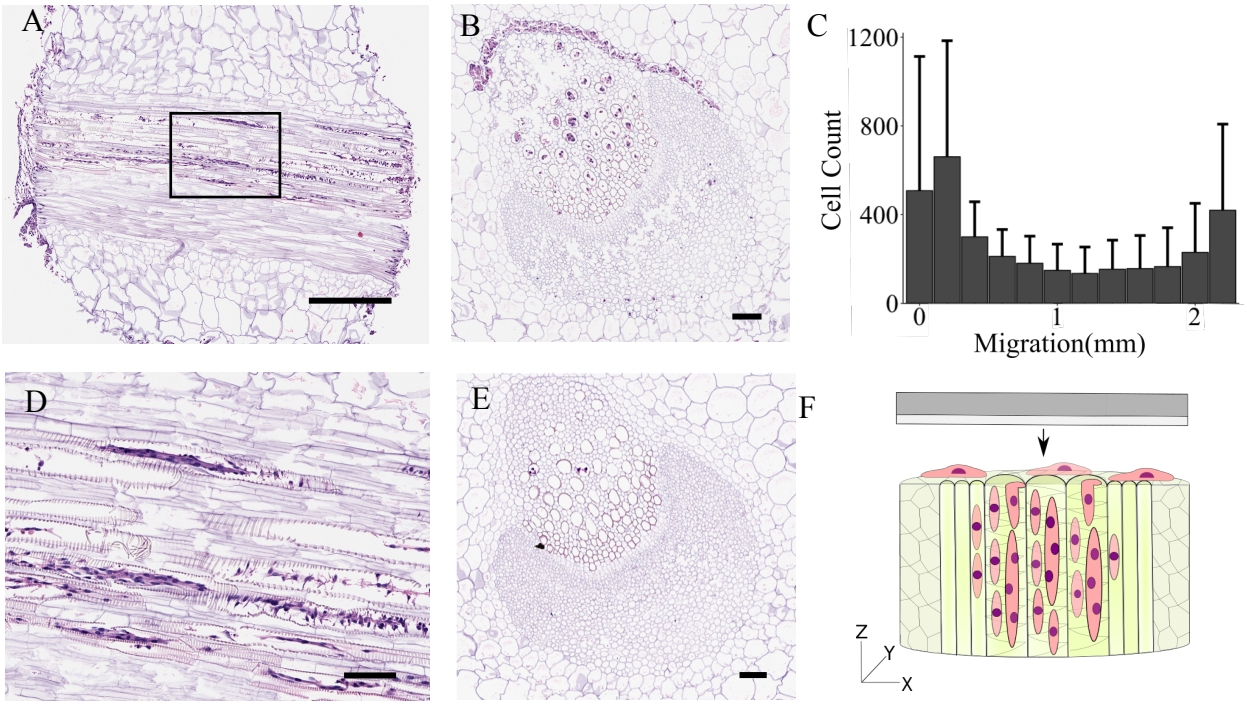

Figure 5. Migration of C2C12 through decellularized vascular bundler of celery at day 10. (A) 4µm wide longitudinal cut of vascular bundle. (F) visual representation of longitudinal cut . (B) Cross section of vascular bundle 100um away from surface. (E) cross section of vascular bundle 800um away from surface. Cells were stained with H&E. (C) Migration distribution of cells throughout the vascular bundle after a 10-day incubation period (N=5)(Mean ± S.D). (A) Scale bar = 500µm. (B-D) Scale bar = 100µm.

Following the observed distribution of cells throughout the vascular bundle after 10 days in growth media, the cross-section scaffolds were placed in differentiation media for 5 days to induce myoblast fusion. Based on immunohistochemical analysis of MYHC expression, myotube formation was not observed (Supplementary material – Figure 3).

4.5 Discussion

Alignment and spatial orientation of cells *in vivo* correlates strongly with tissue functionality (Feng et al., 2013; Komuro et al., 1982; Frontera & Ochala, 2015). In the case of skeletal muscle tissue, muscle precursor cells proliferate, fuse along a predetermined axis, and form fascicles composed of striated myofibers (Chal & Pourquié, 2017). Depolarization of these myofibers leads to the contractions that drive motion in birds (De La Haba et al., 1975), amphibians (Alley & Omerza, 1999), crustaceans (Perry et al., 2009) and mammals (Pette & Staron, 1997).

In order to better understand skeletal muscle tissue, skeletal muscle cells are routinely cultured in stiff and smooth 2D Petri dishes. By underrepresenting the *in vivo* environment, cells appear randomly scattered and display a significant difference in gene expression (Dalrymple et al., 2000; Chal and Pourquie, 2017). In order to recreate alignment *in vitro*, fibers (Soliman et al., 2018; Cooper et al., 2010; Schoenenberger et al., 2018), microchannels of various sizes (Hume et al., 2012; Huang et al., 2010; Leclerc et al., 2013), cyclic strain (Liu et al., 2008; Pennisi et al., 2011) and electrical stimulation (Tanaka et al., 2014) have been shown to influence spatial orientation. *In-vitro* studies have showed that myoblast alignment upregulated the expression of Troponin T, Myogenin and Myosin Heavy Chain II (Cooper et al.,2010). Another group showed

that cell viability and proliferation of smooth muscle cells increased on aligned PHBV nanofibers, alongside an increase in gene expression of contractile markers (Kuppan et al.,2015).

Great emphasis has been placed on microchannel development techniques, such as 3D printing (Tan et al., 2017), electron-beam lithography (Goto et al., 2007), photolithography (Hume et al., 2012; Leclerc et al., 2013; Zhao et al., 2009) and Softlitography (Glawe et al.,2005) due to reproducibility and tunability. Yet, microchannel development is a laborious endeavor which often relies on specialized equipment. Studies on microchannel-influenced cell alignment have shown that 5-200um wide channels significantly influence the spatial orientation of skeletal muscle cells, where 10-100μm wide channels produce optimal alignment and myotube formation. (Hume et al.,2012; Sun et al.,2013).

The vascularization of plants presents a promising topography for guided cell alignment (Fontana et al., 2017). In the case of celery (*A. graveolens)*, the vascular bundle is composed of xylem (which includes cambium) and phloem. The xylem is composed of 17 ± 5μm (N=3) wide channels, whereas the phloem is composed of 16 ± 6μm (N=3.) wide channels (Fig.2A & 2E). By cutting the *A. graveolens* stalk longitudinally, we were able to acquire grooves with diameters within that of intact channels. The decellularization of the *A. graveolens* scaffold was done based on previously published protocol (Fig.1A) (Hickey et al., 2018). As show previously by a number of groups, including our own, decellularized plant tissue can be used as a substrate for 3D cell culture of immortalized and primary mammalian cells (Modulevsky et al. 2014; Gershalk et al., 2017; Fontana et al., 2017; Hickey et al., 2018) That being said, we hypothesize that

C2C12 murine myoblast will adhere, proliferate, differentiate, and align parallel to the vascular bundle of *A. graveolens*.

Following 10 days in culture, the actin filaments and nuclei (direction of apex) of C2C12s were observed to be oriented parallel to the longitudinal axis of the V.B when compared to cells on seeded on the parenchyma ($P = 2 \times 10^{-4}$, N = 10) (Fig.3). Taking into consideration the non-uniform arrangement of channels within the vascular bundle leads us to assume that the diameter of the channels varied. It's then safe to say that in some cases cells were confined and in other cases guided through contact guidance. As reported by Altomare et al. (2010), 25 μm and 50μm wide grooves with a depth between 0.5 and 2.5μm presented enough of a topographical cue for cell alignment. This observation, however, appeared to be cell line specific: C2C12 didn't respond to grooves below 0.5μm as well as primary myoblast (Altomare et al., 2010).

Consideration of myoblast alignment led us to hypothesize that myotubes would also form parallel to the longitudinal axis of the V.B. Following 5 days in differentiation media, the direction of analyzed myotubes was observed to be significantly influenced by the substrate ($P = 2 \times 10^{-6}$, N =10) (Fig.4M & N). An average myotube length of 308 ± 169μm (N=103) was calculated. Myotubes on ground tissue yielded a mostly uniform histogram, whereas myotubes on the V.B. yielded a skewed histogram. The spread of the myotube-histogram is likely due to the noise from non-specific antibody binding, lack of topographical cues (Supplementary data – Figure 2) and partial detachment of cells during the staining steps.

The images analyzed here yield a normalized direction of 1.2 ± 2.0° and 8.6 ± 23.8° (N = 10) for actin and myotubes, respectively. With reference to literature values, cells were considered to be aligned when the normalized direction of myotubes with respect to the substrate was below 10° (Altomare et al., 2010; Chares et al., 2007). This further supports our observation that the microtopography of the vascular bundle induced guided alignment of C2C12 murine myoblast.

Although cells were uniformly distributed throughout the bundle (Fig.5C), myotube formation was not observed following 5 days in differentiation media (Supplementary material - Fig.3). Confluency is a crucial factor in myogenesis; therefore, to obtain optimal myotube development *in vitro*, differentiation media should be introduced into a 85-95% confluent myoblast culture (Hindi et al., 2017). Consequently, MYHC expression has been shown to be influenced by cell density and confluency (Tanaka et al., 2011). We therefore conclude based on the samples tested that confluency was suboptimal for myotube formation. Therefore, we recommend future studies into myogenesis on vascular bundles to introduce longer proliferation periods.

Here we show that the vascular bundle of *A. graveolens* is able to induce alignment of myoblast and subsequently myotubes. However, it lacks a wide array of factors that influence cells *in vitro,* such as biochemical and mechanical cues. As elucidated previously, the xylem and phloem of plants has been determined to be approximately 10^6 (Farahi et al.,2017; Hepworth & Vincent, 1998) and 10^3 (Lee, 1981) times stiffer than muscle tissue (Engler et al., 2004), respectively. With reference to mammalian cells, stiffness has been shown to influence cell

behavior, such as viability, morphology and differentiation (Engler et al., 2004; Levy-Mishali et al., 2009; Wells, 2008). This is turn explains the outlying occurrence in Figure 4D, which portrays a lower number of cells on the xylem compared to the phloem. In addition to the 1000-fold difference in stiffness, we can't disregard the natural hydrophobicity of lignin (Lourenço et al., 2016). As reported by Papenburg and colleagues, hydrophobic surfaces have been shown to improve initial cell attachment of C2C12 pre-myoblast; yet, a reduced proliferation rate and spreading was observed (2010).

In this study, we only tested for the presence of MHC using MF-20. This antibody recognizes all MHC isoforms; therefore, this doesn't provide an insight into the differentiation stage of myotubes without testing for other markers, such as Acta1 and Glut4 (Chal and Pourquie, 2017). Subsequently, based on the centralized location of the nuclei, as opposed to that of mature muscle tissue where the nuclei are found in the periphery (Roman and Gomes, 2018; Cadot et al., 2015), it's safe to say that the myotubes were still immature. It's still unclear if C2C12 cultured on the decellularized vascular bundle of *A. graveolens* can express sarcomeric proteins. Yet, we can't, however, disregard the notion that striated myotubes are rarely observed *in vitro*, especially in immortalized cell lines (Chal & Pourquié, 2017; Denes et al., 2019; Hosseini et al., 2012).

Microchannel fabrication often involves post treatment and coating with bioactive factors to increase cell adhesion (Huang et al., 2010; Leclerc et al., 2013; Wang et al., 2010; Gingras et al., 2009). In contrast, the vascular bundle allowed for adherence and differentiation of muscle cells without a need for a bioactive coating. Yet, we must take into account the role of adhesive

proteins naturally found in FBS (Olivieri et al., 1992; Hayman et al.,1985). We do however postulate that biofunctionalization will improve the substrates biocompatibility and extend the use of this abundant, simple and biocompatible material to more problematic cell types (Fontana et al., 2017). Lastly, we speculate that cells seeded on top of already aligned myotubes can lead to 3D tissue development as shown previously (Hume et al., 2012).

As mentioned previously, the need for anisotropy in 2D cell culture doesn't only apply to myotubes, but also neurons (Basso et al., 2018), tendon derived cells (Foolen et al., 2018) and smooth muscle cells (Kuppan et al., 2016). In addition to somatic cells, the topography presented here can be used to further study the influence of topographical cues on stem cells (Wang et al., 2012). We hereby present a method that will facilitate *in vitro* research on the importance of cellular anisotropy and spatial orientation.

4.6 Conclusion

Here we present a simple, reproducible, abundant, and non-animal derived substrate for guided alignment of C2C12 myoblast. By longitudinally cutting the vascular bundle of decellularized celery (*A. graveolens)*, we were able to acquire grooves in the micrometer scale. After culturing cells in these substrate for 10 days, F-actin filaments and apex of nuclei were observed to be aligned in the direction of the grooves. Subsequently, 5 days in differentiation media led to myoblast fusion alongside MHC expression. Yet, it's still unclear whether myoblast cultured on this substrate have the potential to develop a functional sarcomere.

4.7 Funding

This work was supported by the New Harvest grant number 0005 and the In Vivo Foundation. New Harvest is a 501c3 non-profit research institute based in the US. S.C was also supported by the Queen Elizabeth II graduate scholarships in science and technology (QEII - GSST). We also acknowledge generous support from the Natural Sciences and Engineering Research Council (NSERC) Discovery Grant and Canada Foundation for Innovation grant.

4.8 Acknowledgement

We thank Dr. Yun Liu for the assistance with SEM and Mrs Zaida Ticas for assistance with Histology.

4.9 Supplementary material

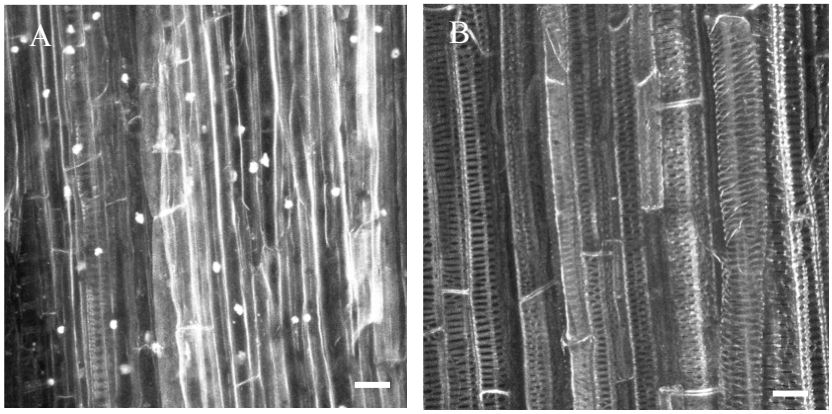

Figure 1. Hoescht 33342 staining of (A) native and (B) decellularized vascular bundle. Nuclei correspond to companion cells of phloem) Scale bar = 25µm.

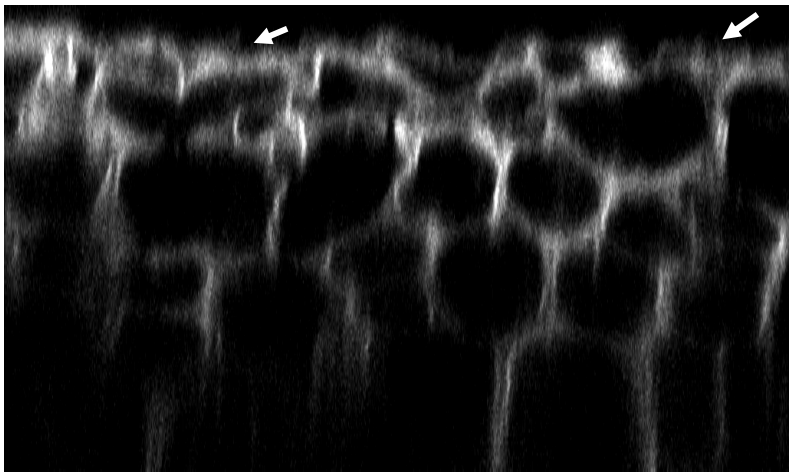

Figure 2. Orthogonal view of phloem microgrooves stained with calcoflour. The image was taken using a multiphoton microscope. Arrows: Smooth areas. 184 x 109 µm orthogonal view

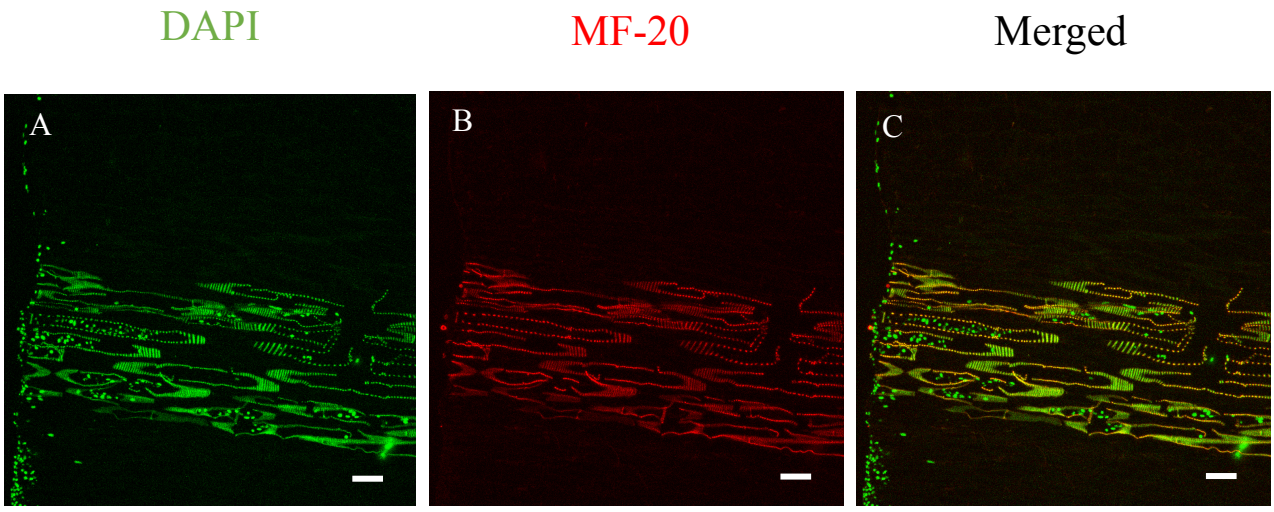

Figure 3. Immunohistochemical analysis of MYHC expression in C2C12 cultured on intact vascular bundles of cross section scaffolds. (A)Myotubes were labeled with MF-20 followed by goat anti-mouse-568 (Red); (B) nuclei were labeled with DAPI (Green). Ribbed structures correspond to fluorescence emission from vascular bundle. Scale bar = 100μm.

CONCLUSION

Great strides have been made towards developing biomaterials for more relevant *in vitro* studies and *in vivo* applications. With the nascent expansion of cellular agriculture as a more sustainable and ethical method of meat production, the development of abundant, food relevant, and biocompatible animal free scaffolds are considered to be a fundamental stepping stone. Decellularized plant tissue has emerged as a simple, abundant and animal free scaffold for applications beyond the biomedical realm. As part of this thesis, I showed how the stiffness of celery parenchyma becomes similar to that of muscle tissue post decellularization. Furthermore, the celery scaffold allowed for extensive proliferation of muscle cells with a physiologically relevant phenotype, and didn't impede differentiation.

Although celery (*Apium graveolens*) parenchyma proved to be a biocompatible substrate with biologically relevant mechanical properties, the limited porosity confined cells to the surface and failed to recreate a crucial characteristic of native skeletal muscle tissue: the alignment of myoblast and myotubes. In an effort to recreate the native spatial orientation of muscle cells, the vascular bundle of celery was cut longitudinally to produce microgrooves with dimensions known to influence the orientation of cells. After 10 days in culture, C2C12 murine myoblast were observed to be align parallel to the vascular bundle. Following 5 days in differentiation media, $MYHC^{+}$ myotubes formed along the vascular bundle grooves. Based on the location of nuclei and arrangement of cytoskeletal proteins (lack of sarcomere), full differentiation was not observed. Although sarcomere formation is rarely observed *in vitro* due to the over simplification of the microenvironment, future studies will build on the results presented here by functionalizing the vascular bundle with ECM relevant protein (e.g. laminin),

introduce recurrent mechanical stimuli (electrical stimulation and cyclic strain), and culture cells in myoblast specific media. Furthermore, future studies will also aim to improve the mechanical properties of the parenchyma and vascular bundle, as substrate stiffness has been shown to influence differentiation. In this thesis, the mean stiffness values of the vascular bundle was determined to be approximately 30x greater than that of skeletal muscle tissue.

Lastly, skeletal muscle is composed of nerve tissue, vascular tissue, nerve tissue and skeletal muscle tissue. Therefore, a more representative *in vitro* model will investigate the importance of a co-culture and possibly recreate the 3D conformation previously shown by Humes et al., 2011.

Concomitantly with sarcomere formation, spontaneous contractions of myotubes known to take place 5-7 days into differentiation treatment was also not observed. In support of the known fact that in vitro contractions lead to myotube detachment, preliminary data showed lower confluency following 10 and 14 days in differentiation media. Observing live contractions on the scaffolds was hindered by the opacity of the scaffold and lack of contrast between the cells and scaffold. Therefore, future studies would benefit from the development of a green-fluorescent-protein or red-fluorescent-protein-C2C12 cell line.

I hereby showed how the vascular bundle of celery can be repurposed as a simple, abundant, and animal free scaffold for *in vitro* studies into the importance of cellular anisotropy. The work presented here will not only facilitate reliable *in vitro* studies but provide foundational work for *in vitro* meat research where animal free scaffolds are expected to be an indispensable

component. This also serves as a reminder that alignment and scaffolding are only two characteristics of a much greater endeavour. The expansion of *in vitro* meat will rely on the development of serum free media, bioreactors, and cell lines or stem cells.

REFERENCES

Allan S.J., De Bank P.A. and Ellis M.J. (2019) Bioprocess Design Considerations for Cultured Meat Production With a Focus on the Expansion Bioreactor. *Front. Sustain. Food Syst.* 3:44. doi: 10.3389/fsufs.2019.00044

Allen, R. E., Sheehan, S. M., Taylor, R. G., Kendall, T. L., & Rice, G. M. (1995). Hepatocyte growth factor activates quiescent skeletal muscle satellite cells in vitro. *Journal of Cellular Physiology*, 165(2), 307. doi: 10.1002/jcp.1041650211

Alley, K. E., & Omerza, F. F. (1999). Neuromuscular remodeling and myofiber turnover in rana pipiens' jaw muscles. *Cells Tissues Organs*, 164(1), 46-58. doi:10.1159/000016642

Allouh, M. Z., Yablonka-Reuveni, Z., & Rosser, B. W. C. (2008). Pax7 reveals a greater frequency and concentration of satellite cells at the ends of growing skeletal muscle fibers. *Journal of Histochemistry and Cytochemistry*, 56(1), 77-87. doi:10.1369/jhc.7A7301.2007

Altomare, L., Gadegaard, N., Visai, L., Tanzi, M. C., & Farè, S. (2010). Biodegradable microgrooved polymeric surfaces obtained by photolithography for skeletal muscle cell orientation and myotube development. *Acta Biomaterialia*, 6(6), 1948-1957. doi:10.1016/j.actbio.2009.12.040

An, B., Kaplan, D. L., & Brodsky, B. (2014). Engineered recombinant bacterial collagen as an alternative collagen-based biomaterial for tissue engineering. *Frontiers in Chemistry*, 2, 40. doi:10.3389/fchem.2014.00040

Antoine, E. E., Vlachos, P. P., & Rylander, M. N. (2014). Review of collagen I hydrogels for bioengineered tissue microenvironments: characterization of mechanics, structure, and transport. *Tissue engineering. Part B, Reviews*, *20*(6), 683–696. doi:10.1089/ten.TEB.2014.0086

Antoni, D., Burckel, H., Josset, E., & Noel, G. (2015). Three-dimensional cell culture: A breakthrough in vivo. *International Journal of Molecular Sciences*, 16(3), 5517-5527. doi:10.3390/ijms16035517

Azuma, K., Osaki, T., Minami, S., & Okamoto, Y. (2015). Anticancer and anti-inflammatory properties of chitin and chitosan oligosaccharides. *Journal of Functional Biomaterials*, 6(1), 33-49. doi:10.3390/jfb6010033

Bader, D. L., & Knight, M. M. (2008). Biomechanical analysis of structural deformation in living cells. *Medical & Biological Engineering & Computing*, 46(10), 951-963. doi:10.1007/s11517-008-0381-4

Badylak, S. F., & Gilbert, T. W. (2007;2008;). Immune response to biologic scaffold materials. *Seminars in Immunology*, 20(2), 109-116. doi:10.1016/j.smim.2007.11.003

Banfield, W.G (1956). Age changes in the swelling capacity of the human achilles tendon. *Journal of Gerontology*, 11(4), 372-372. doi:10.1093/geronj/11.4.372

Basso, J. M. V., Simon, M., & Staii, C. (2018). Neuronal dynamics on patterned substrates measured by fluorescence microscopy. *MRS Communications*, 8(2), 487-492. doi:10.1557/mrc.2018.52

Beauzamy, L., Nakayama, N., & Boudaoud, A. (2014). Flowers under pressure: Ins and outs of turgor regulation in development. *Annals of Botany, 114*(7), 1517-1533.

Beckett, K., & Baylies, M. K. (2007). 3D analysis of founder cell and fusion competent myoblast arrangements outlines a new model of myoblast fusion. *Developmental Biology*, 309(1), 113-125. doi:10.1016/j.ydbio.2007.06.024

Bella, J., Brodsky, B., & Berman, H. M. (1995). Hydration structure of a collagen peptide. *Structure*, 3(9), 893-906. doi:10.1016/S0969-2126(01)00224-6

Benhabiles, M. S., Salah, R., Lounici, H., Drouiche, N., Goosen, M. F. A., & Mameri, N. (2012). Antibacterial activity of chitin, chitosan and its oligomers prepared from shrimp shell waste. *Food Hydrocolloids*, 29(1), 48-56. doi:10.1016/j.foodhyd.2012.02.013

Ben-Yair, R., & Kalcheim, C. (2008). Notch and bone morphogenetic protein differentially act on dermomyotome cells to generate endothelium, smooth, and striated muscle. *The Journal of Cell Biology*, 180(3), 607-618. doi:10.1083/jcb.200707206

Bettadapur, A., Suh, G. C., Geisse, N. A., Wang, E. R., Hua, C., Huber, H. A., . . . McCain, M. L. (2016). Prolonged culture of aligned skeletal myotubes on micromolded gelatin hydrogels. *Scientific Reports*, 6(1), 28855. doi:10.1038/srep28855

Berthod, F., Germain, L., Tremblay, N., & Auger, F. A. (2006). Extracellular matrix deposition by fibroblasts is necessary to promote capillary-like tube formation in vitro. *Journal of Cellular Physiology*, 207(2), 491-498. doi:10.1002/jcp.20584

Bierhalz, A. C. K., Westin, C. B., & Moraes, Â. M. (2016). Comparison of the properties of membranes produced with alginate and chitosan from mushroom and from shrimp. International *Journal of Biological Macromolecules*, 91, 496- 504. doi:10.1016/j.ijbiomac.2016.05.095

Bitar, K. N., & Zakhem, E. (2014). Design strategies of biodegradable scaffolds for tissue regeneration. *Biomedical engineering and computational biology*, *6*, 13–20. doi:10.4137/BECB.S10961

Buckingham, M., Bajard, L., Chang, T., Daubas, P., Hadchouel, J., Meilhac, S., . . . Relaix, F. (2003). The formation of skeletal muscle: From somite to limb. *Journal of Anatomy*, 202(1), 59-68. doi:10.1046/j.1469-7580.2003.00139.x

Breser, M. L., Felipe, V., Bohl, L. P., Orellano, M. S., Isaac, P., Conesa, A., . . . Porporatto, C. (2018). Chitosan and cloxacillin combination improve antibiotic efficacy against different lifestyle of coagulase-negative staphylococcus isolates from chronic bovine mastitis. *Scientific Reports*, 8(1), 5081-13. doi:10.1038/s41598-018-23521-0

Brown, R. B., & Audet, J. (2008). Current techniques for single-cell lysis. *Journal of the Royal Society, Interface*, *5 Suppl 2*(Suppl 2), S131–S138. doi:10.1098/rsif.2008.0009.focus

Cadot, B., Gache, V., & Gomes, E. R. (2015). Moving and positioning the nucleus in skeletal muscle - one step at a time. *Nucleus*, 6(5), 373-381. doi:10.1080/19491034.2015.1090073

Camelliti, P., Kohl, P., McCulloch, A. D., & Gallagher, J. O. (2006). Micropatterned cell cultures on elastic membranes as an in vitro model of myocardium. *Nature Protocols*, 1(3), 1379-1391. doi:10.1038/nprot.2006.203

Carletti E., Motta A., Migliaresi C. (2011) Scaffolds for Tissue Engineering and 3D Cell Culture. In: Haycock J. (eds) 3D Cell Culture. Methods in Molecular Biology (Methods and Protocols), vol 695. Humana Press. doi: 10.1007/978-1-60761-984-0_2

Cavo, M., Fato, M., Peñuela, L., Beltrame, F., Raiteri, R., & Scaglione, S. (2016). Microenvironment complexity and matrix stiffness regulate breast cancer cell activity in a 3D in vitro model. *Scientific Reports*, 6(1), 35367. doi:10.1038/srep35367

Cavka, A., Guo, X., Tang, S. J., Winestrand, S., Jönsson, L. J., & Hong, F. (2013). Production of bacterial cellulose and enzyme from waste fiber sludge. *Biotechnology for biofuels*, *6*(1), 25. doi:10.1186/1754-6834-6-25

Cerino, G., Gaudiello, E., Grussenmeyer, T., Melly, L., Massai, D., Banfi, A., . . . Marsano, A. (2016). Three dimensional multi-cellular muscle-like tissue engineering in perfusion-based bioreactors. *Biotechnology and Bioengineering, 113*(1), 226-236. doi: 10.1002/bit.25688

Cha, S. H., Lee, H. J., & Koh, W. (2017). Study of myoblast differentiation using multi-dimensional scaffolds consisting of nano and micropatterns. Biomaterials Research, 21(1), 1-1. doi:10.1186/s40824-016-0087-x

Chal, J., & Pourquié, O. (2017). Making muscle: Skeletal myogenesisin vivoandin vitro. *Development*, 144(12), 2104- 2122. doi:10.1242/dev.151035

Chan, E. C., Kuo, S., Kong, A. M., Morrison, W. A., Dusting, G. J., Mitchell, G. M., . . . Liu, G. (2016). Three dimensional collagen scaffold promotes intrinsic vascularisation for tissue engineering applications. *PloS One*, 11(2), e0149799. doi:10.1371/journal.pone.0149799

Charest, J. L., García, A. J., & King, W. P. (2007). Myoblast alignment and differentiation on cell culture substrates with microscale topography and model chemistries. *Biomaterials*, 28(13), 2202-2210. doi:10.1016/j.biomaterials.2007.01.020

Chazotte, B. (2011). Labeling nuclear DNA with hoechst 33342. *Cold Spring Harbor Protocols, 2011*(1), Pdb.prot5557.

Cheung, P. C. K. (2013). Mini-review on edible mushrooms as source of dietary fiber: Preparation and health benefits. *Food Science and Human Wellnes*s, 2(3-4), 162-166. doi:10.1016/j.fshw.2013.08.001

Chicatun, F., Pedraza, C. E., Muja, N., Ghezzi, C. E., McKee, M. D., & Nazhat, S. N. (2013). Effect of chitosan incorporation and scaffold geometry on chondrocyte function in dense collagen type I hydrogels. *Tissue engineering. Part A*, *19*(23-24), 2553–2564. doi:10.1089/ten.TEA.2013.0114

Clark, J. F., & Pyne-Geithman, G. (2005). Vascular smooth muscle function: The physiology and pathology of vasoconstriction. *Pathophysiology*, 12(1), 35-45. doi:10.1016/j.pathophys.2005.02.007

Cooper, A., Jana, S., Bhattarai, N., & Zhang, M. (2010). Aligned chitosan-based nanofibers for enhanced myogenesis. *Journal of Materials Chemistry*, 20(40), 8904. doi:10.1039/c0jm01841d

Cornelison, D. D. W. (2008). Context matters: In vivo and in vitro influences on muscle satellite cell activity. *Journal of Cellular Biochemistry*, 105(3), 663-669. doi:10.1002/jcb.21892

Courtenay, J. C., Deneke, C., Lanzoni, E. M., Costa, C. A., Bae, Y., Scott, J. L., & Sharma, R. I. (2018). Modulating cell response on cellulose surfaces; tunable attachment and scaffold mechanics. Cellulose, 25(2), 925-940. doi:10.1007/s10570-017-1612-3

Courtenay, J. C., Johns, M. A., Galembeck, F., Deneke, C., Lanzoni, E. M., Costa, C. A., . . . Sharma, R. I. (2017). Surface modified cellulose scaffolds for tissue engineering. *Cellulose,* 24(1), 253-267. doi:10.1007/s10570-016-1111-y

Croisier, F., & Jérôme, C. (2013). Chitosan-based biomaterials for tissue engineering. *European Polymer Journal*, 49(4), 780-792. doi:10.1016/j.eurpolymj.2012.12.009

Dalrymple, K. R., Prigozy, T. I., & Shuler, C. F. (2000). Embryonic, fetal, and neonatal tongue myoblasts exhibit molecular heterogeneity in vitro. *Differentiation; Research in Biological Diversity,* 66(4-5), 218-226. doi:10.1111/j.1432- 0436.2000.660408.x

Decker, E. -., Von Ohle, C., Weiger, R., Wiech, I., & Brecx, M. (2005). A synergistic chlorhexidine/chitosan combination for improved antiplaque strategies. *Journal of Periodontal Research*, 40(5), 373-377. doi:10.1111/j.1600- 0765.2005.00817.x

De La Haba, G., Kamali, H. M., & Tiede, D. M. (1975). Myogenesis of avian striated muscle in vitro: Role of collagen in myofiber formation. *Proceedings of the National Academy of Sciences of the United States of America*, 72(7), 2729-2732. doi:10.1073/pnas.72.7.2729

Denes, L. T., Riley, L. A., Mijares, J. R., Arboleda, J. D., McKee, K., Esser, K. A., & Wang, E. T. (2019). Culturing C2C12 myotubes on micromolded gelatin hydrogels accelerates myotube maturation. *Skeletal Muscle*, 9(1), 17-10. doi:10.1186/s13395-019-0203-4

Dhanyasi, N., Segal, D., Shimoni, E., Shinder, V., Shilo, B., VijayRaghavan, K., & Schejter, E. D. (2015). Surface apposition and multiple cell contacts promote myoblast fusion in drosophila flight muscles. *The Journal of Cell Biology*, 211(1), 191-203. doi:10.1083/jcb.201503005

Deguchi, S., Tsujii, K., & Horikoshi, K. (2015). In situ microscopic observation of chitin and fungal cells with chitinous cell walls in hydrothermal conditions. *Scientific Reports*, 5(1), 11907. doi:10.1038/srep11907

Derakhshanfar, S., Mbeleck, R., Xu, K., Zhang, X., Zhong, W., & Xing, M. (2018). 3D bioprinting for biomedical devices and tissue engineering: A review of recent trends and advances. *Bioactive Materials*, 3(2), 144-156. doi:10.1016/j.bioactmat.2017.11.008

Donnelly, K., Khodabukus, A., Philp, A., Deldicque, L., Dennis, R., & Baar, K. (2010). A Novel Bioreactor for Stimulating Skeletal Muscle In Vitro. *Tissue Engineering Part C: Methods, 16*(4), 711-8. doi: 10.1089/ten.TEC.2009.0125.

Duckett, J. G., & Pressel, S. (2018). The evolution of the stomatal apparatus: Intercellular spaces and sporophyte water relations in bryophytes-two ignored dimensions. *Philosophical Transactions of the Royal Society of London. Series B, Biological Sciences*, 373(1739), 20160498. doi:10.1098/rstb.2016.0498

Duan, R., Kim, J. H., Shilagardi, K., Schiffhauer, E. S., Lee, D. M., Son, S., . . . Chen, E. H. (2018). Spectrin is a mechanoresponsive protein shaping fusogenic synapse architecture during myoblast fusion. *Nature Cell Biology*, 20(6), 688-698. doi:10.1038/s41556-018-0106-3

Dutta, D., Anant, S., Ruiz-Gomez, M., Bate, M., & VijayRaghavan, K. (2004). Founder myoblasts and fibre number during adult myogenesis in drosophila. *Development,* 131(15), 3761-3772. doi:10.1242/dev.01249

Earles, J. M., Theroux-Rancourt, G., Roddy, A. B., Gilbert, M. E., McElrone, A. J., & Brodersen, C. R. (2018). Beyond porosity: 3D leaf intercellular airspace traits that impact mesophyll conductance. *Plant Physiology*, 178(1), 148-162. doi:10.1104/pp.18.00550

Eloy-Trinquet, S., & Nicolas, J. (2002). Clonal separation and regionalisation during formation of the medial and lateral myotomes in the mouse embryo. *Development*, 129(1), 111-122.

Engler, A. J., Griffin, M. A., Sen, S., Bönnemann, C. G., Sweeney, H. L., & Discher, D. E. (2004). Myotubes differentiate optimally on substrates with tissue-like stiffness: Pathological implications for soft or stiff microenvironments. *The Journal of Cell Biology*, 166(6), 877-887. doi:10.1083/jcb.200405004

Esa, F., Tasirin, S. M., & Rahman, N. A. (2014). Overview of bacterial cellulose production and application. *Agriculture and Agricultural Science Procedia*, 2, 113-119. doi:10.1016/j.aaspro.2014.11.017

Fang, Y., & Eglen, R. M. (2017). Three-Dimensional Cell Cultures in Drug Discovery and Development. *SLAS discovery : advancing life sciences R & D*, *22*(5), 456–472. doi:10.1177/1087057117696795

Farahi, R. H., Charrier, A. M., Tolbert, A., Lereu, A. L., Ragauskas, A., Davison, B. H., & Passian, A. (2017). Plasticity, elasticity, and adhesion energy of plant cell walls: Nanometrology of lignin loss using atomic force microscopy. *Scientific Reports*, 7(1), 152-12. doi:10.1038/s41598-017-00234-4

Fee, T., Surianarayanan, S., Downs, C., Zhou, Y., & Berry, J. (2016). Nanofiber alignment regulates NIH3T3 cell orientation and cytoskeletal gene expression on electrospun PCL+Gelatin nanofibers. *PloS One*, 11(5), e0154806. doi:10.1371/journal.pone.0154806

Feng, Y. N., Li, Y. P., Liu, C. L., & Zhang, Z. J. (2018). Assessing the elastic properties of skeletal muscle and tendon using shearwave ultrasound elastography and MyotonPRO. *Scientific Reports*, 8(1), 17064-9. doi:10.1038/s41598- 018-34719-7

Feng, Y., Okamoto, R. J., Namani, R., Genin, G. M., & Bayly, P. V. (2013). Measurements of mechanical anisotropy in brain tissue and implications for transversely isotropic material models of white matter. *Journal of the Mechanical Behavior of Biomedical Materials*, 23, 117-132. doi:10.1016/j.jmbbm.2013.04.007

Fernandes, Â., Barreira, J. C. M., Antonio, A. L., Morales, P., Férnandez-Ruiz, V., Martins, A., . . . Ferreira, I. C. F. R. (2015). Exquisite wild mushrooms as a source of dietary fiber: Analysis in electron-beam irradiated samples. *LWT - Food Science and Technology*, 60(2), 855-859. doi:10.1016/j.lwt.2014.10.050

Foolen, J., Wunderli, S. L., Loerakker, S., & Snedeker, J. G. (2018). Tissue alignment enhances remodeling potential of tendon-derived cells - lessons from a novel microtissue model of tendon scarring. *Matrix Biology*, 65, 14-29. doi:10.1016/j.matbio.2017.06.002

Fontana, G., Gershlak, J., Adamski, M., Lee, J. S., Matsumoto, S., Le, H. D., … Murphy, W. L. (2017). Biofunctionalized Plants as Diverse Biomaterials for Human Cell Culture. *Advanced healthcare materials*, *6*(8), 10.1002/adhm.201601225. doi:10.1002/adhm.201601225

Forterre, A., Jalabert, A., Berger, E., Baudet, M., Chikh, K., Errazuriz, E., . . . Rome, S. (2014). Proteomic analysis of C2C12 myoblast and myotube exosome-like vesicles: A new paradigm for myoblast-myotube cross talk? *PloS One*, 9(1), e84153-e84153. doi:10.1371/journal.pone.0084153

Franzini-Armstrong, C., & Engel, A. G. (2012). Skeletal muscle : Architecture of membrane systems. In: Hill, J & Olson, E (Eds.). *Muscle* (pp. 763-774). Elsevier Inc. doi:10.1016/B978-0-12-381510-1.00053-3

Frontera, W. R., & Ochala, J. (2015). Skeletal muscle: A brief review of structure and function. Calcified Tissue International, 96(3), 183-195. doi:10.1007/s00223-014-9915-y

Fu, X., Wang, H., & Hu, P. (2015). Stem cell activation in skeletal muscle regeneration. *Cellular and molecular life sciences : CMLS*, *72*(9), 1663–1677. doi:10.1007/s00018-014-1819-5

Fürsatz, M., Skog, M., Sivlér, P., Palm, E., Aronsson, C., Skallberg, A.,… Aili, D.(2018). Functionalization of bacterial cellulose wound dressings with the antimicrobial peptide ε-poly-L-lysine. *Biomedical Materials*, 13(2). Doi: 10.1088/1748-605X/aa9486

Gao, Cao, Dong, Fu, & Wang. (2016). Influence of 3D Microgrooves on C2C12 Cell Proliferation, Migration, Alignment, F-actin Protein Expression and Gene Expression. *Journal of Materials Science & Technology, 32*(9), 901-908. Doi: 10.1016/j.jmst.2016.01.011

García Cruz, D. M., Salmerón-Sánchez, M., & Gómez-Ribelles, J. L. (2012). Stirred flow bioreactor modulates chondrocyte growth and extracellular matrix biosynthesis in chitosan scaffolds. *Journal of Biomedical Materials Research Part A*, 100A(9), 2330-2341. doi:10.1002/jbm.a.34174

Geddis, A. E., & Prockop, D. J. (1993). Expression of human COL1A1 gene in stably transfected HT1080 cells: The production of a thermostable homotrimer of type I collagen in a recombinant system. *Matrix*, 13(5), 399-405. doi:10.1016/S0934-8832(11)80045-4

Gershlak, J., Hernandez, S., Fontana, G., Perreault, L., Hansen, K., Larson, S., . . . Gaudette, G. (2017). Crossing kingdoms: Using decellularized plants as perfusable tissue engineering scaffolds. *Biomaterials*, 125, 13-22. doi:10.1016/j.biomaterials.2017.02.011

Glawe, J. D., Hill, J. B., Mills, D. K., & McShane, M. J. (2005). Influence of channel width on alignment of smooth muscle cells by high-aspect-ratio microfabricated elastomeric cell culture scaffolds. *Journal of Biomedical Materials Research. Part A*, 75(1), 106-114. doi:10.1002/jbm.a.30403

Gilbert, P. M., Havenstrite, K. L., K. E. G. Magnusson, Sacco, A., Leonardi, N. A., Kraft, P., . . . KTH. (2010). Substrate elasticity regulates skeletal muscle stem cell self-renewal in culture. *Science*, 329(5995), 1078-1081. doi:10.1126/science.1191035

Gillies, A. R., & Lieber, R. L. (2011). Structure and function of the skeletal muscle extracellular matrix. *Muscle & nerve*, *44*(3), 318–331. doi:10.1002/mus.22094

Gingras, J., Rioux, R. M., Cuvelier, D., Geisse, N. A., Lichtman, J. W., Whitesides, G. M., . . . Sanes, J. R. (2009). Controlling the orientation and synaptic differentiation of myotubes with

micropatterned substrates. *Biophysical Journal*, 97(10), 2771-2779. doi:10.1016/j.bpj.2009.08.038

Glawe, J. D., Hill, J. B., Mills, D. K., & McShane, M. J. (2005). Influence of channel width on alignment of smooth muscle cells by high-aspect-ratio microfabricated elastomeric cell culture scaffolds. *Journal of Biomedical Materials Research. Part A*, 75(1), 106-114. doi:10.1002/jbm.a.30403

Giusti, S., Mazzei, D., Cacopardo, L., Mattei, G., Domenici, C., & Ahluwalia, A. (2017). Environmental Control in Flow Bioreactors. *Processes, 5*(2), 16. doi:10.3390/pr5020016

Goedecke, N., Bollhalder, M., Bernet, R., Silvan, U., & Snedeker, J. (2015). Easy and accurate mechano-profiling on micropost arrays *MyJove Corporation*. doi:10.5167/uzh-120364

Graham, Z., Gallagher, A., & Cardozo, P. (2015). Focal adhesion kinase and its role in skeletal muscle. *Journal of Muscle Research and Cell Motility, 36*(4-5), 305-315. doi: 10.1007/s10974-015-9415-3

Griffin, M., Sen, S., Sweeney, H., & Discher, D. (2004). Adhesion-contractile balance in myocyte differentiation. *Journal Of Cell Science, 117*(24), 5855-5863.

Gros, J., Serralbo, O., & Marcelle, C. (2009). WNT11 acts as a directional cue to organize the elongation of early muscle fibres. *Nature, 457*(7229), 589-93. doi: 10.1038/nature07564

Ha, J. H., Shehzad, O., Khan, S., Lee, S. Y., Park, J. W., Khan, T., & Park, J. K. (2008). Production of bacterial cellulose by a static cultivation using the waste from beer culture broth. *Korean Journal of Chemical Engineering*, 25(4), 812-815. doi:10.1007/s11814-008-0134-y

Hajiabbas, M., Mashayekhan, S., Nazaripouya, A., Naji, M., Hunkeler, D., Rajabi Zeleti, S., & Sharifiaghdas, F. (2015). Chitosan-gelatin sheets as scaffolds for muscle tissue engineering. *Artificial Cells, Nanomedicine, and Biotechnology*, 43(2), 124-132. doi:10.3109/21691401.2013.852101

Hayman, E. G., Pierschbacher, M. D., Suzuki, S., & Ruoslahti, E. (1985). Vitronectin—A major cell attachmentpromoting protein in fetal bovine serum. *Experimental Cell Research*, 160(2), 245-258. doi:10.1016/0014- 4827(85)90173-9

Heher, P., Maleiner, B., Prüller, J., Teuschl, A. H., Kollmitzer, J., Monforte, X., . . . Fuchs, C. (2015). A novel bioreactor for the generation of highly aligned 3D skeletal muscle-like constructs through orientation of fibrin via application of static strain. *Acta Biomaterialia*, 24, 251-265. doi:10.1016/j.actbio.2015.06.033

Hepworth,D.G. & Vincent, J. F. V. (1998). The mechanical properties of xylem tissue from tobacco plants (nicotiana tabacum‘Samsun’). *Annals of Botany*, 81(6), 751-759. doi:10.1006/anbo.1998.0631

Hickey, R. J., Modulevsky, D. J., Cuerrier, C. M., & Pelling, A. E. (2018). Customizing the shape and microenvironment biochemistry of biocompatible macroscopic plant-derived cellulose scaffolds. *ACS Biomaterials Science & Engineering*, 4(11), 3726-3736. *doi:10.1021/acsbiomaterials.8b00178*

Hickey, R. J., & Pelling, A. E. (2019). Cellulose biomaterials for tissue engineering. *Frontiers in Bioengineering and Biotechnology*, 7, 45-45. doi:10.3389/fbioe.2019.00045

Hindi, L., McMillan, J. D., Afroze, D., Hindi, S. M., & Kumar, A. (2017). Isolation, culturing, and differentiation of primary myoblasts from skeletal muscle of adult mice. *Bio-Protocol*, 7(9) doi:10.21769/BioProtoc.2248

Hindi, S. M., Tajrishi, M. M., & Kumar, A. (2013). Signaling mechanisms in mammalian myoblast fusion. *Science signaling*, *6*(272), re2. doi:10.1126/scisignal.2003832

Hosseini, V., Ahadian, S., Ostrovidov, S., Chen, S., Ramalingam, M., Khademhosseini, A., . . . Kaji, H. (2012). Engineered contractile skeletal muscle tissue on a microgrooved methacrylated gelatin substrate. *Tissue Engineering - Part A*, 18(23-24), 2453-2465.

Huang, L., Xiao, L., Jung Poudel, A., Li, J., Zhou, P., Gauthier, M., . . . Yang, G. (2018). Porous chitosan microspheres as microcarriers for 3D cell culture. *Carbohydrate Polymers*, 202, 611-620. doi:10.1016/j.carbpol.2018.09.021

Huang, N. F., Lee, R. J., & Li, S. (2010). Engineering of aligned skeletal muscle by micropatterning. *American Journal of Translational Research*, 2(1), 43.

Huber, T., Müssig, J., Curnow, O., Pang, S., Bickerton, S., & Staiger, M. P. (2012). A critical review of all-cellulose composites. *Journal of Materials Science*, 47(3), 1171-1186. doi:10.1007/s10853-011-5774-3

Hume, S. L., Hoyt, S. M., Walker, J. S., Sridhar, B. V., Ashley, J. F., Bowman, C. N., & Bryant, S. J. (2012). Alignment of multi-layered muscle cells within three-dimensional hydrogel macrochannels. *Acta Biomaterialia*, 8(6), 2193-2202. doi:10.1016/j.actbio.2012.02.001

Hutter, J., & Bechhoefer. (1993). Calibration of atomic-force microscope tips. *Review of Scientific Instruments*, 64(7), 1868-1873.

Huyck, L., Ampe, C., & Van Troys, M. (2012). The XTT cell proliferation assay applied to cell layers embedded in three-dimensional matrix. *Assay and drug development technologies*, *10*(4), 382–392. doi:10.1089/adt.2011.391

Idota, N., Tsukahara, T., Sato, K., Okano, T., & Kitamori, T. (2009). The use of electron beam lithographic graftpolymerization on thermoresponsive polymers for regulating the directionality of cell attachment and detachment. *Biomaterials,* 30(11), 2095-2101. doi:10.1016/j.biomaterials.2008.12.058

Ishizaki, T., Saito, N., & Takai, O. (2010). Correlation of cell adhesive behaviors on superhydrophobic, superhydrophilic, and micropatterned superhydrophobic/superhydrophilic surfaces to their surface chemistry. Langmuir : *The ACS Journal of Surfaces and Colloids*, 26(11), 8147-8154. doi:10.1021/la904447c

Isobe, N., Komamiya, T., Kimura, S., Kim, U., & Wada, M. (2018). Cellulose hydrogel with tunable shape and mechanical properties: From rigid cylinder to soft scaffold. *International Journal of Biological Macromolecules*, 117, 625-631. doi:10.1016/j.ijbiomac.2018.05.071

Janson, I. A., & Putnam, A. J. (2015). Extracellular matrix elasticity and topography: Material-based cues that affect cell function via conserved mechanisms. *Journal of Biomedical Materials Research Part A*, 103(3), 1246-1258. doi:10.1002/jbm.a.35254

Janssen, I., Heymsfield, S. B., Wang, Z., & Ross, R. (2000). Skeletal muscle mass and distribution in 468 men and women aged 18-88 yr. *Journal of Applied Physiology*, 89(1), 81-88. doi:10.1152/jappl.2000.89.1.81

Jayakumar, R., Chennazhi, K. P., Srinivasan, S., Nair, S. V., Furuike, T., & Tamura, H. (2011). Chitin scaffolds in tissue engineering. *International journal of molecular sciences*, *12*(3), 1876–1887. doi:10.3390/ijms12031876

Jedrzejczak-Silicka, M. (2017). History of Cell Culture in New Insights into Cell Culture Technology, Sivakumar Joghi Thatha Gowder, IntechOpen, DOI: 10.5772/66905. Available from: https://www.intechopen.com/books/new-insights-into-cell-culture-technology/history-of-cell-culture

Jo-Feeney, M., Miller, A. M., & Roupas, P. (2014). Mushrooms—Biologically distinct and nutritionally unique: Exploring a "Third food kingdom". *Nutrition Today*, 49(6), 301-307. doi:10.1097/NT.0000000000000063

John, P. J., Sarvamangala, G. K. and Narasiham, P.(1992),Textural and sensory attributes of curried raw jack fruit, fried and pressure cooked. *Journal of Food Quality*, 15(4): 295-302. doi.org/10.1111/j.1745-4557.1992.tb00993.x

Johns, M. A., Bae, Y., Guimarães, F. E. G., Lanzoni, E. M., Costa, C. A. R., Murray, P. M., . . . Sharma, R. I. (2018). Predicting ligand-free cell attachment on next-generation cellulose-chitosan hydrogels. *ACS Omega*, 3(1), 937-945. doi:10.1021/acsomega.7b01583

Jonas, R., & Farah, L. F. (1998). Production and application of microbial cellulose. *Polymer Degradation and Stability*, 59(1), 101-106. doi:10.1016/S0141-3910(97)00197-3

Kalia, S., Dufresne, A., Cherian, B. M., Kaith, B. S., Avérous, L., Njuguna, J., & Nassiopoulos, E. (2011). Cellulosebased bio- and nanocomposites: A review. *International Journal of Polymer Science,* 2011, 1-35. doi:10.1155/2011/837875

Karavolias, J., Salois, M.J., Baker, K.T. Watkins, K. (2018) Raised without antibiotics: impact on animal welfare and implications for food policy*, Translational Animal Science,* 2(4), 337–348. doi:10.1093/tas/txy016

Karam, G. N. (2005). Biomechanical model of the xylem vessels in vascular plants. *Annals of Botany*, 95(7), 1179- 1186. doi:10.1093/aob/mci130

Kassar-Duchossoy, L., Giacone, E., Gayraud-Morel, B., Jory, A., Gomès, D., & Tajbakhsh, S. (2005). Pax3/Pax7 mark a novel population of primitive myogenic cells during development. *Genes & Development,* 19(12), 1426-1431. doi:10.1101/gad.345505

Kassianidou, E., Probst, D., Jäger, J., Lee, S., Roguet, A., Schwarz, U. S., & Kumar, S. (2019). Extracellular matrix geometry and initial adhesive position determine stress fiber network organization during cell spreading. *Cell Reports,* 27(6), 1897-1909.e4. doi:10.1016/j.celrep.2019.04.035

Keefe, J., Wauk, L., Chu, S., & DeLustro, F. (1992). Clinical use of injectable bovine collagen: A decade of experience. *Clinical Materials*, 9(3), 155-162. doi:10.1016/0267-6605(92)90095-B

Khan, S., Ul-Islam, M., Ikram, M., Ullah, M. W., Israr, M., Subhan, F., . . . Park, J. K. (2016). Three-dimensionally microporous and highly biocompatible bacterial cellulose–gelatin composite scaffolds for tissue engineering applications. *RSC Advances*, 6(112), 110840-110849. doi:10.1039/C6RA18847H

Klemm, D., Heublein, B., Fink, H., & Bohn, A. (2005). Cellulose: Fascinating biopolymer and sustainable raw material. *Angewandte Chemie (International Ed. in English)*, 44(22), 3358-3393. doi:10.1002/anie.200460587

Kohn, R. R., & Rollerson, E. (1960). Aging of human collagen in relation to susceptibility to the action of collagenase. *Journal of Gerontology*, 15(1), 10-14. doi:10.1093/geronj/15.1.10

Komuro, T., Desaki, J., & Uehara, Y. (1982). Three-dimensional organization of smooth muscle cells in blood vessels of laboratory rodents. *Cell and Tissue Research*, 227(2), 429-437. doi:10.1007/BF00210897

Kraham S.J. (2017) Environmental Impacts of Industrial Livestock Production. In: Steier G., Patel K. (eds) International Farm Animal, Wildlife and Food Safety Law. Springer, Cham. doi: 10.1007/978-3-319-18002-1_1

Kulangara, K., & Leong, K. W. (2009). Substrate topography shapes cell function. *Soft Matter*, 5(21), 4072. doi:10.1039/b910132m

Kuo, I. Y., & Ehrlich, B. E. (2015). Signaling in muscle contraction. *Cold Spring Harbor perspectives in biology*, *7*(2), a006023. doi:10.1101/cshperspect.a006023

Kumar, A., Murphy, R., Robinson, P., Wei, L., & Boriek, A. M. (2004). Cyclic mechanical strain inhibits skeletal myogenesis through activation of focal adhesion kinase, rac-1 GTPase, and NF-κB transcription factor. *The FASEB Journa*l, 18(13), 1524-1535. doi:10.1096/fj.04-2414com

Kuppan, P., Sethuraman, S., & Krishnan, U. M. (2016). Interaction of human smooth muscle cells on random and aligned nanofibrous scaffolds of PHBV and PHBV-gelatin. International *Journal of Polymeric Materials and Polymeric Biomaterials*, 65(16), 816. doi:10.1080/00914037.2016.1163562

Kurniawan, H., Lai, J., & Wang, M. (2012). Biofunctionalized bacterial cellulose membranes by cold plasmas. *Cellulose,* 19(6), 1975-1988. doi:10.1007/s10570-012-9785-2

Kwon, S. G., Kwon, Y. W., Lee, T. W., Park, G. T., & Kim, J. H. (2018). Recent advances in stem cell therapeutics and tissue engineering strategies. *Biomaterials Research*, 22(1), 36-36. doi:10.1186/s40824-018-0148-4

Lang, I., Sassmann, S., Schmidt, B., & Komis, G. (2014). Plasmolysis: Loss of turgor and beyond. *Plants (Basel, Switzerland),* 3(4), 583-593. doi:10.3390/plants3040583

Leclerc, A., Tremblay, D., Hadjiantoniou, S., Bukoreshtliev, N. V., Rogowski, J. L., Godin, M., & Pelling, A. E. (2013). Three dimensional spatial separation of cells in response to microtopography. *Biomaterials*, 34(33), 8097-8104. doi:10.1016/j.biomaterials.2013.07.047

Lee, D. R. (1981). Elasticity of phloem tissues. *Journal of Experimental Botany*, 32(126), 251-260.

Lee, P., Lin, R., Moon, J., & Lee, L. P. (2006). Microfluidic alignment of collagen fibers for in vitro cell culture. *Biomedical Microdevices*, 8(1), 35-41. doi:10.1007/s10544-006-6380-z

Lee, K. Y., & Mooney, D. J. (2012). Alginate: Properties and biomedical applications. *Progress in Polymer Science*, 37(1), 106-126. doi:10.1016/j.progpolymsci.2011.06.003

Lemke, S. B., & Schnorrer, F. (2017;2016;). Mechanical forces during muscle development. *Mechanisms of Development*, 144(Pt A), 92-101. doi:10.1016/j.mod.2016.11.003

Lepper, C., & Fan, C. M. (2010). Inducible lineage tracing of Pax7-descendant cells reveals embryonic origin of adult satellite cells. *Genesis (New York, N.Y. : 2000)*, *48*(7), 424–436. doi:10.1002/dvg.20630

Levy-Mishali, M., Zoldan, J., & Levenberg, S. (2009). Effect of scaffold stiffness on myoblast differentiation. *Tissue Engineering. Part A*, 15(4), 935-944. doi:10.1089/ten.tea.2008.0111

Li, Y., Xu, C., & Ma, T. (2014). In vitro organogenesis from pluripotent stem cells. *Organogenesis*, 10(2), 159-163. doi:10.4161/org.28918

Li, J., Chen, M., Wei, X., Hao, Y., & Wang, J. (2017). Evaluation of 3D-printed polycaprolactone scaffolds coated with freeze-dried platelet-rich plasma for bone regeneration. *Materials (Basel, Switzerland),* 10(7), 831. doi:10.3390/ma10070831

Lin, K. W., & Lin, H. Y. (2004). Quality characteristics of Chinese-style meatball containing bacterial cellulose (nata). *Journal of Food Science*, 69(3), SNQ107-SNQ111. doi:10.1111/j.1365-2621.2004.tb13378.x

Listrat, A., Lebret, B., Louveau, I., Astruc, T., Bonnet, M., Lefaucheur, L., . . . Bugeon, J. (2016). How muscle structure and composition influence meat and flesh quality. *The scientific world journal*, 2016(3182746), 3182746-14. doi:10.1155/2016/3182746

Liu, W., Merrett, K., Griffith, M., Fagerholm, P., Dravida, S., Heyne, B., . . . Hälsouniversitetet. (2007;2008;). Recombinant human collagen for tissue engineered corneal substitutes. *Biomaterials*, 29(9), 1147-1158. doi:10.1016/j.biomaterials.2007.11.011

Liu, B., Qu, M., Qin, K., Li, Z., Li, H., Shen, B., & Jiang, Z. (2008;2007;). Role of cyclic strain frequency in regulating the alignment of vascular smooth muscle cells in vitro. *Biophysical Journal*, 94(4), 1497-1507. doi:10.1529/biophysj.106.098574

Lopes, T. D., Riegel-Vidotti, I. C., Grein, A., Tischer, C. A., & Faria-Tischer, Paula Cristina de Sousa. (2014). Bacterial cellulose and hyaluronic acid hybrid membranes: Production and characterization. *International Journal of Biological Macromolecules*, 67, 401-408. doi:10.1016/j.ijbiomac.2014.03.047

Lourenço, A., Rencoret, J., Chemetova, C., Gominho, J., Gutiérrez, A., del Río, J. C., & Pereira, H. (2016). Lignin composition and structure differs between xylem, phloem and phellem in quercus suber L. *Frontiers in Plant Science*, 7 doi:10.3389/fpls.2016.01612

Lukomski, S., Nakashima, K., Abdi, I., Cipriano, V. J., Ireland, R. M., Reid, S. D., . . . Musser, J. M. (2000). Identification and characterization of the scl gene encoding a group A streptococcus extracellular protein virulence factor with similarity to human collagen. *Infection and Immunity*, 68(12), 6542-6553. doi:10.1128/IAI.68.12.6542-6553.2000

Lukomski, S., Nakashima, K., Abdi, I., Cipriano, V. J., Shelvin, B. J., Graviss, E. A., & Musser, J. M. (2001). Identification and characterization of a second extracellular collagen-like protein made by group A streptococcus: Control of production at the level of translation. *Infection and Immunity*, 69(3), 1729-1738. doi:10.1128/IAI.69.3.1729-1738.2001

Lynch, J. & Pierrehumbert, R. (2019) Climate Impacts of Cultured Meat and Beef Cattle. *Front. Sustain. Food Syst*. 3, 5. doi: 10.3389/fsufs.2019.00005

Madihally, S. V., & Matthew, H. W. T. (1999). Porous chitosan scaffolds for tissue engineering. *Biomaterials*, 20(12), 1133-1142. doi:10.1016/S0142-9612(99)00011-3

Maleiner, B., Tomasch, J., Heher, P., Spadiut, O., Rünzler, D., & Fuchs, C. (2018). The Importance of Biophysical and Biochemical Stimuli in Dynamic Skeletal Muscle Models. *Frontiers in physiology*, *9*, 1130. doi:10.3389/fphys.2018.01130

Martin, S. L., Vrhovski, B., & Weiss, A. S. (1995). Total synthesis and expression in escherichia coli of a gene encoding human tropoelastin. *Gene*, 154(2), 159-66. doi: 10.1016/0378-1119(94)00848-M

McDougall, G. J., Morrison, I. M., Stewart, D., & Hillman, J. R. (1996). Plant cell walls as dietary fibre: Range, structure, processing and function. *Journal of the Science of Food and Agriculture*, 70(2), 133-150. doi:10.1002/(SICI)1097- 0010(199602)70:23.0.CO;2-4

Mim, C., & Unger, V. M. (2012). Membrane curvature and its generation by BAR proteins. *Trends in Biochemical Sciences*, 37(12), 526-533. doi:10.1016/j.tibs.2012.09.001

Modulevsky, D. J., Cuerrier, C. M., & Pelling, A. E. (2016). Biocompatibility of subcutaneously implanted plant-derived cellulose biomaterials. *Plos One*, 11(6), e0157894. doi:10.1371/journal.pone.0157894

Modulevsky, D. J., Lefebvre, C., Haase, K., Al-Rekabi, Z., & Pelling, A. E. (2014). Apple derived cellulose scaffolds for 3D mammalian cell culture. *PloS One*, 9(5), e97835. doi:10.1371/journal.pone.0097835

Moniri, M., Boroumand Moghaddam, A., Azizi, S., Abdul Rahim, R., Bin Ariff, A., Zuhainis Saad, W., . . . Mohamad, R. (2017). Production and status of bacterial cellulose in biomedical engineering. Nanomaterials, 7(9), 257. doi:10.3390/nano7090257

Mozetic, P., Giannitelli, S. M., Gori, M., Trombetta, M., & Rainer, A. (2017). Engineering muscle cell alignment through 3D bioprinting. *Journal of Biomedical Materials Research Part A*, 105(9), 2582-2588. doi:10.1002/jbm.a.36117

Münsterberg, A. E., Kitajewski, J., Bumcrot, D. A., McMahon, A. P., & Lassar, A. B. (1995). Combinatorial signaling by sonic hedgehog and wnt family members induces myogenic bHLH gene expression in the somite. *Genes & Development*, 9(23), 2911-2922. doi:10.1101/gad.9.23.2911

Murphy, & Kardon. (2011). Origin of Vertebrate Limb Muscle: The Role of Progenitor and Myoblast Populations. *Current Topics in Developmental Biology, 96*, 1-32. doi: 10.1016/B978-0-12-385940-2.00001-2.

Muzzarelli, R. A. A. (1997). Human enzymatic activities related to the therapeutic administration of chitin derivatives. *Cellular and Molecular Life Sciences*, 53(2), 131-140. doi:10.1007/PL00000584

Myburg, A. A., Lev-Yadun, S. and Sederoff, R. R. (2013). Xylem Structure and Function. *In eLS, John Wiley & Sons, Ltd (Ed*.). doi:10.1002/9780470015902.a0001302.pub2

Myllyharju, J., Lamberg, A., Notbohm, H., Fietzek, P. P., Pihlajaniemi, T., & Kivirikko, K. I. (1997). Expression of wild-type and modified proα chains of human type I procollagen in insect cells leads to the formation of stable [α1(I)]2α2(I) collagen heterotrimers and [α1(I)]3Homotrimers but not [α2(I)]3Homotrimers. *Journal of Biological Chemistry*, 272(35), 21824-21830. doi:10.1074/jbc.272.35.218

Myllyharju, J., Nokelainen, M., Vuorela, A., & Kivirikko, K. I. (2000). Expression of recombinant human type I-III collagens in the yeast pichia pastoris. *Biochemical Society Transactions*, 28(4), 353-357. doi:10.1042/0300-5127:0280353

Narayanan, T., Lombardi, V., Lucii, L., Reconditi, M., Sun, Y., Linari, M., . . . Irving, M. (2002). Mechanism of force generation by myosin heads in skeletal muscle. *Nature*, 415(6872), 659-662. doi:10.1038/415659a

Novotna, K., Havelka, P., Sopuch, T., Kolarova, K., Vosmanska, V., Lisa, V., . . . Bacakova, L. (2013). Cellulose-based materials as scaffolds for tissue engineering. *Cellulose*, 20(5), 2263-2278. doi:10.1007/s10570-013-0006-4

O'Brien, F. J. (2011). Biomaterials & scaffolds for tissue engineering. *Materials Today*, 14(3), 88-95. doi:10.1016/S1369- 7021(11)70058-X

Oh, S. K. W., Chen, A. K., Chen, X., Mok, Y., Lim, U., Chin, A., . . . Reuveny, S. (2009). Long-term microcarrier suspension cultures of human embryonic stem cells. *Stem Cell Research*, 2(3), 219-230. doi:10.1016/j.scr.2009.02.005

Olivieri, M. P., Kittle, K. H., Tweden, K. S., & Loomis, R. E. (1992). Comparative biophysical study of adsorbed calf serum, fetal bovine serum and mussel adhesive protein films. *Biomaterials*, 13(4), 201-208. doi:10.1016/0142- 9612(92)90185-Q

Olsen, D. R., Leigh, S. D., Chang, R., McMullin, H., Ong, W., Tai, E., . . . Toman, P. D. (2001). Production of human type I collagen in yeast reveals unexpected new insights into the molecular assembly of collagen trimers. *Journal of Biological Chemistry*, 276(26), 24038-24043. doi:10.1074/jbc.M101613200

Ontell, M., & Kozeka, K. (1984). The organogenesis of murine striated muscle: A cytoarchitectural study. *The American Journal of Anatomy*, 171(2), 133-148. doi:10.1002/aja.1001710202

O'Sullivan, A. C. (1997). Cellulose: The structure slowly unravels. *Cellulose*, 4(3), 173-207. doi:10.1023/A:1018431705579

Ostadhossein, F., Mahmoudi, N., Morales-Cid, G., Tamjid, E., Navas-Martos, F. J., Soriano-Cuadrado, B., . . . Simchi, A. (2015). Development of Chitosan/Bacterial cellulose composite films containing nanodiamonds as a potential flexible platform for wound dressing. *Materials (Basel, Switzerland)*, 8(9), 6401-6418. doi:10.3390/ma8095309

Pacheco, G., Mello, C. V., Chiari-Andréo, B. G., Isaac, V. L. B., Ribeiro, S. J. L., Pecoraro, É., & Trovatti, E. (2018;2017;). Bacterial cellulose skin masks—Properties and sensory tests. *Journal of Cosmetic Dermatology*, 17(5), 840-847. doi:10.1111/jocd.12441

Pakkanen, O., Hämäläinen, E., Kivirikko, K. I., & Myllyharju, J. (2003). Assembly of stable human type I and III collagen molecules from hydroxylated recombinant chains in the yeast pichia pastoris. effect of an engineered C-terminal oligomerization domain foldon. *The Journal of Biological Chemistry*, 278(34), 32478-32483. doi:

Papenburg, B. J., Roigues, E. D., Roigues, E. D., Wessling, M., & Stamatialis, D. (2010). Insights into the role of material surface topography and wettability on cell-material interactions. *Soft Matter*, 6(18), 4377-4388. doi:10.1039/b927207k

Pangestuti, R., & Kim, S. (2010). Neuroprotective properties of chitosan and its derivatives. *Marine Drugs*, 8(7), 2117- 2128. doi:10.3390/md8072117

Peng, Y. Y., Yoshizumi, A., Danon, S. J., Glattauer, V., Prokopenko, O., Mirochnitchenko, O., . . . Ramshaw, J. A. M. (2009;2010;). A streptococcus pyogenes derived collagen-like protein as a non-cytotoxic and non-immunogenic crosslinkable biomaterial. *Biomaterials*, 31(10), 2755-2761. doi:10.1016/j.biomaterials.2009.12.040

Perry, M. J., Tait, J., Hu, J., White, S. C., & Medler, S. (2009). Skeletal muscle fiber types in the ghost crab, ocypode quadrata: Implications for running performance. *The Journal of Experimental Biology*, 212(Pt 5), 673-683. doi:10.1242/jeb.023481

Pette, D., & Staron, R. S. (1997). Mammalian skeletal muscle fiber type transitions. *International Review of Cytology*, 170, 143. doi: 10.1016/S0074-7696(08)61622-8

Pennisi, C. P., Olesen, C. G., de Zee, M., Rasmussen, J., & Zachar, V. (2011). Uniaxial cyclic strain drives assembly and differentiation of skeletal myocytes. *Tissue Engineering Part A,* 17(19-20), 2543-2550. doi:10.1089/ten.tea.2011.0089

Petersen, N., Gatenholm, P. (2011). Bacterial cellulose-based materials and medical devices: Current state and perspectives. *Applied Microbiology and Biotechnology*, 91(5), 1277-1286. doi:10.1007/s00253-011-3432-y

Percot, A., Viton, C., & Domard, A. (2003). Optimization of chitin extraction from shrimp shells. *Biomacromolecules*, 4(1), 12-18. doi:10.1021/bm025602k

Pihlajaniemi, T., Myllylä, R., & Kivirikko, K. I. (1991). Prolyl 4-hydroxylase and its role in collagen synthesis. *Journal of Hepatology*, 13, S2-S7. doi:10.1016/0168-8278(91)90002-S

Ravi, M., Paramesh, V., Kaviya, S. R., Anuradha, E., & Solomon, F. D. P. (2015). 3D cell culture systems: Advantages and applications. *Journal of Cellular Physiology*, 230(1), 16-26. doi:10.1002/jcp.24683

Ren, X., Chen, C., Hou, Y., Huang, M., Li, Y., Wang, D., & Zhang, L. (2018). Biodegradable chitosan-based composites with dual functions acting as the bone scaffold and the inflammation inhibitor in the treatment of bone defects. International Journal of Polymeric *Materials and Polymeric Biomaterials*, 67(12), 703-710. doi:10.1080/00914037.2017.1376196

Reshef, R., Maroto, M., & Lassar, A. B. (1998). Regulation of dorsal somitic cell fates: BMPs and noggin control the timing and pattern of myogenic regulator expression. *Genes & Development,* 12(3), 290-303. doi:10.1101/gad.12.3.290

Revin, V., Liyaskina, E., Nazarkina, M., Bogatyreva, A., & Shchankin, M. (2018). Cost-effective production of bacterial cellulose using acidic food industry by-products. *Brazilian Journal of Microbiology*, doi:10.1016/j.bjm.2017.12.012

Rich, A. & F. H. C. Crick. (1955). The Structure of Collagen. *Nature*, 176(4489), 915-916.

Rich, A., & Crick, F. (1961). The molecular structure of collagen. *Journal of Molecular Biology,* 3, 483-506.

Riedl, A., Schlederer, M., Pudelko, K., Stadler, M., Walter, S., Unterleuthner, D., . . . Dolznig, H. (2017). Comparison of cancer cells in 2D vs 3D culture reveals differences in AKT-mTOR-S6K signaling and drug responses. *Journal of Cell Science*, 130(1), 203-218. doi:10.1242/jcs.188102

Rodríguez-Vázquez, M., Vega-Ruiz, B., Ramos-Zúñiga, R., Saldaña-Koppel, D. A., & Quiñones-Olvera, L. F. (2015). Chitosan and its potential use as a scaffold for tissue engineering in regenerative medicine. *BioMed Research International*, 2015. doi:10.1155/2015/821279

Roman, W., & Gomes, E. R. (2018). Nuclear positioning in skeletal muscle. *Seminars in Cell & Developmental Biology*, 82, 51-56. doi:10.1016/j.semcdb.2017.11.005

Romanazzo, S., Forte, G., Ebara, M., Uto, K., Pagliari, S., Aoyagi, T., . . . Taniguchi, A. (2012). Substrate stiffness affects skeletal myoblast differentiation in vitro. *Science and Technology of Advanced Materials*, 13(6), 064211-064211. doi:10.1088/1468-6996/13/6/064211

Ruotsalainen, H., Sipilä, L., Vapola, M., Sormunen, R., Salo, A. M., Uitto, L., . . . Myllylä, R. (2006). Glycosylation catalyzed by lysyl hydroxylase 3 is essential for basement membranes. *Journal of Cell Science*, 119(Pt 4), 625-635. doi:10.1242/jcs.02780

Ruottinen, M., Bollok, M., Kögler, M., Neubauer, A., Krause, M., Hämäläinen, E., . . . Neubauer, P. (2008). Improved production of human type II procollagen in the yeast pichia pastoris in shake flasks by a wireless-controlled fed-batch system. *BMC Biotechnology*, 8(1), 33-33. doi:10.1186/1472-6750-8-33

Sabourin, L. A. and Rudnicki, M. A. (2000), The molecular regulation of myogenesis. *Clinical Genetics,* 57(1), 16-25. doi:10.1034/j.1399-0004.2000.570103.x

Sacks, L. D., Cann, G. M., William Nikovits, J., Conlon, S., Espinoza, N. R., & Stockdale, F. E. (2003). Regulation of myosin expression during myotome formation. *Development*, 130(15), 3391-3402. doi:10.1242/dev.00541

Sammalkorpi, M., Karttunen, M. M., & Haataja, M. (2009). Ionic surfactant aggregates in saline solutions: Sodium dodecyl sulfate (SDS) in the presence of excess sodium chloride (NaCl) or calcium chloride (CaCl2). *Journal of Physical Chemistry B*, 113(17), 5863-5870. doi:10.1021/jp901228v

Sampath, S. C., Sampath, S. C., & Millay, D. P. (2018). Myoblast fusion confusion: The resolution begins. *Skeletal Muscle*, *8*(1), 3-3. doi:10.1186/s13395-017-0149-3

Saska, S., Teixeira, L. N., Tambasco de Oliveira, P., Minarelli Gaspar, A. M., Lima Ribeiro, S. J., Messaddeq, Y., & Marchetto, R. (2012). Bacterial cellulose-collagen nanocomposite for bone tissue engineering. *Journal of Materials Chemistry*, 22(41), 2212-22112. doi:10.1039/c2jm33762b

Sato, K., Saida, K., Yanagawa, T., Fukuda, T., Shirakura, K., Shinozaki, H., & Watanabe, H. (2011). Differential Responses of Myogenic C2C12 Cells to Hypoxia between Growth and Muscle-Induction Phases: Growth, Differentiation and Motility. *Journal Of Physical Therapy Science, 23*(1), 161-169.

Scarpella, E., & Meijer, A. (2004). Pattern formation in the vascular system of monocot and dicot plant species. *New Phytologist, 164*(2), 209-242.

Schramm, M., & Hestrin, S. (1954). Factors affecting production of cellulose at the air/ liquid interface of a culture of acetobacter xylinum. *Journal of General Microbiology*, 11(1), 123-129. doi:10.1099/00221287-11-1-123

Schiaffino, S., Rossi, A. C., Smerdu, V., Leinwand, L. A., & Reggiani, C. (2015). Developmental myosins: Expression patterns and functional significance. *Skeletal Muscle*, 5(1), 22-22. doi:10.1186/s13395-015-0046-6

Schoenenberger, A. D., Foolen, J., Moor, P., Silvan, U., & Snedeker, J. G. (2018). Substrate fiber alignment mediates tendon cell response to inflammatory signaling. *Acta Biomaterialia*, 71, 306-317. doi:10.1016/j.actbio.2018.03.004

Schuetz, M., Smith, R., & Ellis, B. (2013). Xylem tissue specification, patterning, and differentiation mechanisms. *Journal of Experimental Botany*, 64(1), 11-31. doi:10.1093/jxb/ers287

Serra, T., Planell, J. A., & Navarro, M. (2013). High-resolution PLA-based composite scaffolds via 3-D printing technology. *Acta Biomaterialia*, 9(3), 5521-5530. doi:10.1016/j.actbio.2012.10.041

Sheetz, M., & Vogel, V. (2006). Local force and geometry sensing regulate cell functions. *Nature Reviews Molecular Cell Biology*, 7(4), 265-275. doi:10.1038/nrm1890

Shi, Z., Zhang, Y., Phillips, G. O., & Yang, G. (2014). Utilization of bacterial cellulose in food. *Food Hydrocolloids*, 35, 539-545. doi:10.1016/j.foodhyd.2013.07.012

Shilo, S., Roth, S., Amzel, T., Harel-Adar, T., Tamir, E., Grynspan, F., & Shoseyov, O. (2013). Cutaneous wound healing after treatment with plant-derived human recombinant collagen flowable gel. *Tissue engineering. Part A*, *19*(13-14), 1519–1526. doi:10.1089/ten.TEA.2012.0345

Shoseyov, O., Posen, Y., & Grynspan, F. (2013). Human Recombinant Type I Collagen Produced in Plants. *Tissue Engineering Part A*, 19(13-14), 1527-33. doi:10.1089/ten.TEA.2012.0347

Shoseyov, O., Posen, Y., & Grynspan, F. (2014). Human collagen produced in plants: More than just another molecule. *Bioengineered*, 5(1), 49-52. doi:10.4161/bioe.26002. doi:10.4161/bioe.26002

Smith, M., McFetridge, P., Bodamyali, T., Chaudhuri, J. B., Howell, J. A., Stevens, C. R., & Horrocks, M. (2000). Porcine-derived collagen as a scaffold for tissue engineering. *Food and Bioproducts Processing*, 78(1), 19-24. doi:10.1205/096030800532680

Soliman, E., Bianchi, F., Sleigh, J. N., George, J. H., Cader, M. Z., Cui, Z., & Ye, H. (2018). Aligned electrospun fibers for neural patterning. *Biotechnology Letters*, 40(3), 601-607. doi:10.1007/s10529-017-2494-z

Somers, S. M., Spector, A. A., DiGirolamo, D. J., & Grayson, W. L. (2017). Biophysical Stimulation for Engineering Functional Skeletal Muscle. *Tissue engineering. Part B, Reviews*, *23*(4), 362–372. doi:10.1089/ten.TEB.2016.0444

Specht, E. A., Welch, D. R., Rees Clayton, E. M., & Lagally, C. D. (2018). Opportunities for applying biomedical production and manufacturing methods to the development of the clean meat industry. *Biochemical Engineering Journal,* 132, 161-168. doi:10.1016/j.bej.2018.01.015

Staunton D., Millard C., Aricescu A., Campbell I. (2009) Preparation of recombinant fibronectin fragments for functional and structural studies. In: Even-Ram S., Artym V. (eds) Extracellular Matrix Protocols. Methods in Molecular Biology (Methods and Protocols), vol 522. Humana Press. doi: 10.1007/978-1-59745-413-1_5

Stein, H., Wilensky, M., Tsafrir, Y., Rosenthal, M., Amir, R., Avraham, T., . . . Shoseyov, O. (2009). Production of bioactive, post-translationally modified, heterotrimeric, human recombinant type-I collagen in transgenic tobacco. *Biomacromolecules*, 10(9), 2640-2645. doi:10.1021/bm900571b

Stephens, N., Di Silvio, L., Dunsford, I., Ellis, M., Glencross, A., & Sexton, A. (2018). Bringing cultured meat to market: Technical, socio-political, and regulatory challenges in cellular agriculture. *Trends in Food Science & Technology*, 78, 155-166. doi:10.1016/j.tifs.2018.04.010

Sun, Y., Duffy, R., Lee, A., & Feinberg, A. W. (2013). Optimizing the structure and contractility of engineered skeletal muscle thin films. *Acta Biomaterialia*, 9(8), 7885-7894. doi:10.1016/j.actbio.2013.04.036

Szczesna, D. D., Guzman, G., Miller, T., Zhao, J., Farokhi, K., Ellemberger, H., & Potter, J. (1996). The role of the four Ca 2 binding sites of troponin C in the regulation of skeletal muscle contraction. *Journal of Biological Chemistry, 271*(14), 8381-8386. doi: 10.1074/jbc.271.14.8381

Szustakowski, Lee, Marrese, Kosinski, Nirmala, & Kemp. (2006). Identification of novel pathway regulation during myogenic differentiation. *Genomics, 87*(1), 129-138

Tamura, H., Furuike, T., Nair, S. V., & Jayakumar, R. (2011). Biomedical applications of chitin hydrogel membranes and scaffolds. *Carbohydrate Polymers*, 84(2), 820-824. doi:10.1016/j.carbpol.2010.06.001

Tan, Z., Liu, T., Zhong, J., Yang, Y., & Tan, W. (2017). Control of cell growth on 3D-printed cell culture platforms for tissue engineering. *Journal of Biomedical Materials Research Part A*, 105(12), 3281-3292. doi:10.1002/jbm.a.36188

Tanaka, T., Hattori-Aramaki, N., Sunohara, A., Okabe, K., Sakamoto, Y., Ochiai, H., . . . Kishi, K. (2014). Alignment of skeletal muscle cells cultured in collagen gel by mechanical and electrical stimulation. *International Journal of Tissue Engineering*, 2014, 1-5. doi:10.1155/2014/621529

Tanaka, K., Sato, K., Yoshida, T., Fukuda, T., Hanamura, K., Kojima, N., . . . Watanabe, H. (2011). Evidence for cell density affecting C2C12 myogenesis: Possible regulation of myogenesis by cell–cell communication. *Muscle & Nerve*, 44(6), 968-977. doi:10.1002/mus.22224

Teixeira, A. I., Abrams, G. A., Bertics, P. J., Murphy, C. J., & Nealey, P. F. (2003). Epithelial contact guidance on welldefined micro- and nanostructured substrates. *Journal of Cell Science*, 116(Pt 10), 1881-1892. doi:10.1242/jcs.00383

Tchemtchoua, V. T., Atanasova, G., Aqil, A., Filée, P., Garbacki, N., Vanhooteghem, O., . . . Colige, A. (2011). Development of a chitosan nanofibrillar scaffold for skin repair and regeneration. *Biomacromolecules*, 12(9), 3194- 3204. doi:10.1021/bm200680q

Thanner, S., Drissner, D., & Walsh, F. (2016). Antimicrobial Resistance in Agriculture. *mBio*, *7*(2), e02227-15. doi:10.1128/mBio.02227-15

Thirumala, S., Gimble, J. M., & Devireddy, R. V. (2013). Methylcellulose based thermally reversible hydrogel system for tissue engineering applications. *Cells*, 2(3), 460-475. doi:10.3390/cells2030460

Thorsteinsdóttir, S., Deries, M., Cachaço, A. S., & Bajanca, F. (2011). The extracellular matrix dimension of skeletal muscle development. *Developmental Biology*, 354(2), 191-207. doi:10.1016/j.ydbio.2011.03.015

Tijore, A., Irvine, S. A., Sarig, U., Mhaisalkar, P., Baisane, V., & Venkatraman, S. (2018). Contact guidance for cardiac tissue engineering using 3D bioprinted gelatin patterned hydrogel. *Biofabrication*, 10(2), 025003. doi:10.1088/1758- 5090/aaa15d

Tin, S., Sakharkar, K. R., Lim, C. S., & Sakharkar, M. K. (2009). Activity of chitosans in combination with antibiotics in pseudomonas aeruginosa. *International Journal of Biological Sciences*, 5(2), 153-160. doi:10.7150/ijbs.5.153

Tintignac, L. A., Brenner, H., & Rüegg, M. A. (2015). Mechanisms regulating neuromuscular junction development and function and causes of muscle wasting. *Physiological Reviews*, 95(3), 809-852. doi:10.1152/physrev.00033.2014

Trensz, F., Lucien, F., Couture, V., Söllrald, T., Drouin, G., Rouleau, A., . . . Grenier, G. (2015). Increased microenvironment stiffness in damaged myofibers promotes myogenic progenitor cell proliferation. *Skeletal Muscle*, 5(1), 5-5. doi:10.1186/s13395-015-0030-1

Tomihata, K., & Ikada, Y. (1997). In vitro and in vivo degradation of films of chitin and its deacetylated derivatives. *Biomaterials*, 18(7), 567-575. doi:10.1016/S0142-9612(96)00167-6

Tuomisto, H. L., & de Mattos, M Joost Teixeira. (2011). Environmental impacts of cultured meat production. *Environmental Science & Technology*, 45(14), 6117-6123. doi:10.1021/es200130u

Turoverova, L. V., Khotin, M. G., Yudintseva, N. M., Magnusson, K. -., Blinova, M. I., Pinaev, G. P., . . . Hälsouniversitetet. (2009). Analysis of extracellular matrix proteins produced by cultured cells. *Cell and Tissue Biology*, 3(5), 497-502. doi:10.1134/S1990519X09050137

Turnbull, G., Clarke, J., Picard, F., Riches, P., Jia, L., Han, F., . . . Shu, W. (2018;2017;). 3D bioactive composite scaffolds for bone tissue engineering. *Bioactive Materials*, 3(3), 278-314. doi:10.1016/j.bioactmat.2017.10.001

Varley, M. C., Markaki, A. E., & Brooks, R. A. (2017). Effect of Rotation on Scaffold Motion and Cell Growth in Rotating Bioreactors. *Tissue engineering. Part A*, *23*(11-12), 522–534. doi:10.1089/ten.TEA.2016.0357

Verbeke, W. A. J., & Viaene, J. (2000). Ethical challenges for livestock production:Meeting consumer concerns about meat safety and AnimalWelfare. *Journal of Agricultural and Environmental Ethics*, 12(2), 141-151. doi:10.1023/A:1009538613588

Vernon, R. B., Gooden, M. D., Lara, S. L., & Wight, T. N. (2005). Microgrooved fibrillar collagen membranes as scaffolds for cell support and alignment. *Biomaterials*, 26(16), 3131-3140. doi:10.1016/j.biomaterials.2004.08.011

Vogel, V., & Sheetz, M. (2006). Local force and geometry sensing regulate cell functions. *Nature Reviews Molecular Cell Biology, 7*(4), 265-75.

von Maltzahn, J., Chang, N. C., Bentzinger, C. F., & Rudnicki, M. A. (2012). Wnt signaling in myogenesis. *Trends in Cell Biology*, 22(11), 602-609. doi:10.1016/j.tcb.2012.07.008

Wang, X., Wang, G., Liu, L., & Zhang, D. (2016). The mechanism of a chitosan-collagen composite film used as biomaterial support for MC3T3-E1 cell differentiation. *Scientific Reports*, 6, 39322. doi:10.1038/srep39322

Wang, P., Li, W., Yu, J., & Tsai, W. (2012). Modulation of osteogenic, adipogenic and myogenic differentiation of mesenchymal stem cells by submicron grooved topography. *Journal of Materials Science: Materials in Medicine*, 23(12), 3015-3028. doi:10.1007/s10856-012-4748-6

Wang, P., Yu, H., & Tsai, W. (2010). Modulation of alignment and differentiation of skeletal myoblasts by submicron ridges/grooves surface structure. *Biotechnology and Bioengineering*, 106(2), 285-n/a. doi:10.1002/bit.22697

Werkmeister, J. A., & Ramshaw, J. A. M. (2012). Recombinant protein scaffolds for tissue engineering. *Biomedical Materials*, 7(1), 012002. doi:10.1088/1748-6041/7/1/012002

Widhe, M., Bysell, H., Nystedt, S., Schenning, I., Malmsten, M., Johansson, J., . . . Farmaceutiska fakulteten. (2010). Recombinant spider silk as matrices for cell culture. *Biomaterials*, 31(36), 9575-9585. doi:10.1016/j.biomaterials.2010.08.061

Wells, R. G. (2008). The role of matrix stiffness in regulating cell behavior. *Hepatology*, 47(4), 1394-1400. doi:10.1002/hep.22193

Wiebe, H. H. (1978). The significance of plant vacuoles. *Bioscience*, 28(5), 327-331. doi:10.2307/1307374

Willard, J. J., Drexler, J. W., Das, A., Roy, S., Shilo, S., Shoseyov, O., & Powell, H. M. (2013). Plant-derived human collagen scaffolds for skin tissue engineering. *Tissue engineering. Part A*, *19*(13-14), 1507–1518. doi:10.1089/ten.TEA.2012.0338

Wozniak, M. (2004). Focal adhesion regulation of cell behavior. *Biochimica Et Biophysica Acta (BBA) - Molecular Cell Research*, doi:10.1016/S0167-4889(04)00099-0

Wu, X., Peng, C., Huang, F., Kuang, J., Yu, S., Dong, Y., & Han, B. (2011). Preparation and characterization of chitosan porous microcarriers for hepatocyte culture. *Hepatobiliary & Pancreatic Diseases International,* 10(5), 509-515. doi:10.1016/S1499-3872(11)60086-6

Wu, Y. J., Chen, T., Chen, I., Kuo, S. M., & Chuang, C. W. (2018). Developing highly porous collagen scaffolds by using alginate microsphere porogens for stem cell cultures. *Materials Letters*, 223, 120-123. doi:10.1016/j.matlet.2018.04.039

Yeong, W. Y., Yu, H., Lim, K. P., Ka Lai Gary Ng, Yin Chiang Freddy Boey, Subbu, V. S., & Tan, L. P. (2010). Multiscale topological guidance for cell alignment via direct laser writing on biodegradable polymer. *Tissue Engineering Part C: Methods,* 16(5), 1011. doi:10.1089/ten.tec.2009.0604

Xu, X., Gan, Q., Clough, R. C., Pappu, K. M., Howard, J. A., Baez, J. A., & Wang, K. (2011). Hydroxylation of recombinant human collagen type I alpha 1 in transgenic maize co-expressed with a recombinant human prolyl 4- hydroxylase. *BMC Biotechnology*, 11(1), 69-69. doi:10.1186/1472-6750-11-69

Yang, T. (2011). Chitin-based materials in tissue engineering: Applications in soft tissue and epithelial organ. *International Journal of Molecular Sciences,* 12(3), 1936-1963. doi:10.3390/ijms12031936

Yu, Z., An, B., Ramshaw, J. A. M., & Brodsky, B. (2014). Bacterial collagen-like proteins that form triple-helical structures. *Journal of Structural Biology*, 186(3), 451-461. doi:10.1016/j.jsb.2014.01.003

Zakhem, E., Raghavan, S., Gilmont, R. R., & Bitar, K. N. (2012). Chitosan-based scaffolds for the support of smooth muscle constructs in intestinal tissue engineering. *Biomaterials*, 33(19), 4810-4817. doi:10.1016/j.biomaterials.2012.03.051

Zeiger, A. S., Hinton, B., & Van Vliet, K. J. (2013). Why the dish makes a difference: Quantitative comparison of polystyrene culture surfaces. *Acta Biomaterialia*, 9(7), 7354-7361. doi:10.1016/j.actbio.2013.02.035

Zhao, Y., Zeng, H., Nam, J., & Agarwal, S. (2009). Fabrication of skeletal muscle constructs by topographic activation of cell alignment. *Biotechnology and Bioengineering*, 102(2), 624-631. doi:10.1002/bit.22080

Zhao, H., Xia, J., Wang, J., Yan, X., Wang, C., Lei, T., . . . Zhang, H. (2018). Production of bacterial cellulose using polysaccharide fermentation wastewater as inexpensive nutrient sources. *Biotechnology & Biotechnological Equipment*, 32(2), 350-356. doi:10.1080/13102818.2017.1418673

Zheng, X., Baker, H., Hancock, W. S., Fawaz, F., McCaman, M., & Pungor, J., Erno. (2006). Proteomic analysis for the assessment of different lots of fetal bovine serum as a raw material for cell culture. part IV. application of proteomics to the manufacture of biological drugs. *Biotechnology Progress*, 22(5), 1294-1300. doi:10.1021/bp060121o

APPENDIX I

Python script for measuring vascular bundle channel diameter

```
# Python script for measuring vascular bundle vessel diameter (Python 3.7.x)
# November 2019
# Written by Santiago Campuzano
# Open Computer Vision (OpenCV) based Python script for measuring the area of Contours
# (enclosed structures). The script takes the path to an image (i.e. the location in the computer)
# , applies Canny edge detection to the image (Binary image containing edges), and draws
# contours around an enclosed structure.
# Prior to exporting data in the form of an xlsx file, an area- threshold is set based on the size
# of the smallest and largest vessel diameter to reduce noise.
# OpenCV supports TIFF, JPEG, PNG and JPEG2000. To find out more about imag- file
reading,
# refer to the documentation page:
# https://docs.opencv.org/4.2.0/d4/da8/group__imgcodecs.html

import cv2
import numpy as np
import pandas as pd
import math

# Declare global variables
areas = []
BelowThr = []
tool = list(range(0, 1000))
df = pd.DataFrame({}, tool)

#open image in provided PATH
img = cv2.imread('PATH')

# Resize image to fit screen
newImgMask = cv2.resize(img, (0,0), fx=0.7, fy=0.7)

#convert to from RGB to BGR
bw = cv2.cvtColor(newImgMask, cv2.COLOR_RGB2BGR)

#Isolate edges using OpenCV's Canny edge detection method
edges = cv2.Canny(bw,200,300)

#find and draw OpenCV Contours
contours, hierachy = cv2.findContours(edges,
cv2.RETR_TREE,cv2.CHAIN_APPROX_SIMPLE)
img = cv2.drawContours(newImgMask, contours, -1, (0,0,255), 1)
```

 # For all of the contours in the "contours" list calculate the area and determine the diameter
based on the correlation between surface area and diameter. In an effort to reduce noise, thresholds for min and max area were set based on manual measurements. Once the diameter is calculated, the values are appended to an excel file (PATH),

```
for c in contours:
   if ((math.sqrt((cv2.contourArea(c)*1.48)/math.pi))*2) < 10:
      BelowThr.append((math.sqrt((cv2.contourArea(c)*1.48)/math.pi))*2)

   elif ((math.sqrt((cv2.contourArea(c)*1.48)/math.pi))*2) >= 55:
      BelowThr.append((math.sqrt((cv2.contourArea(c) * 1.48) / math.pi)) * 2)

   else:
      areas.append((math.sqrt((cv2.contourArea(c)*1.48)/math.pi))*2)

writer = pd.ExcelWriter("PATH", engine='xlsxwriter')
dataY = np.array(BelowThr)
dataX = np.array(areas)
df['area'] = pd.Series(dataX)
df['BelowThr'] = pd.Series(dataY)
```

#display the images

```
cv2.imshow('f',edges)
cv2.imshow('G', newImgMask)
print(areas)

cv2.waitKey(0)
```

 # Write data to excel file on exit

```
df.to_excel(writer, sheet_name='Sheet1')
print(df)
writer.save()

cv2.destroyAllWindows()
```

 # Test conditions for contour area (channel surface area). In an effort to reduce noise and ignore parenchyma plant cells, a threshold was set as shown below. This was done based on manual measurements of the largest and smallest channel for the xylem and phloem. If conditional statement is met, the value will be appended to a list.

```
for c in contours:
   if ((math.sqrt((cv2.contourArea(c)*1.48)/math.pi))*2) < 12:
            BelowThr.append((math.sqrt((cv2.contourArea(c)*1.48)/math.pi))*2)
```

```
    elif ((math.sqrt((cv2.contourArea(c)*1.48)/math.pi))*2) >= 55:
        BelowThr.append((math.sqrt((cv2.contourArea(c) * 1.48) /    math.pi)) * 2)

    else:
        areas.append((math.sqrt((cv2.contourArea(c)*1.48)/math.pi))*2)

# Create an excel file with the contour area generated lists
writer = pd.ExcelWriter("PATH", engine='xlsxwriter')

dataY = np.array(BelowThr)
dataX = np.array(areas)
df['area'] = pd.Series(dataX)
df['BelowThr'] = pd.Series(dataY)

# Display the image to confirm optimal contour detection
cv2.imshow('f',edges)
cv2.imshow('G', newImgMask)
print(areas)
cv2.waitKey(0)

# Send list values to the PATH chosen previously
df.to_excel(writer, sheet_name='Sheet1')
print(df)
writer.save()
cv2.destroyAllWindows()
```

APPENDIX II

Python script for measuring cell migration through vascular bundle

```
# Python script for measuring cell migration through vascular bundle (Python 3.7.x)
# November 2019
# Written by Santiago Campuzano
# Open Computer Vision (OpenCV) based Python script for detecting mouse clicks on image
# files. The script will detect, mark with a green circle, and record the location of a mouse- click
# in the X,Y coordinate system. The user has the option to batch process images by providing
# the path to a folder containing images. The script will automatically export the data as an xlsx
# file.
# OpenCV supports TIFF, JPEG, PNG and JPEG2000. To find out more about reading image
files,
# please refer to the documentation page:
# https://docs.opencv.org/4.2.0/d4/da8/group__imgcodecs.html

# Import required packages
import cv2
import pandas as pd
import glob2 as glob
import os
import numpy as np

# Declare global variables and lists
images = []
my_listX = []
my_listY = []
x = 0
y = 0
AddColX = 0
AddColY = 0
tool = list(range(0, 1000))
df = pd.DataFrame({}, tool)

# mouse-click callback function. Each time a mouse click is detected, the function will
append the x and y coordinates

def draw_circle(event,x,y,flags,param):
    if event == cv2.EVENT_LBUTTONDOWN:
        cv2.circle(n,(x,y),2,(0,255,0),-1)
        my_listX.append(x)
        my_listY.append(y)

# Use glob.glob to batch upload images from the declared PATH.
```

Create separate excel columns for x and y coordinates.

```
for img in glob.glob("PATH"):
    writer = pd.ExcelWriter("PATH", engine='xlsxwriter')
    ColX = "(X){}".format(os.path.basename(img))
    ColY = "(Y){}".format(os.path.basename(img))
    Text = "{}".format(img)
    n = cv2.imread(Text)
    cv2.namedWindow(Text)
    cv2.setMouseCallback(Text, draw_circle)
    images.append(Text)
    print(Text)

    while True:
        cv2.imshow(Text, n)

# Once the spacebar is pressed, the list will be added to the excel file
        if cv2.waitKey(10) == 32:
            print(my_listY)
            print(my_listX)
            cv2.destroyWindow(Text)
            dataX = np.array(my_listX)
            dataY = np.array(my_listY)
            df[ColX] = pd.Series(dataX)
            df[ColY] = pd.Series(dataY)
            del my_listY[:]
            del my_listX[:]
            break

df.to_excel(writer, sheet_name='Sheet1')
print(df)
writer.save()
```